UNIVERSITY OF NAIROBI

SYNTHESIS, CHARACTERIZATION AND ANTI-CANCER APPLICATION OF PLATINUM(II) THIOSEMICARBAZONE COMPLEXES

By

JASMINE NEHEMA ALOISE

I56/13548/2018

Research Thesis Submitted in Partial Fulfillment of the Requirements for Award of the Degree of Master of Science in Chemistry of the University of Nairobi.

2021

DECLARATION

I declare that this thesis is my original work and has not been submitted elsewhere for examination. Where other people's work or my own work has been used, this has properly been acknowledged and referenced in accordance with the University of Nairobi's requirements.

Signed: Date: 30th/11/2021

Jasmine Nehema Aloise

I56/13548/2018

This thesis is submitted for examination with our approval as supervisors:

Dr. Ruth Odhiambo,   Signed…… ……..   Date …30/11/2021……..

Department of chemistry,

University of Nairobi

odhiambor@uonbi.ac.ke

Prof. Lydia Njenga,   Signed…………………   Date …30/11/2021……..

Department of chemistry,

University of Nairobi

lnjenga@uonbi.ac.ke

Prof. Martin Onani,   Signed … ……….Date …30-11-2021……….

Department of chemistry,

University of the Western Cape (SA)

monani@uwc.ac.za

DEDICATION

This thesis is dedicated to my parents, Aloise Thiringi and Celina Karea, for their prayers, love, support, guidance, and encouragement throughout my life, especially during my master's degree.

ACKNOWLEDGEMENT

ABSTRACT

Coordination compounds have great potential as drug molecules. However, their instability, poor water solubility, and multi-drug resistance limit their use. Unstable coordination compounds may undergo unnecessary ligand exchange reactions when introduced into biological systems. While literature reports that bulky ligands can help stabilize the metal center, their use with platinum metal centers has not been explored extensively. This work involved the synthesis of stable metal complexes to be used as anticancer agents. Four thiosemicarbazone ligands; 2-((5-ethylthiophen-2-yl)methylene-*N*-phenylhydrazine carbothiomide (**L1**), 2-((5-ethylthiophene-2-yl)methylene)-1-methylhydrazine carbothiomide (**L2**), *N,N*–dimethyl–2-((4-nitrophene-2-yl)methylene)hydrazine carbothiomide (**L3**), and 2-([2,2'-bithiophen]-5-ylmethylene-1-methylhydrazine carbothiomide (**L4**) were synthesized through condensation reactions of aldehydes and amines. Their respective platinum(II) complexes 2-((5-ethylthiophen-2-yl)methylene-*N*-phenylhydrazinecarbothiomide platinum(II) chloride (**C1**), 2-((5-ethylthiophene-2-yl) methylene)-1-methylhydrazine carbothiomide platinum(II) chloride (**C2**), *N,N*–dimethyl–2-((4-nitrophene-2-yl)methylene)hydrazinecarbothiomide platinum(II) chloride (**C3**), and 2-([2,2'-bithiophen]-5-ylmethylene-1-methylhydrazine carbothiomide platinum(II) (**C4**) were synthesized by reacting the ligands with K_2PtCl_4. The synthesis reactions were all performed under mild conditions, and refluxing was the preferred reaction technique. The yields of the thiosemicarbazone ligands ranged between 89% and 99% while the yields of the complexes were between 77% and 88%. The yields of the complexes were significantly lower than those of the ligands, which can be attributed to the steric shielding of the heavy ligands to the platinum metal center. The compounds exhibited sharp melting points. The characterization techniques employed were: FTIR, UV-Vis, ^{1}H NMR, ^{13}C NMR, elemental analysis, and XRD. The ligands were bidentate and coordinated via sulphur and nitrogen atoms. The mode of coordination was established by the disappearance of the thioamide proton and changes in chemical shifts observed in the NMR spectra of the complexes. The anti-cancer activities of the thiosemicarbazone ligands and complexes were performed in *vitro* on four human cell lines; three cancerous cell lines (HeLa, Caco-2 and HT-29) and the non-cancerous KMST-6, and *cis*platin was used as the positive control. The results revealed that three ligands (**L1**, **L2,** and **L4**) had less anti-cancer activity compared to their complexes. **L3** was lethal to Caco-2 (IC_{50} = 3.412 µg/mL), HT-29 (IC_{50} = 0.6886 µg/mL) and HeLa (IC_{50} = 0.107 µg/mL) cell lines at lower concentrations than *cis*platin. However, **L3** was also lethal to KMST-6 (IC_{50} = 2.1 µg/mL). Complexes exhibited varying anti-cancer activity on the different cell lines. **C1** had a low inhibition value of (IC_{50} = 45.42 µg/mL) for the Caco-2 cell line. **C2** showed inhibition values of; (IC_{50} = 31.63 µg/mL) for HT-29 and (IC_{50} = 41.82 µg/mL) for Caco-2 cell line, suggesting that it had better activity than *cis*platin, which had inhibition values (IC_{50} = 35.5 µg/mL) for HT-29 and (IC_{50} = 48.83 µg/mL) for Caco-2 cell lines. **C3** showed inhibition values of (IC_{50} = 0.0001973 µg/mL) for HeLa, suggesting better activity than *cis*platin, whose inhibition was (IC_{50} = 0.1099 µg/mL). Altogether, this study shows that these some of these thiosemicarbazone (II) complexes offer a promising alternative to other platinum complexes in cancer therapy.

TABLE OF CONTENTS

LIST OF FIGURES

LIST OF SCHEMES

LIST OF TABLES

LIST OF ABBREVIATIONS

ATR-IR   Attenuated Total Reflectance Infrared

Caco-2   Colon Carcinoma (Human Colorectal Adenocarcinoma Cells)

CFSE   Crystal Field Stabilization Energy

***Cis*platin**   *Cis*-dichlorodiammineplatinum

COSY   Correlated Spectroscopy

DEPT   Distortionless Enhancement by Polarization Transfer

DMF   Dimethylformamide

DMSO   Dimethyl Sulfoxide

DNA   Deoxyribonucleic Acid

EDTA   Ethylenediaminetetraacetic Acid

FTIR   Fourier Transform Infrared Spectroscopy

Hela   Henrietta Lacks (Cervical Cancer Cell Line)

HMBC   Heteronuclear Multiple Bond Correlation

HOMO   Highest Occupied Molecular Orbital

HSQC   Heteronuclear Single Quantum Coherence Spectroscopy

HT-29   Human Colorectal Adenocarcinoma Cell Line

IC_{50}   Half-Maximal Inhibitory Concentration

IR   Infrared Spectroscopy

KBr   Potassium Bromide

KMST-6   Human Fibroblast Cell Line

LUMO   Lowest Unoccupied Molecular Orbital

MLCT   Metal to Ligand Charge Transfer

NMR   Nuclear Magnetic Resonance

TMS   Tetramethylsilane

TSC   Thiosemicarbazone

UV-Vis   Ultraviolet - Visble

XRD   X-Ray Diffraction

CHAPTER 1

INTRODUCTION

1.1 Background Information

1.1.1 Application of Metal Complexes

Coordination compounds have been studied for several decades now, emphasizing their synthesis, characterization, and applications. Their unique properties, such as varying oxidation states, distinct colours, magnetic susceptibility, and volatility, have made the compounds attractive in many fields. One of these areas is catalysis, like in the case of triscyclomatalated homoleptic iridium(III) complexes (Njogu *et al.,* 2019). The iridium complexes can be installed in equipment that utilizes solar energy, thus helping to conserve energy. Metal complexes have also been used in environmental control, such as crown ether chelates (Odhiambo *et al.,* 2018), which can detect the heavy metals they have a high affinity to.

Another use of coordination metal complexes is in biological applications, where they have been used to treat several ailments. For instance, the gold complex, auranofin (Jurca *et al.,* 2017), treats rheumatoid arthritis. Lanthanum carbonate is a compound used as a phosphate binder in clinical practice and has been used on patients with severe kidney diseases. The biological activity of the compounds has been found to increase with chelation, which proves the importance of using complexes and not only the ligands on their own.

Coordination compounds have been widely used as anticancer drug agents such as *cis*platin, nedaplatin, and carboplatin (Parkin *et al*., 2021). Although many cancer treatments are available, they are prescribed based on the cancer type and how advanced it is. Many patients use a combination of therapies to achieve the best results. While newer therapies like stem cell therapy and immunotherapy are coming up, chemotherapy remains a superior treatment method because it is a systematic approach to treating cancer (Jurca *et al*., 2017). This means that the drug travels to all body parts and kills all metastasized cells, making it ideal for cure, palliation, or control purposes (Dasari & Tchounwou 2014).

1.1.2 The Cancer Burden

In GLOBCAN survey of 2020, as summarized by Sung *et al.* (2021), cancer was responsible for ten million deaths in 2020 alone. An estimated nine million new cancer cases were reported in 2020. In the same year, female breast cancer was reported to have been the most commonly diagnosed cancer type, not lung cancer as reported in the previous year (Sung *et al.,* 2021). Out of the 183 countries involved in the GLOBCAN study, cancer was the primary cause of death for people under 70 years old in 112 nations. The statistics indicate that cancer is a prominent cause of death and is a considerable impediment to increasing life expectancy across the globe. As the world's population continues to increase, it is expected that the global cancer burden will continue to rise. Therefore, it is no doubt that the need for speedy solutions and effective cancer therapies is a priority.

1.1.3 Coordination Complexes Used in Cancer Treatment

The earliest complex used in cancer treatment was *Cis*-dichlorodiammineplatinum (*cis*platin) (**1**), which had chloro and amino ligands and a platinum metal center (Pitt *et al.,* 2016).

$$
\begin{array}{ccc}
Cl & & NH_3 \\
 & Pt & \\
Cl & & NH_3 \\
\end{array}
$$

1
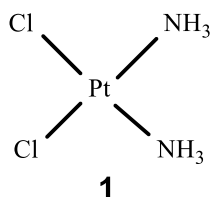
Before its introduction, scientists had not managed to control the toxic effects of metal-based drugs while harnessing their benefits (Dasari & Tchounwou 2014). This made *cis*platin a significant success. When *cis*platin is introduced into a biological system, the chlorine atoms are quickly replaced by water molecules to bind with DNA since they are more labile than the amino groups (Kellinger *et al.,* 2013). However, sometimes the amino ligands on the *cis*platin molecule are replaced by Sulphur-containing bioligands, abundant in the body. When this happens, the drug changes its form and cannot treat cancer as it was intended to. This usually causes drug resistance, and the patient may not get better.

The challenges posed by *cis*platin prompted the development of *cis*platin analogs known as platins (Zalba & Garrido, 2013). Their mode of action requires them first to undergo aquation. One or more ligands is replaced with water molecules in the body, allowing the compound to

bind to DNA and prevent replication and transcription. This causes the cancer cells to die. One of the first analogs was the nedaplatin (**2**) (Shimada *et al.,* 2013), which has amine carrier ligands like *cis*platin, but the leaving group is a bulky five-membered ring compound.

2
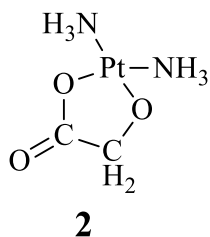
Its mechanism is similar to *cis*platin because it prevents DNA duplication, but nedaplatin is more stable and has a shorter elimination life than *cis*platin (Niioka *et al.,* 2007). Another analog is carboplatin (**3**) (Liu *et al.,* 2014), which has good chemical stability, due to its large ligands that increase steric hindrance.

3
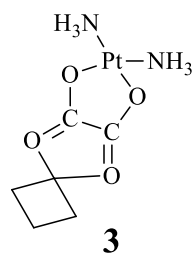
Fewer doses of carboplatin are required to treat cancer than what is needed when using *cis*platin (Zalba & Garrido, 2013). Oxaliplatin (**4**) (Lévi *et al.,* 2012), a second-generation *cis*platin analog, has a diamino cyclohexane ligand and a platinum metal center, increasing the compound's chemical stability.

4
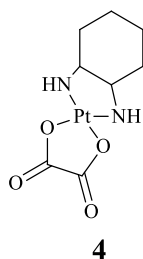
Oxaliplatin is a significant upgrade from *cis*platin because it doesn't have a high resistance profile like *cis*platin (Graham *et al.,* 2004). Several platinum-based drugs are under clinical trials like dicyloplatin (**5**) (Yu *et al.,* 2014), a carboplatin analog under evaluation.

3

5
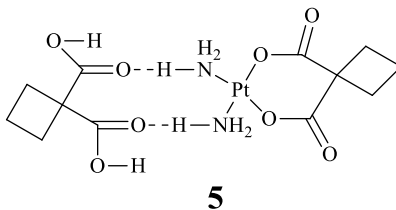
Oxaliplatin has three ligands, and the extra ligand slows down the rate of the molecule's aquation in the body, thus stabilizing it (Yu *et al.,* 2014). The LA-12 compound (**6**) is a platinum (IV) drug under clinical trial (Bouchal *et. al.,* 2011).

6
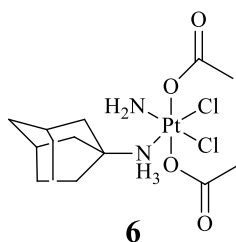
The chloro ligands of LA-12 undergo aquation for it to bind to DNA. Interestingly, this molecule's acetate groups are released in the biological system; the compound is reduced to platinum(II). Another drug under clinical examination is phenanthriplatin (**7**) (Kellinger *et al.,* 2013), 40 times more efficient than *cis*platin (Johnstone *et al.,* 2014).

7
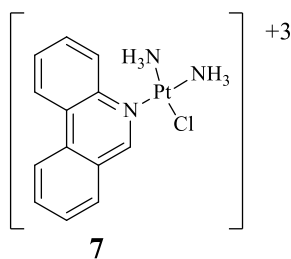
1.1.4 Thiophene-Based Platinum Thiosemicarbazone Complexes as the Future of Cancer Therapies

From the literature, it is clear that platinum-based drugs have superior biological properties, especially when treating cancer. As cancer becomes a global problem, platinum metal complexes to treat cancer could help reduce the cancer burden. Unfortunately, out of the thousands of newly synthesized platinum complexes, only a few make it to clinical trials because many are unstable (El-Saied *et al,* 2019). In addition, many complexes are only effective on specific cancer types,

hence the need to synthesize new compounds and test them for their anti-cancer properties to ease the cancer challenge.

While complexation plays a crucial role in developing drug molecules, the ligands used have a significant impact, such as the compound's stability. For instance, steric hindrance is desired when designing molecules for anti-cancer agents because it prevents unnecessary ligand substitution reactions (Kayed *et al.,* 2016). It allows improved selectivity when the compound is binding to DNA. That is why thiosemicarbazone ligands are the desired option when designing potential anti-cancer compounds.

Previous use of thiophene-based compounds in biological applications such as anti-cancer, anti-inflammatory, anti-anxiety, anti-mitotic, anti-psychotic, anti-fungal, anti-arrhythmic, and anti-microbial shows great success. Substituting the thiophene ring (**8**) with bulky substituents shows improved anti-proliferative activity (Oliveira *et al.,* 2015).

8
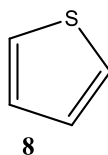
While substituting the thiophene ring on positions 2 and 3 has been widely studied, there is limited research on substitution on position 5, which requires some attention. Research by Mbugua *et al.* (2020) emphasizes the potential of using thiosemicarbazone ligands with a substituted thiophene ring as anticancer agents. From the study, the introduction of bromine to the thiophene ring showed better activity.

The high steric hindrance offered by thiosemicarbazone ligands, coupled with the anti-proliferative activity of thiophene and the success of platinum-based complexes, is likely to yield stable compounds to be used drug molecules. The use of thiophene-based thiosemicarbazone platinum complexes for anti-cancer application is yet to be well studied, despite showing great potential. That is what this study seeks to achieve.

1.2 Statement of the Problem

Coordination complexes have great potential for use as drug molecules, such as anticancer agents, with statistics showing that almost half of all cancer patients receive a platinum-based drug (Sava & Dyson, 2006). Although countless complexes have been synthesized, many are unstable. This has led to issues with resistance because the compounds undergo unnecessary ligand exchange reactions and do not reach the target cells in their intended state. The challenge has prevented the full utilization of metal complexes as medicinal agents.

Literature suggests that using bulky ligands increases steric hindrance and consequently reduces the ligand substitution reaction rate. In this case, the ease of displacing the ligands reduces significantly, and the compound can get to the target cells with minimal alterations. However, the use of bulky ligands has not been studied extensively.

Therefore, it is essential to synthesize new platinum complexes with better stability to make them more useful, particularly for biological applications. Thiosemicarbazone complexes could offer a suitable solution. TSC ligands are highly sterically hindered and good anti-cancer agents with anti-proliferative properties. Therefore, newly synthesized thiosemicarbazone platinum(II) complexes are likely to be stable enough for use as anticancer agents.

1.3 Objectives

1.3.1 General Objective

To synthesize and screen for the anti-cancer activities of novel platinum(II) thiosemicarbazone complexes.

1.3.2 Specific Objectives

1. To synthesize thiosemicarbazone ligands
2. To synthesize platinum(II) thiosemicarbazone complexes
3. To screen for the anti-cancer activities of the thiosemicarbazone ligands and their platinum complexes against HeLa, Caco-2, HT-29, and KMST-6 cell lines.

1.4 Justification and Significance of the Study

Cancer is a leading cause of death and it contributes to disease and economic burden globally. While chemotherapy is a desired approach to fighting the disease, multi-drug resistance and undesired side effects decrease its effectiveness.

Platinum complexes, such as thiosemicarbazone complexes, have shown potential as good anti-cancer agents. Since thiosemicarbazone ligands are bulky, they are unlikely to undergo unnecessary ligand exchange reactions. The steric hindrance TSC ligands exhibit may also increase their selectivity when used as drugs. Platinum(II) is suitable for biological applications because it is relatively inert and has a low ligand exchange rate. Therefore, when thiosemicarbazone platinum(II) complexes are introduced in a biological system, the ligands aren't replaced easily, which means that the drug is likely to get to the target cells in its intended state.

It is expected that this research will contribute to Universal Health care which is one of the big four agendas because of their medicinal application. Since the study contributes to cancer development, it will also enhance the achievement of good health and well-being, which is anchored in the Sustainable Development Goals (SDGs).

Research, innovation and scientific research is one of the sectors that Vision 2030 seeks to reform to achieve a prosperous nation and improve the quality of life. Therefore, this research will contribute positively to the achievement of innovation goals as stated in this plan

CHAPTER 2
LITERATURE REVIEW

2.1 Applications of Metal Complexes

Coordination complexes have been studied since 1798, with the first study being the Tassaert study (Jurca *et al*., 2017). Several advances have been made ever since in organic and inorganic chemistry on their synthesis, characterization, and applications. Complexes do not fit the typical valence theory because the overall ratios of the elements outdo their valences. The structural variety and many complexes have made it difficult to have a general classification criterion. However, attempts have been made to use criteria such as the number of central atoms, types of ligands, coordination number, and charge of the complex ion.

Nature has provided several metal complexes that are part of critical biological mechanisms such as transportation of oxygen in the blood, enzymatic reactions, photosynthesis, and coordination of metabolic processes. Some are bio-molecules (carboxylic acids, peptides, amino acids) while others have healing effects, such as antidepressants, diuretics, and antimicrobial because of the coordination of the metallic ions like Zn^{2+}, Fe^{2+}, Cu^{2+}, and Fe^{2+} (Kumble *et al.,* 2017). Hemoglobin (**9**) is an iron-porphyrin complex that transports oxygen from the lungs to body tissues.

9
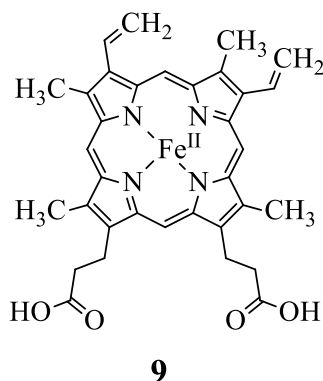
Chlorophyll is a Mg-porphyrin complex (**10**), and it is responsible for the green coloring in most plant leaves. It aids photosynthesis and is thus critical for survival.
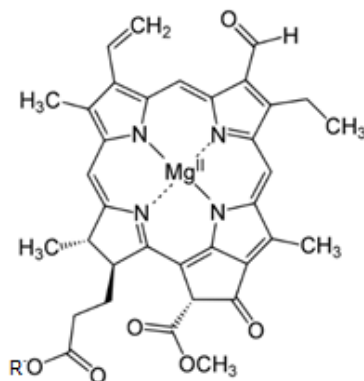
10

Coordination metal complexes have found use in many fields, one of them being catalysis, especially transition metals since they have varying oxidation states. An emerging study area on photo redox catalysts showed that triscyclomatalated homoleptic iridium(III) complexes could be applied (Njogu *et al.,* 2019). The study was on developing Ir (III) complex sensitizers that utilize solar energy sources. The focus was on homoleptic tris-C, N iridium complexes, with most efforts dedicated to the 2-phenyl-pyridine ligands. In this regard, (Njogu *et al.,* 2019) synthesized a new group of triscyclometalated Ir(III) complexes, in which the ligand was replaced by electron-donating methoxy or methyl groups. The complexes exhibited a long triplet lifetime of 1386 to 3692 ns and were strongly luminescent (588 to 610 nm). Therefore, the complexes can be used on equipment to conserve energy. One of the complexes (**11**) is shown below.
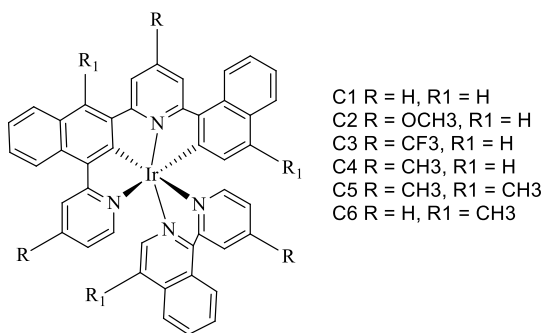
C1 R = H, R1 = H
C2 R = OCH3, R1 = H
C3 R = CF3, R1 = H
C4 R = CH3, R1 = H
C5 R = CH3, R1 = CH3
C6 R = H, R1 = CH3

11

Another application is the chemical sensing of environmental pollutants. Metal ions pose significant environmental pollution challenges because of their bio-accumulation and non-biodegradability. The need to develop highly selective and sensitive sensors is a priority to prevent the excessive accumulation of metal ions in the environment. The focus is on developing

detection techniques with a high affinity to the specific metal ions. An example of highly selective metal ion detectors is crown ether chelates developed by (Odhiambo *et al.,* 2018). Some of the ruthenium complexes were found to have an affinity towards Hg^{2+} and Cd^{2+}. Therefore, they could potentially be used to detect these heavy metals. Ru(bpy)$_2$-(1,10-Dioxa-4,7-dithiacyclobutaoctano[2,3-f][1,10]-phenanthroline)][PF6]$_2$ (**12**) is one of the complexes.
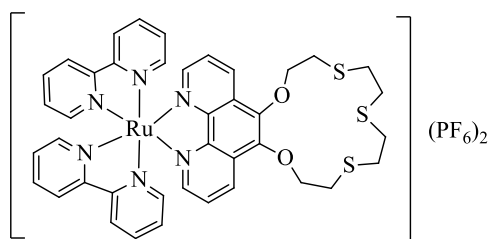
12

Another major use of metal complexes is for therapeutic purposes. Studies of metal ions and ligands showing biological, pathophysiological, and physiological properties have revealed that metal ions have great importance in biological functions (Jurca *et al.,* 2017). The use of ligands, chelates and complexes for biological applications is important because when introduced to living organisms like bacteria and viruses, they have been found to deprive them of macronutrients important for their survival (Jurca *et al*., 2017). With this regard, several coordination complexes have been utilized in medicine containing metals like gold (as auranofin) for rheumatoid arthritis, *cis*platin for anti-cancer, and rhenium in radiotherapy. (2,3,4,6-Tetra-*O*-acetyl-1-thio-β-L-glucopyranosato-κS1)(triethylphosphoranyliden)gold (**13**), trades as auranofin, and is used for rheumatoid arthritis. Lanthanum carbonate (**14**), which trades under the name Fosrenol, is a metal complex used as a phosphate binder in clinical practice. It is used mainly for patients with severe kidney ailments.
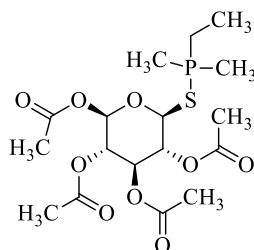
13
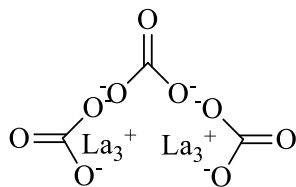
14

Biological activity has been shown to increase upon chelation because it makes the ligand a more powerful agent (Archibald & Smith, 2013). Metal complexes have emerged as a vital tool in drug discovery because they are widely used as therapeutic compounds to treat numerous human diseases like viral, bacterial, inflammatory, tumors, and neurological disorders (Abu-Surraha *et al.,* 2010).

2.2 Cancer

Over the past few decades, emphasis has been on increasing life expectancy, but cancer has been a significant impediment to this pursuit. The World Health Organization reported that cancer was the first or second leading cause of death in people under the age of 70 years in 112 countries, out of the 183 countries that were surveyed. That is a little over 60%, and that rate is quite alarming. While cancer is on the rise, other chronic lifestyle diseases like coronary heart disease and stroke are declining.

2.2.1 Cancer Statistics

The burden of cancer is increasing steadily all over the globe. Changes in the prevalence of the risk factors behind the causes of cancer and an ageing population are some of the forces behind this trend (Sung *et al.,* 2021). In 2020 alone, about 19.3 million new cases of cancer diagnosis and 10 million deaths were linked to cancer. Out of these figures, Africa accounts for 7.2 percent of the deaths and 5.7 percent of the new incidents. Europe has the highest figures, with 22.8 percent of the total new cases and 19.6 percent of the cancer deaths, even though the region represents only 9.7 percent of the global population (Sung *et al.,* 2021). In America, the incidence rate is 20.9 percent, while the mortality rate is 14.2 percent. Asia accounts for 58 percent of the mortalities and 49.3 percent of the new cases.

Lung cancer remains the leading cause of mortalities, as lung tumors cause about 1.8 million deaths (18%). Colorectal cancer follows with about 9.4 percent of all deaths resulting from cancer in 2020. Liver cancer was responsible for 8.3 percent of mortalities, while stomach and breast cancer was responsible for 7.7 percent and 6.9 percent of all deaths that year (Ferlay *et al.,* 2021). In Kenya, cancer is the third largest cause of death; after infectious diseases and cardiovascular ailments. These statistics prove that the global cancer burden is increasing globally, and the effects are an adverse physical, financial, and emotional strain on the patients and their families. Therefore, it is paramount that researchers look for suitable ways of solving this global challenge.

2.2.2 Cancer drug resistance

Despite the availability of over 60 different chemotherapy drug agents, drug resistance remains a serious challenge, especially in the systemic treatment of cancer. Only a few cancer types are susceptible to the curative agents, including some hematological malignancies, several pediatric tumors, and testicular germ cell tumors (Parkin *et al.,* 2021). Many adult epithelial cancers are not as curable, and many of them are diagnosed in their advanced stages (Ward *et al.,* 2021). Even as advances continue to be made to find better curative agents, the problem of drug resistance is still a considerable barrier to the realization of these therapies.

Medically speaking, resistance is categorized into two, where there is acquired resistance and intrinsic resistance. In acquired resistance, the tumor is initially sensitive to treatment, but it shows increasing unresponsiveness to the same therapy used to treat the malignancy initially (Goldie, 2001). This is one of the biggest challenges with cancer drugs, but the same trend is also observable in antibiotics by pathogenic microorganisms. Intrinsic resistance is the state where cancer shows minimal or low sensitivity to chemotherapeutic drugs. In this case, the malignancy had not been exposed to the agent before, so it rejects the drug on the first attempt.

Acquired resistance seems to originate from random mutations that occur over the evolution of the malignant DNA. Sometimes, the tumor may be treated with a higher dose or increased duration, but this depends on the type of mutation and cancer itself. Sometimes, the drug causes this mutation to happen (Chaturvedi *et al.,* 2017). Further research on how this occurs

biologically needs to be undertaken to be able to exclude such cases. Clinically, some cases of drug resistance happen very quickly, such that one may assume that this is an induced event.

Some of the clinical interventions under development to control cancer drug resistance include personalized medicine (Pitt *et al.,* 2016). Thanks to the readily available genetic information through gene sequencing, scientists can access a patient's genetic data and tailor small molecule drugs like *cis*platin to brain metastasis. Another technique is to use alternative or additional active pathways. This is because some tumours minimize the uptake of a cancer drug molecule, which has been found to reduce the drug's effectiveness and increase resistance. Although many of the solutions to cancer drug resistance control are from a clinical perspective, scientists need to improve the drugs from the development stage to curb resistance challenges.

2.3 The Use of Platinum Compounds in Cancer Treatment

Several cancer treatments exist and are given subject to the nature of cancer and how advanced it is. While some people will have only one treatment, others are subjected to a combination of methods (Jurca *et al*., 2017). One of them is surgery, where the doctor removes the tumor from the body. Another one is radiation therapy that utilizes radiation to reduce the tumor or get rid of it completely. Sometimes doctors recommend immunotherapy treatment, which involves the empowering of the immune system to fight cancerous cells (Shimada *et al.,* 2013). There is also hormone therapy that is commonly used to treat prostate and breast cancers. Recently, stem cell transplant has been introduced as a cancer treatment method that restores the blood-creating stem cells in people whose stem cells have been destroyed by chemotherapy or radiation treatment (Ndagi *et al.,* 2017).

Chemotherapy is a standard method of cancer treatment. Essentially, chemotherapy (chemo) refers to the use of drugs to treat an illness (Shimada *et al.,* 2013). Chemotherapy is a systemic treatment in that the drug travels throughout the body and kills cells that have metastasized in other body parts besides where the primary tumour was at. That characteristic makes chemo a unique method, unlike radiation and surgery that only focus on one body part. There are three main goals of chemotherapy: control, cure, or palliation purposes.

Although many drug molecules are organic, metals are critical therapeutic applications. Their study dates back to more than 5,000 years ago (Pan *et al,* 2014). The modern organometallic complex for pharmaceutical use was pioneered by Kopf and Maier in the early 1970s (Dasari & Tchounwou 2014). They researched how transition metal complexes could be used as anti-cancer compounds. Their research led to the introduction of *cis*platin (**1**) to oncology. Before this discovery, scientists had challenges distinguishing between therapeutic and toxic doses (Dasari & Tchounwou 2014). Therefore, the introduction of *cis*platin was a breakthrough in cancer treatment. *Cis*platin has been a benchmark for cancer chemotherapy since its discovery. *Cis*platin is particularly important in treating testicular cancer. Several *cis*platin analogues have been synthesized and used in anti-cancer treatment (Motswainyana *et al.,* 2012).

The isomer of *cis*platin (*trans*platin) (**15**) is inactive against anti-cancer.

15
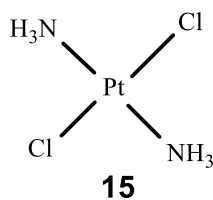
Its inactivity is because of the trans effect, defined as the labilization (making it more reactive) of the ligand that is trans to another ligand, known as the trans-directing ligand. Trans effect is caused by electronic effects and is common in square planar complexes but may at times be observed in tetrahedral complexes (Corint *et al.,* 2017). Therefore, *trans*platin is more stable than *cis*platin, and more energy is needed to remove the chlorine atoms in *trans*platin than what is required for *cis*platin. Also, the N-Pt-N angle in the *cis* form is lower than that in the Trans form, which means that *cis*platin can react readily with DNA than *trans*platin.

The activity of metal complexes relies heavily on particular interactions with DNA, which causes the ultimate destruction and death of the cancerous cells (Jurca *et al.,* 2017). Before reacting with the DNA, complexes usually undergo ligand exchange reactions, where one or more labile ligand is exchanged with a biomolecule. When *cis*platin enters biological systems, it might experience an unexpected ligand exchange reaction, where Sulphur-containing bioligands like cysteine replace the amino ligands (Mbugua *et al.,* 2020). When this happens, the nature of the drug

molecule is completely altered, and it cannot function as it should. This is what causes the resistance experienced by some patients when they take *cis*platin to treat cancer (Motswainyana *et al.,* 2012).

2.3.1 The Development of *Cis*platin Analogs

The development of inorganic compounds for cancer treatment has advanced widely, and today, it encompasses a variety of metals and ligands. Some complexes have been found to have better activity than conventional *cis*platin. Although *cis*platin faces resistance challenges, its development led to the discovery of other metal complexes as cancer therapies. Almost half of all cancer patients receive a platinum-based drug (Sava & Dyson, 2006). It led to a generation of platinum drugs known as the 'platins,' which have two types of ligands attached to the central platinum cation. They are the labile chloride or carboxylate ligands and amine carriers (Dasari & Tchounwou, 2014). All the platin molecules act as prodrugs in that they must undergo aquation of their labile ligands within the target cancer cells for them to bind with the N7 atom on adenosine and guanine bases. When this binding occurs, it prevents DNA transcription and replication, which results in cellular apoptosis (Zalba & Garrido, 2013).

One of the second-generation platin drugs to be produced after *cis*platin was nedaplatin (*cis*-diamine-glycolatoplatinum) (**2**). It has similar amine carrier ligands as *cis*platin, but the leaving group is bulkier, consisting of a five-membered ring compound, where the glycolate binds to the platinum ion as a bidentate ligand (Shimada *et al.,* 2013). The mode of action of nedaplatin as a drug is to react with nucleosides in the body to create a nucleoside-platinum complex, which is quite similar to how *cis*platin works. Biological studies have confirmed that the bases that form after nedaplatin reacts with bases in the body are similar to what is produced by *cis*platin. Once nedaplatin is taken up by the cells, its glycolate portion is cleaved by hydrolysis. It thus forms an active species, which interconverts between a sequence of other active species, all of which are in equilibrium (Niioka *et al.,* 2007). This mechanism is similar to that of *cis*platin because it inhibits DNA duplication. However, nedaplatin has a relatively short elimination half-life, ranging between 1.1 and 4.4 hours. Nedaplatin is used to treat non-small cell lung cancer, uterine cancer, head & neck cancer, cervical cancer, and urothelial cancer.

Another second-generation drug from *cis*platin was the carboplatin [diammine(1,1-cyclobutanedicarboxylato) platinum(II)] (**3**), which is very promising and has better chemical stability than *cis*platin. Its good chemical stability explains its reduced reactivity with nucleophilic DNA sites (Kellinger *et al.,* 2013). That is why a higher dose is needed to give the same antitumor effect of *cis*platin. It also has a lower reactivity with proteins, which explains why it is not as nephrotoxic as nedaplatin and *cis*platin. That is why the success rate of treating ovarian cancer and small cell lung cancer has been higher when using carboplatin as opposed to *cis*platin (Zalba & Garrido, 2013).

The second generation of *cis*platin drugs was oxaliplatin, which is a coordination compound consisting of platinum and diaminocylohexane (DACH) ligand. Since oxaliplatin has bulky ligands, it has a high steric hindrance and is very stable. (Lévi *et al.,* 2012). The DACH ligand plays a crucial role in inhibiting DNA duplication of the cancerous cells, preventing cross-resistance, as observed in *cis*platin. Since oxaliplatin is highly lipophilic, it easily crosses the cellular membrane, and its distribution half-life is between 10 and 25 minutes upon administration. (Graham *et al.,* 2004). Its prolonged stability makes it possible for continuous infusions of up to five days. The drug is used as a combination therapy with other chemotherapeutic agents in the treatment of non-small cell lung cancer and lung cancer. From studies, oxaliplatin (**4**) has a more promising safety profile than *cis*platin, and has shown positive effects in patients who could not tolerate *cis*platin previously.

From the three platinum-based chemotherapeutic drugs discussed above, it is evident that the choice of ligands leans towards the bulkier side. From *cis*platin to nedaplatin, the chloride ligands in the former are replaced by a five-membered ring structure, which bears better anti-cancer activity. The five-membered ring is enhanced further with a bulkier ligand, and the new molecule has better anti-cancer activity than nedaplatin. In the case of oxaliplatin, the amine ligands are replaced with diaminocylohexane, which has a high steric hindrance and better stability than its predecessors. This is because bulky ligands have a more significant steric hindrance, which prevents unnecessary ligand exchange reactions in the body by sulphur, abundant in biological systems. Therefore, in developing new drug molecules, the focus should

be on stabilizing the metal center by coordinating it with bulky ligands. From the activity of previously synthesized molecules, stabilizing the metal center results in lower resistance and decreased side effects.

2.3.2 Chiral platinum complexes

The biological activities of chiral compounds have attracted great interest because they are highly selective and specific when used as chemotherapeutic drugs (Ndagi *et al.,* 2017. Since *cis*platin and its analogues have had significant challenges, especially with high toxicity levels, it has become necessary to approach drug design from the angle of chirality. A potentially positive solution is the use of metal-drug synergism. This is attained by combining a metal-based complex with a known active organic compound. The DNA structure and other biomolecules in the body can be probed using chiral metallic complexes. That way, the biological activities are considerably influenced by the chiral molecules existing in the system. Research by Ellena *et al*. (2015) involving chiral platinum complexes surveyed the DNA binding properties of platinum complexes combined with the chemical properties of chloroquine and phosphine. The phosphine and chloroquine platinum(II) complexes had lower biological activity, high affinity for blood plasma protein and high DNA interaction. Since the compounds have a high affinity to protein, the effect of DNA is reduced substantially, and consequently, the cytotoxic effect is also minimized. For this method to work, there is a need to reduce or eliminate the plasma binding of the compounds to improve their DNA interactions and eventually make them better anti-cancer agents. Otherwise, this method is not a sustainable chemotherapy treatment in its current state. Therefore, chiral platinum complexes have not shown much positive progress for them to be introduced as potential anti-cancer agents.

2.3.4 New Platinum Drugs Under Pre-Clinical Development and Clinical Trials

New platin drugs continue to be developed because this class of compounds has depicted unlimited potential in cancer therapy. One of them is dicyloplatin (**5**), a carboplatin analogue, currently under clinical trial evaluation in China (Yu *et al.,* 2014). The formulation consists of an additional carboxylate ligand that is hydrogen-bonded to the drug while in solid-state. When the drug is dissolved in water, the extra ligand slows down the rate of the drug's aquation, thus making the molecule more stable. The first human trials of dicyloplatin (**5**) were completed in

2003, and the reported safety profiles were very close to those of carboplatin (Liu *et al.,* 2014). The study was a double-blinded trial comparing dicyloplatin (**5**) and carboplatin, and the results show no significant differences between the two.

Another platinum-based drug under clinical trial is phenanthriplatin (**7**) by Blend Therapeutics in the USA (Johnstone *et al.,* 2014). It is based on *cis*platin's structure, but one chloro ligand in *cis*platin has been replaced with phenanthridine. Since the compound has only one labile ligand, it can only form monofunctional adducts with DNA (Kellinger *et al.,* 2013). Therefore, the drug alters the DNA structure to a relatively low scope compared to *cis*platin. While this modification may be expected to affect the compound's activity negatively, it is still significantly effective in obstructing the action of RNA polymerase II by inhibiting the DNA transcript. As determined by the National Cancer Institute, phenathriplatin is 40 times more effective than *cis*platin, and it has a high cellular uptake (Johnstone *et al.,* 2014). Therefore, phenathriplatin has the potential as a viable anti-cancer therapy.

The LA-12 is a platinum (IV)- based compound (**6**), whose mode of action is an intracellular reduction to platinum(II) by ascorbate and glutathione. The chloride ligands must also undergo aquation before the drug molecule can bind DNA (Wexselblatt & Gibson, 2012). LA-12 is active because of the lipophilic ligands. The adamantylamine carrier ligand is similar to memantine, an already approved drug for Alzheimer's disease (Kozubík *et al.,* 2005). The axial acetate groups of the LA-12 are released when the platinum (IV) is reduced to platinum(II). Although the drug is reported to be in clinical trials, the researchers are yet to release published data from phase I or phase II of the study. The only available findings are those comparing serum protein binding in animal models to samples extracted from patients (Bouchal *et al.,* 2011). Once LA-12 (**20**) passes all the clinical trials successfully, it will likely impact cancer treatment significantly.

The compounds discussed above that are under clinical trials are all platinum derivatives, implying that the potential for platinum-based drugs is endless. As long as scientists can get rid of the resistance challenge that the current platinum drugs face, they can contribute significantly to the treatment of various cancer types. From the molecules that are already under clinical trials, it is evident that the solubility of drug molecules plays a critical role in a drug's efficiency. LA-

12 and dicyloplatin undergo aquation when they enter biological systems, facilitating their binding to DNA molecules more quickly.

2.4 Thiophene-based Compounds and their Applications

Heterocyclic compounds are essential in medicinal chemistry and organic chemistry because of their diverse biological functions. Sulphur, nitrogen, and oxygen-containing heterocyclic compounds are vital to medicinal research because of their varied pharmacological profiles (Zhao *et al.,* 2019). One such heterocycle – thiophene – is a five-membered ring with sulphur heteroatom.

With a molecular mass of 84.14 g/mol and a 1.051 g/mL density, thiophene is soluble in most organic solvents. The electron pairs on the thiophene sulphur are delocalized in the pi-electron system, increasing its reactivity, almost to a benzene derivative (Shah & Verma, 2018). Therefore, it can be easily sulfonated, halogenated, acylated, and nitrated. It can also undergo coupling diazonium salts formation and reamer-Tiemann reaction. Thiophene's heat of combustion is 22 to 28 K.Cal.mol, which is somehow less than the resonance energy of benzene. Thiophene is considered aromatic based on these properties, as it also obeys the $4n + 2$ π electron rule. The ability of thiophene to be sulphonated makes it suitable for use in biological applications because it can quickly be introduced in human cells. However, unlike most sulphides, thiophene does not undergo oxidation, making their derivatives relatively stable to oxygen.

Thiophene-based compounds feature in various applications, including anti-cancer, anti-inflammatory, anti-anxiety, anti-mitotic, anti-psychotic, anti-fungal, anti-arrhythmic, and anti-microbial. The world's population is increasing steadily, and health concerns are rising at an alarming rate (Archna *et al.,* 2020). That is why scientists need to discover and design new drug molecules with the potential for treating these concerns. Thiophene-based molecules are likely to offer solutions to the cancer challenge because of their universal synthetic applicability and biological activity to help medicinal chemists design and device new strategies to discover better drugs.

2.4.1 Thiophene Derivatives as Anticancer Agents

Several thiophene derivatives with diverse substitutions, such as mono-substitution, di-substitution and tri-substitution, have found significant application as anti-cancer compounds. Many of the mono-substituted compounds reported so far are at the 2nd and 3rd positions. Some of the compounds reported by (Saad *et al.,* 2011) possessed significant cytotoxicity against a range of cancer cell lines. The anti-proliferative potential of the compounds was attributed to the presence of the thioether and thiol groups of these compounds. The compound (**16**) was the most potent against HCT-116 cancer cell line.

16
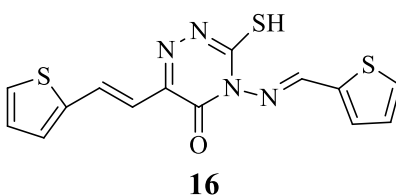
(Oliveira *et al.,* 2015) developed thiophene-2-thiosemicarbazones and screened them against nine cancer cells, including MCF-7, U251, PC-3, NCI-H460, NCIADR/RES, HT-29, and 786-0. Although some of the unsubstituted compounds had remarkable selectivity to K-562 cell lines, introducing an alkyl group to the aromatic ring increased the cytostatic effect against leukemia. Introducing a phenyl ring was also crucial for activity, while substituting a 1-naphthyl ring or 3-pyridyl ring showed better anti-proliferative effects. Their findings indicate that thiophene-based thiosemicarbazones are a promising class of anti-cancer therapies. The compound (**17**) is a substituted thiophene-2-thiosemicarbazone with good anti-proliferative effects.

17
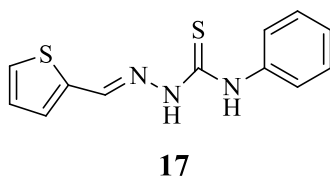
2.5 Thiosemicarbazone Ligands and Complexes

Thiosemicarbazones are Schiff bases, which are synthesized by condensation reactions between amines and aldehydes or ketones. The ligands have a broad biological application. In the solution form, thiosemicarbazones are in an equilibrium mixture of thione and thiol, as shown in Figure 2.1. The thione is a neutral bidentate ligand, transforming to the thiol form when it loses a

proton. Although thiosemicarbazone complexes can be positively charged, negatively charged or neutral, most studies have considered the neutral form
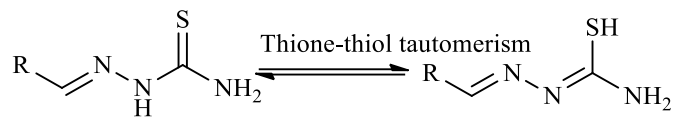
Figure 2.1: Thione-thiol tautomerism of thiosemicarbazones

Thiosemicarbazone complexes have been found to dominate a large share of transition metal complexes, which echoes the importance of sulphur coordination based on its acid-soft base preference.

The thione tautomer is a neutral bidentate ligand (**18**).

18
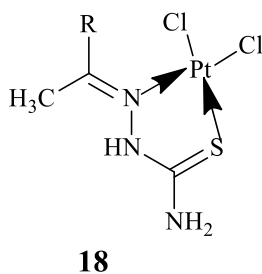
The thiol tautomer forms complex by proton loss (**19**).

19
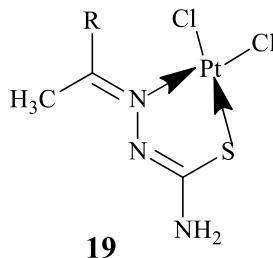
If additional binding sites are adjacent to the S-N donor system, the ligand behaves like a tridentate species (**20**).
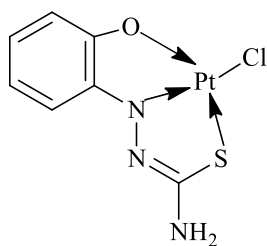
20

In many instances, the third coordinating species will be in the form of an aldehyde moiety or ketonic. The presence of a third coordinating species may result in the formation of polymeric species or might change the coordinating environment of the metal ion. The changes that take place might affect the biological properties of a compound.

The stereochemistry of the thiosemicarbazones relies on the additional coordination sites on the structure and the charge. This affects the thiol-thione equilibrium in the reaction medium. The equilibrium and nature of the complexation of the thione-thiol structure depend on the pH of the solvents used.

When coordinating to a metal ion, thiosemicarbazones are in the Z-form, such as (*1R,5S*)-*N'*-((*Z*)-1-(3-methylpyrazin-2-yl)ethylidene)-3-azabicyclo[3.3.2]decane-3-carbothiohydrazide (**21**).
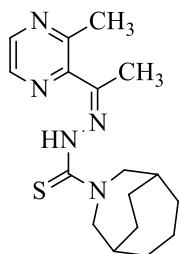
21

This may result in chelation and consequently increased stability because of improved electron delocalization in the chelated ring system. That is what is responsible for the coordination with the metal center. Thiosemicarbazones usually act as neutral bidentate ligands, thus resulting in the formation of square planar and octahedral geometrics. Their derivatives show increased

22

biological activity, antitumor, and antimalarial properties. Studies show that the ligand's stereochemistry relies on the substituent's steric effects in the thiosemicarbazones structure.

2.5.1 Applications of Thiosemicarbazone Ligands and Complexes

Thiosemicarbazone ligands and complexes can be applied to medicinal and catalysis, among other industries (Netalkar *et al.,* 2015). One of the applications of thiosemicarbazone ligands and complexes is in environmental pollution control. Ecological protection is directly proportional to the sustainable economics and development in a society. The management of significant pollutants in the air, land and water remains a challenge worldwide. Atmospheric pollutants like NO_x, volatile organic compounds, and carbon monoxide originating from transport vehicles and industrial activities pose severe health effects. Catalysis is among the most effective and economically viable methods of controlling environmental pollution. In the past, catalysts have been developed for pollution control. At the moment, numerous transition metals have been reported to have a positive correlation with NOx reduction. Some of the well-known catalysts are TiO_2-supported V_2O_5, Fe_2O_3, CuO, MnO_x, and CeO_x. While the use of thiosemicarbazone complexes in catalysis has not been explored thoroughly, significant developments have been made. For instance, (Nabil *et al.,* 2012) developed a TSC copper complex (**22**) used as a catalyst.
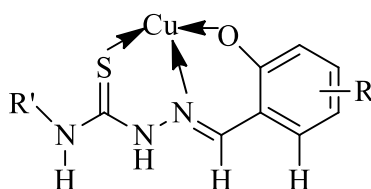
22

2.5.2 The Use of Thiosemicarbazone ligands and Complexes in Cancer Treatment

Metal thiosemicarbazone complexes are emerging as a new class of anticancer therapies because they show inhibitory activities against cancer (Prajapati & Patel, 2019). Since thiosemicarbazone complexes have both sulphur and nitrogen as donor ligands, notable biological activities are observed. Their biological activity also depends on the non-coordinating groups since some of the thiosemicarbazone complexes have additional functional groups that are not coordinated by the "primary" metal ion. The role of thiosemicarbazone complexes in cancer treatment is based on the fact that they act as ion chelators; thus, they interfere with DNA synthesis and prevent its production (El-Saied *et al*., 2019).

Serda and his group designed two new thiosemicarbazone compounds for anti-cancer application (Serda *et al.,* 2014). They did so by combining the active moieties of known potency; thiosemicarbazone bioeffectors and quinolone. The ligand is known as 2,2'-(7-amino-2-methyl quinoline-5,8-diyl)bis(*N*-methylhydrazine-1-carbothioamide) (**23**). They were found to have notable effects against HCT 116 cancer cells.
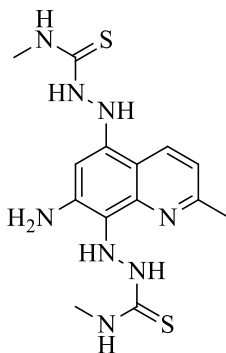
23

Subasi *et al.* (2019) also synthesized a thiosemicarbazone-functionalized organoruthenium(II)-arene complex (**24**). The complex was found active against colorectal cancer.
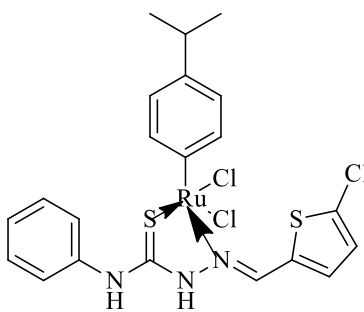
24

Transitional metal complexes with nitrogen-donor groups have been under continuous survey because of their interesting biological applications, especially anti-tumour applications, in search of more selective and less toxic drugs (Abu-Surraha *et al.*, 2010). One of the exciting facts have to do with how ligands govern the metal ions' reactivity and the shared effects that the metal ions have on the ligands.

24

Of great importance are square planar complexes that mimic *cis*platin. Square planar complexes are vital in cancer treatment because they minimize deactivation levels by thiol-containing compounds in biological systems without interfering with DNA binding (Motswainyana *et al.,* 2012). Bidentate ligands are essential in averting trans-labilization and the undesirable ligand displacement by nitrogen and Sulphur- containing bioligands.

2.6 Synthesis of thiosemicarbazone ligands and their complexes

Thiosemicarbazone derivatives are a vital class of organic compounds because of their diverse synthesis and pharmaceutical, medicinal and biological applications. Previous research has found them useful as antifungal, antibacterial, antitumor, anticancer, anti-inflammatory, anti-diabetic, herbicidal, and anti-proliferative agents. Thanks to the versatility of thiosemicarbazone ligands, they show better coordination tendency, stability and selectivity towards various metal ions. They also adopt many coordination modes with the different metals. Heterocyclic TSCs have been cited as critical medicinal agents because they quickly diffuse via semipermeable membranes of cell lines. How TSC ligands coordinate to metal ions has also been found useful in enhancing their activity and minimizing the side effects of the ligands when used for medicinal applications. So far, a significant amount of data has been published regarding the development of metal-TSC synthesis, characterization and their applications. This section reviews some of the synthetic, characterization, analytical and biological applications of thiosemicarbazone complexes. Thiosemicarbazones can coordinate both in deprotonated and neutral forms (Prajapati & Patel, 2019). Therefore, it is possible to have deprotonated and neutral TSC derivatives in a complex. From the review, researchers have opted to use reflux reactions when synthesizing the ligands and their complexes.

(El-Saied *et al.,* 2019) synthesized new coordination complexes with the potential for biological applications. They used isatin-N(4)anti-pyrinethiosemicarbazone ligand with iron, zinc, copper, nickel and cobalt ions. The complexes were further evaluated for their anti-cancer properties. The complexes were stable at room temperature and non-hygroscopic. However, they were insoluble in water and most organic solvents, but they were entirely soluble in DMF and DMSO. Some of the complexes did not show any signal analogous to the N-N(2)H of thiosemicarbazone, suggesting they had coordinated to the metal center by proton loss. The characteristic of the

νC=N bands of the isatin molecule shifted to lower wave numbers, indicating the involvement of the C=N moiety in coordination; via the nitrogen atom. This was the case for all the complexes. The IR spectra of some of the metal complexes corresponding to the C=O moiety of isatin were observed at lower wavenumbers than the ligands. This confirmed that coordination may have involved the carbonyl oxygen atom. The νC=S bands appear at lower wavenumbers, indicating the participation of the C=S group in coordination in all the complexes. Two of the complexes comprised two ligand molecules binding to one metal center, and the IR showed that the two ligands had different binding modes. The nickel(II) complexes were paramagnetic, which confirmed the absence of square planar configuration. They displayed magnetic moments at 2.98 and 3.06 BM, which are attributed to the two unpaired electrons. This suggests that there are other geometries besides square planar.

Nyawade *et al.* (2020) synthesized new TSC complexes to be used as anti-cancer agents. They observed that since the TSCs ligands exist as thione-thiol tautomers, they could coordinate to the metal center as neutral or anionic forms resulting from the loss of a proton. They also noted that the biological activities of thiosemicarbazones was dependent on the parent ketone or aldehyde and the metal ion used in complexation. Because of the presence of a thioamine functional group on thiosemicarbazone ligands, they can exhibit thione-thiol tautomeric forms. The S-H vibration observed between 2600 and 2500 cm^{-1} confirmed that the thione firm was predominant in the synthesized ligands. A proton signal associated with -SH protons at 4.00 ppm was absent in the ^{1}HNMR, which shows that the thione-thiol tautomerism exists even in polar solvents like DMSO. The tautomerism was further confirmed from the XRD data. Thiosemicarbazones can also exist in E and Z isomers in the solutions. The ^{1}H NMR signals attributed to N-NH signals of Z isomers exist in the range of 14.00 to 15.00 ppm, while those of the E isomers occur between 9.00 and 12.00 ppm. The ligands, in this case, were observed between 10.32 and 10.24 ppm, confirming that they exist as E isomers in the DMSO solution. Carbon signals representing C=N are observed between 142.5 ppm and 44.5 ppm. The C=S signals are between 177.9 ppm and 178.9 ppm, which confirms the existence of the ligands in the thione tautomer. The characterization results showed that the ligands exist in the E form of the thione.

Mbugua *et al.* (2020) synthesized thiosemicarbazone ligands with a substituted thiophene ring as anticancer agents. The ligand with an unsubstituted ring had the highest frequencies for the imine band. On introducing bromine to the thiophene ring, the frequency was lowered because its electron-withdrawing effect raises the single bond character.

When the bromine was at position 5, the ligand had a lower frequency shift than on position 4. This showed a possible resonance donation from the lone pair of nonbonding electrons that increased electron density. The azomethine for palladium complexes had higher energy than for platinum complexes. This could be because platinum has a higher nuclear charge, meaning that the ligand would be more attracted to platinum than to palladium. This causes the azomethine region to have a single bond character and a lower electron density than palladium complexes. The bond dissociation energies for the metal-ligand bond are higher in platinum than palladium because of the lower steric crowding around the Pt metal center. In NMR analysis, the azomethine proton in the complex occurred 8.25 ppm compared to 7.13, 7.45 and 7.65 in the ligands. The azomethine protons on the complex with bromine on position 4 appeared further downfield, at 7.53 and 7.75 ppm. This was because of the deshielding effect of bromine. The complex with bromine at position five showed an upfield shift of the azomethine proton to 8.16 ppm because there is resonance at position five. For the electronic spectra of the compounds, the ligand with bromine at position 5 had a higher bathochromic shift of 7 nm than the one with bromine at position four with a shift of 3nm. At position five, there is better p-π conjugation with the entire pi system from the likely donation of the lone pair on bromine.

CHAPTER 3
MATERIALS AND METHODS

3.1 Chemicals

The chemicals used in this research were of analytical grade and were purchased from Sigma Aldrich South Africa. The reagents used were K_2PtCl_4 (98%), 5-nitrothiophene-2-carbaldehyde (98%), 5-ethyl-2-thiophenecarboxyaldehyde (98%), 2, 2′-Bithiophene-5-carboxaldehyde (98%), 5′-Bromo-2,2′-bithiophene-5 carboxaldehyde (97%), 2-Methyl-3-thiosemicarbazide (97%), 4-Ethyl-3-thiosemicarbazide (97%), 4,4'-dimethyl-3-thiosemicarbazide (98%), 4-phenylthiosemicarbazide (99%), 4-methyl-3-thiosemicarbazide (97%). The solvents used for the experimental procedures were: dichloromethane, *n*-hexane, methanol, dimethyl sulfoxide, acetone, acetonitrile, and dimethylformamide. All solvents used in the reactions were dried following their respective drying techniques and stored under activated molecular sieves to maintain their purity. Methanol was dried using magnesium and calcium oxide; *n*-hexane was dried under sodium wire with benzophenone as the indicator; dichloromethane was dried using calcium chloride.

3.2 Equipment

The equipment used in this study were Parkin Etmer FTIR spectrometer/Spectrum-two for obtaining the FTIR spectra, GBC UV-VIS 920 for obtaining UV-Vis data, Bruker Asend TM 400MHz Advance III HD NMR Spectrophotometer equipped with 5 mm BBI probe at 298K, and standard 1D and 2D NMR pulse frequencies for acquiring NMR spectra in deuterated solvents, Server 112 Series Elemental Analyzer for acquiring C, H, N, S data, SMP10 melting point apparatus using open capillaries for analyzing melting points of the compounds, and Bruker SMART CCD APEXII diffractometer with graphite monochromated Mo Kαradiation (k = 0.71073 Å) for acquiring single-crystal structure for **L2**.

3.3 Synthesis of Thiosemicarbazone Ligands (L1-L4)

Four thiosemicarbazone ligands were synthesized by standard condensation reactions of thiosemicarbazides and aldehydes, as described by (Mbugua *et al.,* 2020). All reactions were carried out under an inert atmosphere using a standard schlenk line with a dual vacuum/nitrogen channel. Magnetic stirrers were used for all reactions. The yields were calculated using the formula:

$$\frac{\textit{moles of the product}}{\textit{moles of the starting material}} \times 100$$

3.3.1 Synthesis of 2-((5-ethylthiophen-2-yl)methylene-*N*-phenylhydrazinecarbothiomide (L1)

A mass of 0.0836g (0.5 mmol) of 4- phenyl thiosemicarbazide was dissolved in 15mL methanol and stirred for ten minutes. A mass of 0.0701g (0.5 mmol) of 5-ethyl-2-thiophenecarboxyaldehyde was dissolved in 15 mL methanol and stirred for ten minutes. The 4-phenyl thiosemicarbazide in the MeOH mixture was added into the 5-ethyl-2-thiophenecarboxyaldehyde in the MeOH mixture dropwise and stirred for ten minutes. The reaction mixture was heated at 60^OC under reflux for 4 hours. After that, the solvent was removed under reduced pressure under nitrogen, and the product was re-crystallized from dichloromethane and *n*-hexane.

The Scheme 3.1 below represents the synthesis of **L1**.
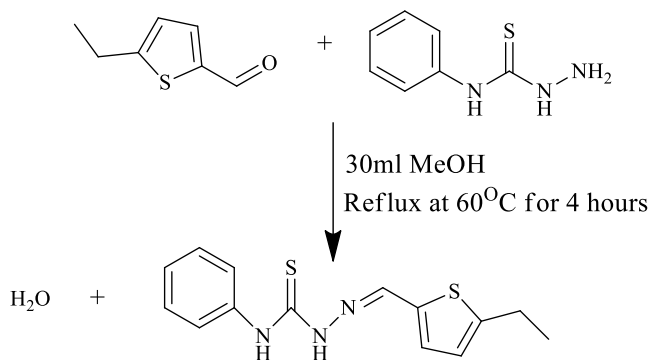
Scheme 3.1: Synthesis of **L1**

3.3.2 Synthesis of 2-((5-ethylthiophene-2-yl) methylene)-1-methylhydrazine carbothiomide (L2)

A mass of 0.1051 g (1.0 mmol) of 2-methyl-3-thiosemicarbazide was dissolved in 15 mL methanol and stirred for ten minutes. A mass of 0.1420 g (0.5 mmol) of 5-ethyl-2-thiophene carboxyaldehyde was dissolved in 15 mL methanol and stirred for ten minutes. The 2-methyl-3-thiosemicarbazide in the MeOH mixture was added into the 5-ethyl-2-thiophene

carboxyaldehyde in the MeOH mixture dropwise and stirred for ten minutes. The reaction mixture was heated at 60^OC under reflux for 6 hours. After that, the solvent was removed under reduced pressure under nitrogen and a precipitate was obtained. This was re-crystallized from DCM and *n*-hexane.

The Scheme 3.2 below represents the synthesis of **L2**.
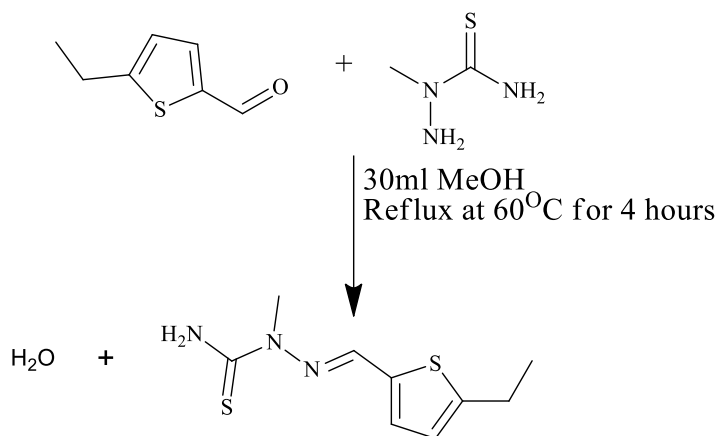
Scheme 3.2: Synthesis of **L2**

3.3.3 Synthesis of *N,N*–dimethyl–2-((4-nitrophene-2-yl)methylene)hydrazinecarbothiomide (L3)

A mass of 0.0596 g of 4,4'-dimethyl-3-thiosemicarbazide was dissolved in 15 mL methanol and stirred for ten minutes. A mass of 0.0785g (0.5 mmol) of 5-nitro-2-thiophene carboxyaldehyde was dissolved in 15 mL methanol and stirred for ten minutes. The 4,4'-dimethyl-3-thiosemicarbazide in MeOH mixture was added into the 5-nitro-2-thiophene carboxyaldehyde in MeOH mixture drop wise and stirred for ten minutes. The reaction mixture was heated at 60^OC under reflux for 4 hours. After that, the solvent was removed under reduced pressure while under nitrogen and the product was re-crystallized from dichloromethane and *n*-hexane.

The Scheme 3.3 below represents the synthesis of **L3**.
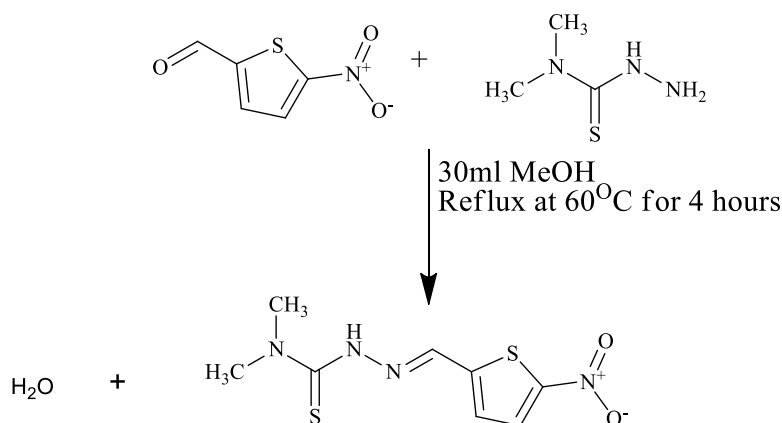
Scheme 3.3: Synthesis of **L3**

3.3.4 Synthesis of 2-([2,2'-bithiophen]-5-ylmethylene-1-methylhydrazinecarbothiomide (L4)

A mass of 0.1352 g (1.2 mmol) of 2-methyl-3-thiosemicarbazide was dissolved in 15 mL methanol and stirred for ten minutes. A mass of 0.2500 g (1.2 mmol) of 2,2'-bithiophene-5-carboxyaldehyde was dissolved in 15 mL methanol and stirred for ten minutes. The 2-methyl-3-thiosemicarbazide in MeOH mixture was added into the 2,2'-bithiophene-5-carboxyaldehyde in MeOH mixture drop wise and stirred for ten minutes. The reaction mixture was heated at 60°C under reflux for 4 hours. After that, the solvent was removed under reduced pressure under nitrogen, and the product was re-crystallized from DCM and *n*-hexane.

The Scheme 3.4 below represents the synthesis of **L4**.

Scheme 3.4: Synthesis of **L4**

31

3.4 Synthesis of Thiosemicarbazone Complexes (C1-C4)

Four thiosemicarbazone complexes were prepared from the ligands synthesized earlier. The metal percussor used for all reactions was K_2PtCl_4, and its solubility was taken into account when selecting the solvents used for the reactions. The reactions were monitored using FTIR and were stopped when the end point was attained. The yields were calculated using the formula:

$$\frac{moles\ of\ the\ product}{moles\ of\ the\ starting\ material} \times 100$$

3.4.1 Synthesis of 2-((5-ethylthiophen-2-yl)methylene-*N*-phenylhydrazinecarbothiomide platinum(II) chloride (C1)

A mass of 0.0868g (0.3 mmol) of the thiosemicarbazone 2-((5-ethylthiophen-2-yl)methylene-*N*-phenylhydrazinecarbothiomide) was dissolved in 10 mL methanol, and 5 mL of DCM was added to improve its solubility. The yellow solution was added to a solution of 0.1245g of K_2PtCl_4 (0.3 mmol) dissolved in 10mL MeOH: H_2O (1:1). It was stirred for 12 hours and then filtered, and the precipitate was washed with MeOH and dried under reduced pressure under nitrogen.

The Scheme 3.5 below represents the synthesis of **C1**.
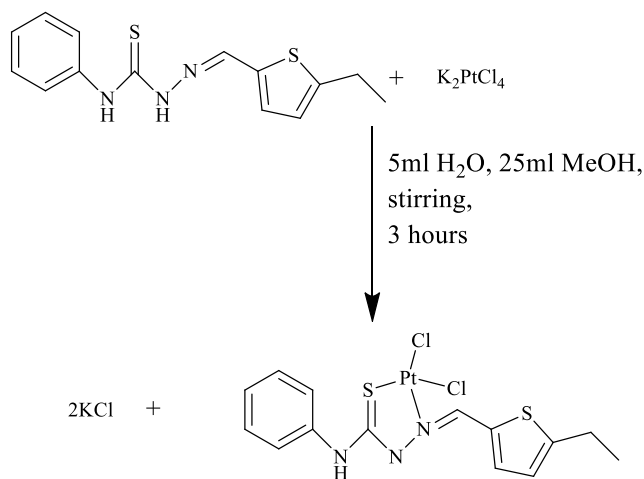
Scheme 3.5: Synthesis of **C1**

3.4.2 Synthesis of 2-((5-ethylthiophene-2-yl) methylene)-1-methylhydrazine carbothiomide platinum(II) chloride (C2)

A mass of 0.0682 g (0.3 mmol) of the thiosemicarbazone 2-((5-ethylthiophene-2-yl) methylene)-1-methylhydrazinecarbothiomide) was dissolved in 10 mL methanol, and 5 mL of DCM was added to improve its solubility. The yellow solution was added to a solution of 0.1245g of K_2PtCl_4 (0.3 mmol) dissolved in 10 mL MeOH: H_2O (1:1). It was stirred for 8 hours, then filtered, and the precipitate was washed with MeOH and dried under reduced pressure.

The Scheme 3.6 below represents the synthesis of **C2**
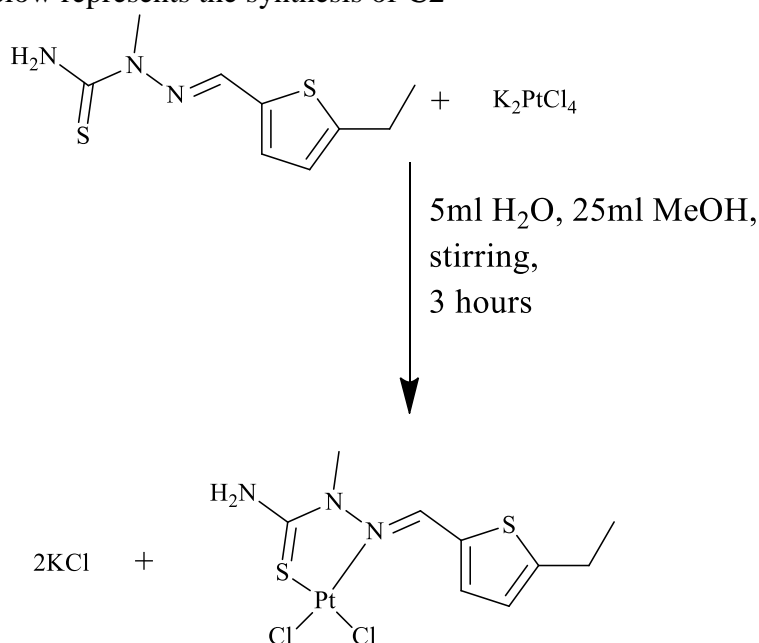
Scheme 3.5: Synthesis of **C2**

3.4.3 Synthesis of *N*,*N*–dimethyl–2-((4-nitrophene-2-yl)methylene)hydrazinecarbothiomide platinum(II) chloride (C3)

A mass of 0.0774 g (0.3 mmol) of the thiosemicarbazone *N*,*N*–dimethyl–2-((4-nitrophene-2-yl)methylene)hydrazine carbothiomide was dissolved in 10 mL methanol, and 5 mL of DCM was added to improve its solubility. The yellow solution was added to a solution of 0.1245g of K_2PtCl_4 (0.3 mmol) dissolved in 10 mL MeOH: H_2O (1:1). It was stirred for 12 hours, and the precipitate was filtered. The product was washed with MeOH and dried under reduced pressure. The Scheme 3.7 below represents the synthesis of **C3**.
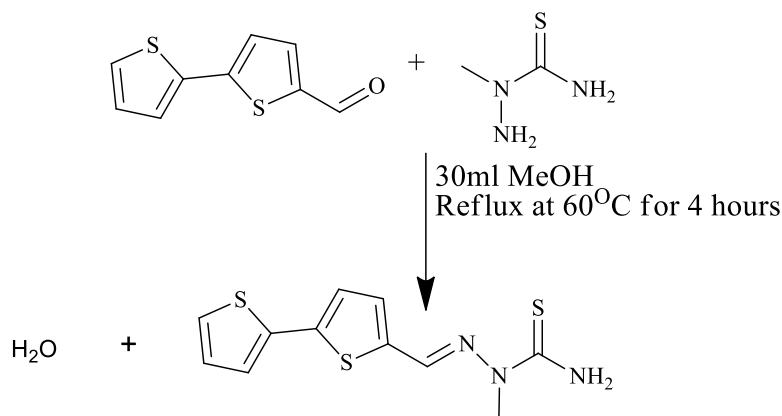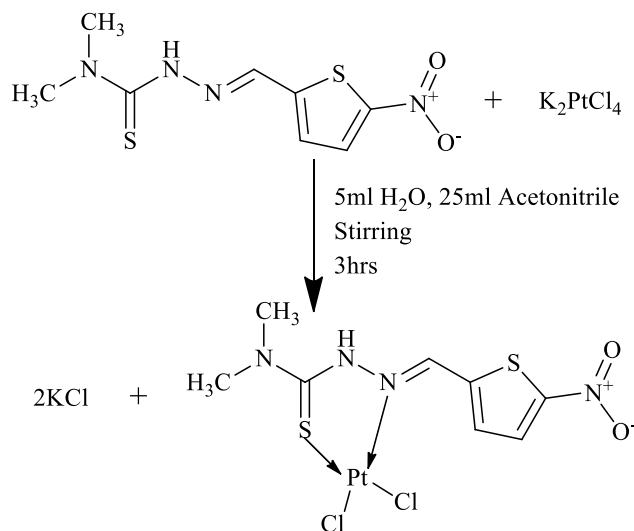
Scheme 3.6: Synthesis of **C3**

3.4.4 Synthesis of 2-([2,2'-bithiophen]-5-ylmethylene-1-methylhydrazine carbothiomide platinum(II) (C4)

A mass of 0.0844 g (0.3 mmol) of the thiosemicarbazone 2-([2,2'-bithiophen]-5-ylmethylene-1-methylhydrazinecarbothiomide was dissolved in 10 mL methanol, and 5 mL of DCM was added to improve its solubility. The yellow solution was added to a solution of 0.1245 g of K_2PtCl_4 (0.3 mmol) dissolved in 10 mL MeOH: H_2O (1:1). It was stirred for 10 hours and then filtered, and the precipitate was washed with MeOH and dried under reduced pressure under nitrogen.

The Scheme 3.8 below represents the synthesis of **C4**

34
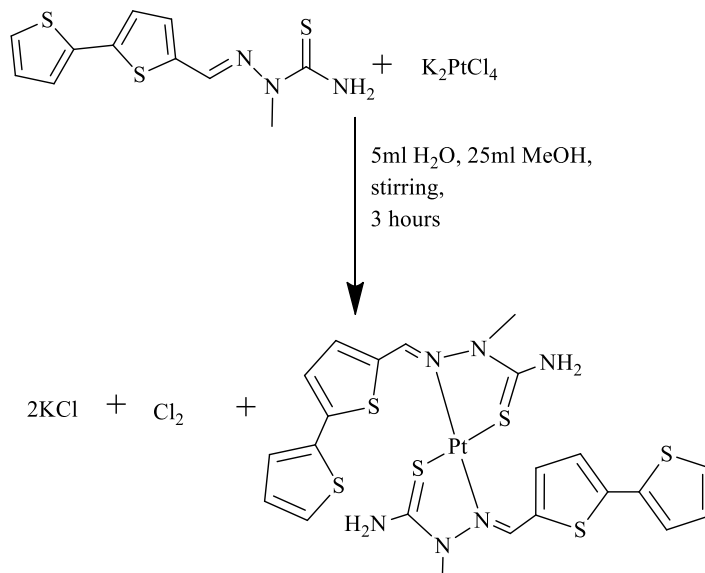
Scheme 3.7: Synthesis of **C4**

## 3.5. Characterization of the Ligands and Complexes

The following techniques were used to characterize the thiosemicarbazone ligands and platinum(II) thiosemicarbazone complexes synthesized above.

3.5.1 Fourier Transform Infrared Spectroscopy (FTIR)

FTIR data was obtained from Perkin-Elmer Spectrum 100 Series FT-IR instrument using KBr pellets. Once the sample was prepared and ready for analysis, it was placed in the stainless-steel disks and compressed using the hydraulic press. The disks were then removed from the press and pulled apart. The film was confirmed to be homogenous and transparent in appearance and inserted into the IR sample holder. After that, the spectrum was run, and data was obtained.

3.5.2 UV-Visible Spectroscopy (UV-Vis)

The UV-Vis data was obtained from the GBC UV-VIS 920 equipment. The data were recorded within a spectral range of 200 to 800 nm. The initial concentration used was 1.0×10^{-3} M. Where a peak would not be observed the first time, serial dilutions were made until the correct concentration was achieved and a peak was obtained.

3.5.3 Nuclear Magnetic Resonance Spectroscopy

The ^{1}H NMR data was obtained from a Bruker 400 MHz spectrometer. The samples were dissolved in deuterated solvents containing a small amount of TMS as indicated by the

manufacturer, and it was used as the internal reference. The samples were then placed in NMR tubes for analysis.

3.5.4 Elemental Analysis (C, H, N, S)

The instrument used for elemental analysis was the Server 1112 Series Elemental analyzer. The facility was provided by Stellenbosch University, South Africa. Since the investigation involves the combustion of the sample, part of the preparation procedure was to ensure the samples did not contain any residual solvent or moisture to obtain reliable results. Therefore, the samples were left overnight in Schlenk tubes and under nitrogen to dry for 24 hours. Their weights were carefully taken to ensure the accuracy of the results.

3.5.5 Single Crystal X-ray Crystallography

The single-crystal x-ray crystallography data was obtained from a Bruker CCD APEXII area-detector diffractometer, courtesy of Rutgers University, USA. The analysis was performed on **L2**, which gave suitable crystals. The **L2** crystals were mounted as they were on the goniometer, which positioned the crystal at appropriate orientations. The crystal was illuminated using focused monochromatic x-ray beams. The diffraction patterns obtained were regularly spaced spots in a two-dimensional fashion. The images taken were then converted to three-dimensional models and presented for comparisons for any unusual or unexpected bonding.

3.6 Anticancer Screening of Ligands and Complexes

The ligands and complexes were subjected to cytotoxicity assays. The assays were performed using commercially available cancer cells, and standard procedures were followed.

3.6.1 Preparation of Solutions for the Ligands and Complexes

Stock solutions (1 mg/mL) of the newly synthesized ligands and complexes were prepared by dissolving each compound in 10 μL dimethylsulfoxide and 990 μL of Dulbecco's Modified Eagle's Medium (DMEM), and the solutions were stored at 40^0C.

3.6.2 Cell culture

The cancerous cell lines colon cancer (Caco-2 and HT-29), cervical cancer (HELA) and the non-cancerous cell line (KMST-6) were obtained and cultured in complete Dulbecco's Modified Eagle's Medium (DMEM + 10% FBS + 5% Penicillin-Streptomycin) in 25 cm tissue culture flasks and were left to grow in an incubator set at 37^0C with 5% CO_2 atmospheric pressure to 90% confluence. The cells were then harvested using trypsin, which is an enzyme that breaks

down proteins to detach adherent cells from the flasks in which they were cultured. Once trypsinized, the cells were pushed into the solution and were ready for further analysis.

3.6.3 Morphological Evaluation

Serial dilutions (50 mL, 12.5 mL and 6.25 mL) of the ligands and complexes were prepared in Dulbecco's Modified Eagle's Medium. The medium was removed from the wells and replaced with the respective concentrations of ligands and complexes. Untreated cells were included as a negative control, and 12.5 μL of *cis*platin-treated cells were included as a positive control. The experiment was performed in triplicates. The cells were then incubated for 24 hours at 37^0C in a 5% humidified CO_2 incubator. After the lapse of 24 hours, the cells were inspected under a light microscope and pictures taken to study the morphology of the cells.

3.6.4 MTT Assay

After 24 hours, the respective treatments were removed from the wells and replaced with 0.5 mg/mL of MTT in Dulbecco's Modified Eagle's Medium (DMEM). The cells were incubated for 3 hours. After the lapse of the incubation period, the MTT was removed from the wells and replaced with 100% DMSO and incubated for 15-20 min. Absorbance readings at 570 nm and at 700 nm were obtained using the PLATEREADER NAME.

CHAPTER 4
RESULTS AND DISCUSSION

4.1 Background

This chapter presents the results obtained and the characterization techniques used to determine the structures of ligands (**L1-L4**) and complexes (**C1-C4**). The FTIR spectra of the ligands indicated the completion of the reactions because of the disappearance of the aldehyde peaks. The measurements were taken in solid-state using potassium bromide pellets, and the readings were between $400cm^{-1}$ to $4000cm^{-1}$. Generally, all ligands showed similar FTIR spectroscopic features. The functional groups of interest on FTIR spectra were: aldehyde (O=CH), amide (O=CHN), amine (C=N) and (C=S). The ligands were further characterized by ^1H NMR and ^{13}C NMR against a Tetramethylsilane (TMS) reference standard. 1D NMR spectra showed splitting in some of the peaks, which were assigned singlet *(s)*, doublet *(d)*, triplet *(t)*, multiplet *(m)* or broad (*br*) depending on the extent of coupling of the specific atoms. The observed shifts were explained depending on the different chemical environments, substituents and steric effects. The compounds were also analyzed using 2D NMR techniques, namely Distortionless Enhancement by Polarization Transfer (DEPT), Heteronuclear Single Quantum Correlation (HSQC), Heteronuclear Multiple Bond Correlation (HMBC) and Correlation Spectroscopy (COSY). Data from the 2D NMR spectra further confirmed the chemical shifts assignments deduced from 1D NMR and consequently confirmed the structures of the ligands. UV-Visible spectra for the ligands were recorded in dimethyl suphoxide solvent within the range of 200 to 800 nm using quartz cells. The concentration used was 1.0×10^{-3} M, and dilutions were made where necessary. All Platinum(II) thiosemicarbazone complexes were synthesized using the characterized thiosemicarbazone ligands and K_2PtCl_4 in the molar ratio of 1:1 while monitoring the reaction. The thiosemicarbazone complexes were characterized using FTIR, ^1HNMR, UV-VIS and elemental analysis.

4.2 Characterization of Ligands

All ligands (**L1 to L4**) were characterized using FTIR, ^1H NMR, ^{13}C NMR, 2D NMR techniques, UV-Vis, and elemental analysis. **L2** crystals were obtained and analyzed using XRD crystallography.

4.2.1 Characterization and Structure of 2-((5-ethylthiophen-2-yl)methylene-*N*-phenylhydrazine carbothiomide (L1)

L1 was a yellow solid with a melting point of 170^OC – 171^OC. The yield was 98%. It dissolved in dichloromethane, dimethyl sulfoxide, acetone, acetonitrile, and dimethylformamide.

Infrared (IR) spectroscopy was the first characterization technique used. Figure 4.1 shows Attenuated Total Reflectance Infrared (ATR-IR) spectra of the starting material (5-ethyl-2-thiophenecarboxyaldehyde).
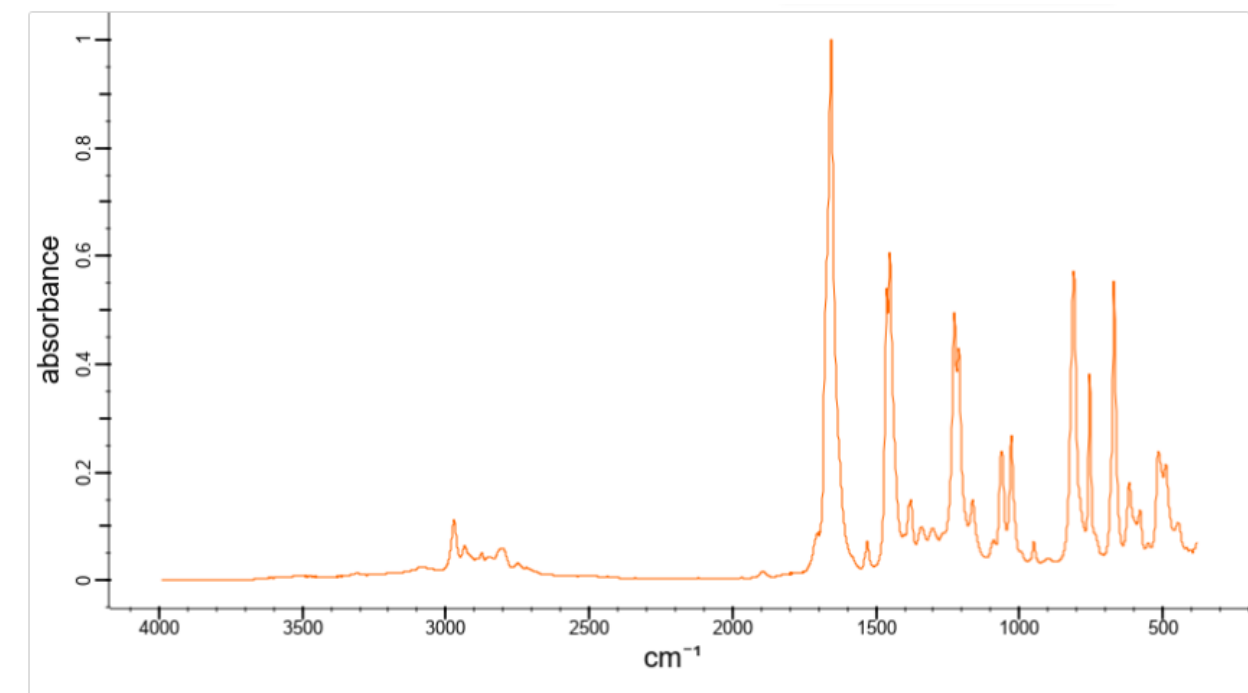
Figure 4.1: ATR-IR spectrum of 5-ethyl-2-thiophenecarboxyaldehyde

Figure 4.2 shows the product (**L1**).
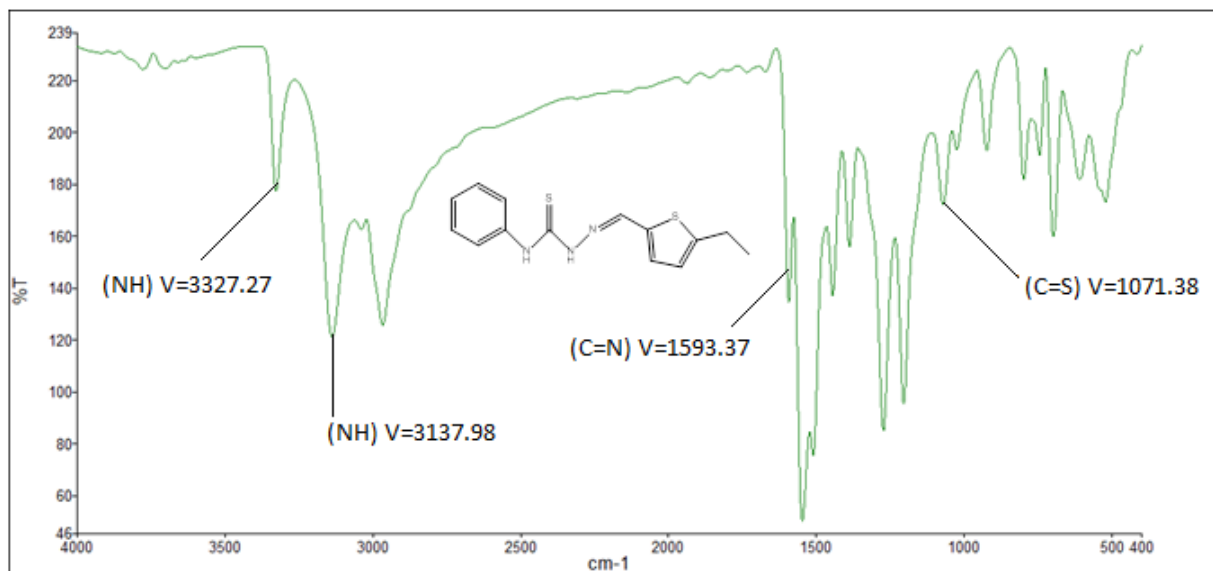
Figure 4.2: FTIR spectrum for **L1**

The aldehyde functional group that was observed at 1690 cm^{-1} was not observed in the ligand FTIR spectra. The imine peak at 1593.37 cm^{-1}, which was not in the aldehyde spectra was observed in the ligand's spectra. There was also an appearance of the C=S at 1071.38 cm^{-1} and (NH - 1) at 3137.98 cm^{-1} and (NH -2) at 3327.27 cm^{-1}. These observations confirmed that the product of interest had been formed. These results agree with previous published studies by Nyawade *et al.* (2020) and Mbugua *et al.* (2020), who found functional groups of interest (C=N), (C=S) and (NH) within the same range.

UV – VIS spectroscopy for **L1** is as shown in figure 4.3.
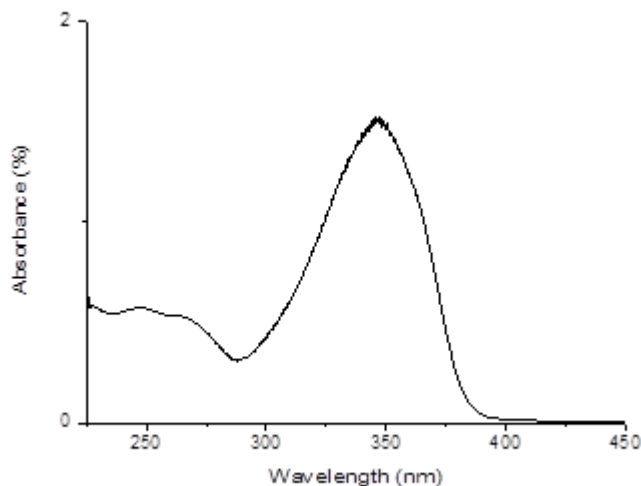
Figure 4.3: UV-Vis peaks for **L1**

The UV-Vis spectra displayed a $\pi \to \pi^*$ transition at 346.13 nm and $\eta \to \pi^*$ transition at 246.00 nm. This agrees with previous research on thiosemicarbazone ligands Motswainyana *et al.* (2013). The $\pi \to \pi^*$ transition is synonymous with molecules with pi bonds or those with a nonbonding orbital. In this case, the shift can be attributed to the aromatic units in the structure. The $\eta \to \pi^*$ transition observed at lower energy usually has high energies and consequently shorter wavelengths. It can be associated with the N-C-S chromophore, which agrees with research by Khanmohammadi *et al.* (2009). These bands can be associated with electronic transitions corresponding to HOMO (Highest Occupied Molecular Orbital) found in the imine region and LUMO (Lowest Unoccupied Molecular Orbital) in the thione.

^{1}H NMR was also used to characterize the ligand. Figure 4.4 shows the ^{1}H NMR of the starting material (5-ethyl-2-thiophenecarboxyaldehyde.
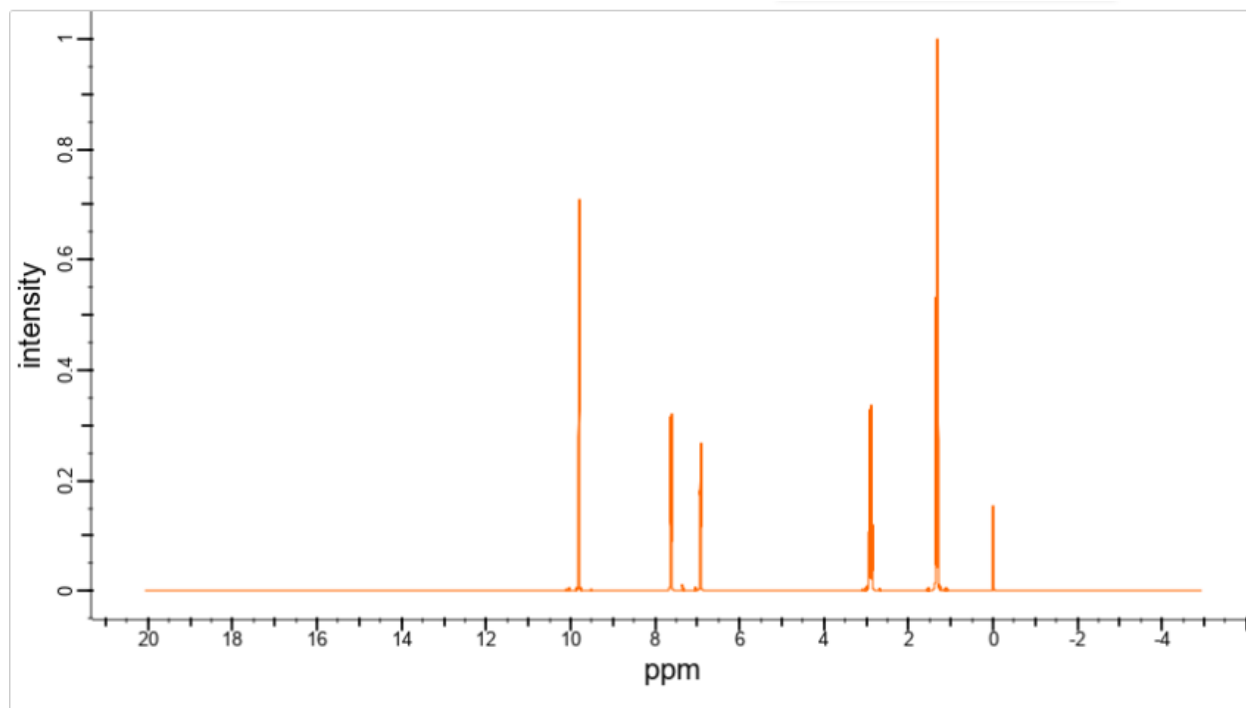
Figure 4.4: ^{1}H NMR spectrum for 5-ethyl-2-thiophenecarboxyaldehyde

The proton peak assignments on ^{1}H NMR spectra as shown in figure 4.5 were made folllowing chemical shift intution, by considering the nature of the substituents and the effect they had on the overall chemical structure.
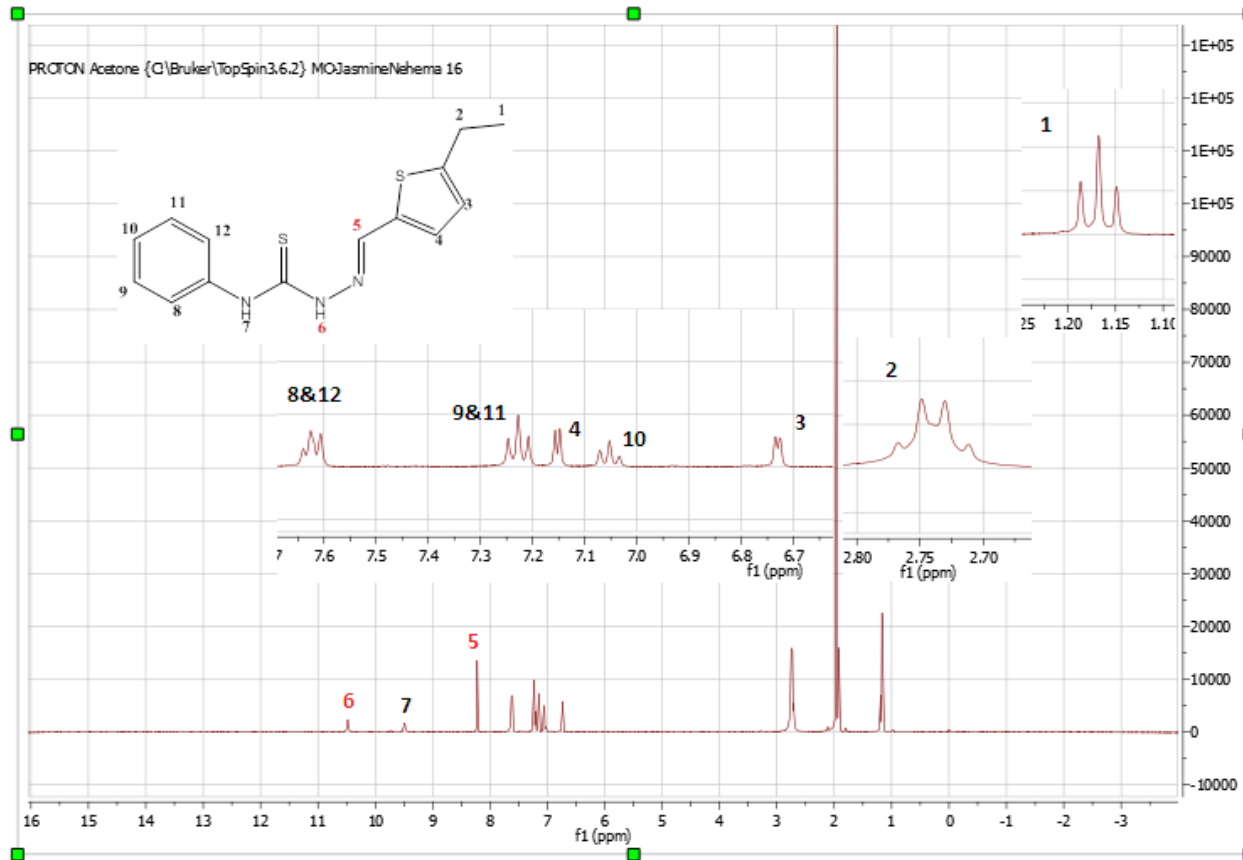
Figure 4.5: ^{1}H NMR spectrum for **L1**

The imine proton, observed at δ 8.23 ppm, is a singlet, indicating that the thiosemicarbazone ligand was successfully formed, resulting from the reaction between the aldehyde and the amine. The first peak was a triplet, observed at δ 1.15 ppm, which was assigned to position one on the ligand. The peak shows as a triplet in the ratio of 1:2:1 because of the methyl protons at position one that couple with each other, thus accounting for three protons. The second peak is observed at δ 2.8 ppm, which is a quartet in the ratio of 1:3:3:1 because of the methylene protons at position two that couple with each other and the neighbouring methyl, thus accounting for two protons. The multiplicity deduction for peaks one and two can be seconded by the fact that methyl and methylene protons have a high electron density, which results in greater shielding. Because the protons experience lower external magnetic fields, they require a lower frequency to achieve resonance, thus explaining the upfield chemical shifts. The proton peaks on the thiophene moiety (3 and 4) are observed at δ 6.70 ppm and δ 7.15 ppm, with each of the peaks accounting for one proton. Both peaks three and four are doublets because they couple with each

other since they are only three bonds away ($J3$). Three peaks represent the protons on the benzene moiety. Protons 8 and 12 are in the same chemical and magnetic environment, and their peak is observed at δ 7.65 ppm, representing two protons, which is a triplet because it couples with protons 9 and 11. Protons 9 and 11 are also in the same chemical and magnetic environment, which is why they are observed as a single peak at δ 7.20 ppm, representing two protons. The peak is a triplet because protons 9 and 11 couple with protons 8 and 12. The third aromatic proton peak is observed at δ 7.0 ppm, which represents proton 10. The peak appears as a triplet because it couples with protons 9 and 11. The hydrazine protons, 6 and 7, are observed at δ 10.5 ppm and δ 9.50 ppm, respectively. Both peaks are observed downfield because of the strong deshielding effect of the nitrogen. Another confirmation that the peaks are indeed for the hydrazine protons is that they are broad singlets because they are exchangeable and do not couple with neighbouring protons.

The ^{13}C NMR assignements for **L1** are shown in figure 4.6

Figure 4.6: ^{13}C NMR peaks for **L1**

The imine carbon shift at δ 137.92 ppm indicates the formation of the thiosemicarbazone ligand. This agrees with Mbugua *et al.* (2020), who found imine shifts within a similar range. The absence of an aldehyde carbon peak, which usually appears between δ 195.00 ppm and 205.00 ppm, indicates the successful formation of the TSC ligand. In addition, all the ^{13}C NMR peaks are accounted for and assigned, respectively. Other researchers have reported this trend in Motswainyana *et al.*(2012) and Mbugua *et al.* (2020).

2D NMR spectra were used to confirm the results of ^{1}H NMR and ^{13}CNMR. The DEPT, HSQC, HMBC and COSY spectra were obtained.

Distortionless enhancement by polarization transfer (DEPT) data for **L1** is as shown in figure 4.7.

Figure 4.7: DEPT spectra for **L1**

DEPT is an NMR technique used to determine the presence of primary, secondary and tertiary carbon atoms. There is only one negative resonance with a chemical shift of 23.37 ppm associated with methylene carbon. The methyl carbon and the aromatic carbons all have positive resonances. Quaternary carbon peaks 139.19 ppm, 151.21 ppm, and 176.00 ppm, are not visible on the DEPT NMR spectrum. This corresponds to the previous assignments of the ^{13}C NMR spectrum.

The Heteronuclear Single Quantum Coherence (HSQC) data for **L1** is shown in Figure 4.8.
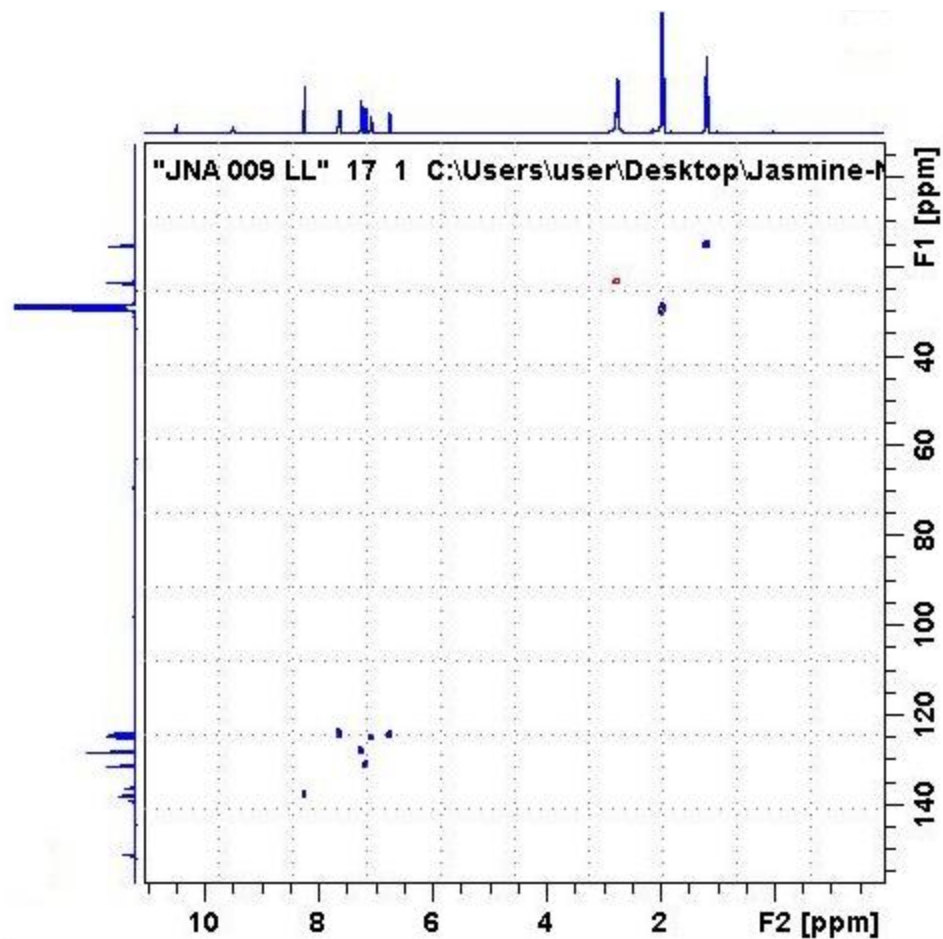
Figure 4.8: HSQC peaks for **L1**

HSQC is a 2D NMR technique used to determine proton-carbon single bond correlations. Deductions were made from the HSQC spectrum to determine the carbon nuclei separated from proton nuclei by one bond. This further confirmed the assignments made from 1D NMR.

Heteronuclear Multiple Bond Correlation (HMBC) data for **L1** is shown in figure 4.9.
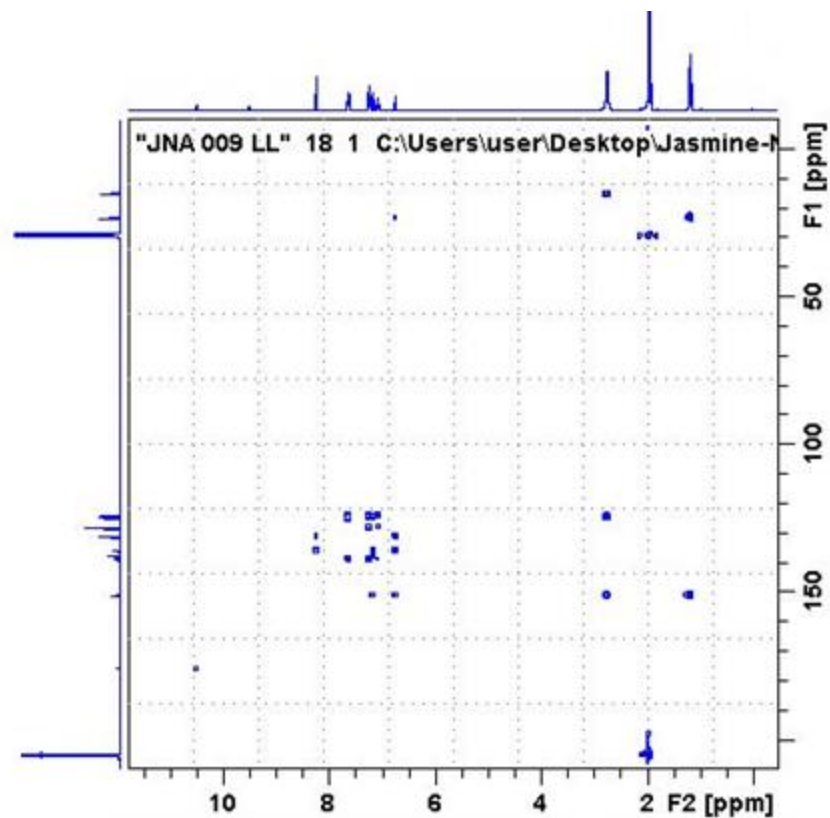
Figure 4.9: HMBC peaks for **L1**

HMBC shows the correlation between protons and heteroatoms separated by two, three or four bonds and is based on small coupling constants. The HMBC spectrum showed the caborn atoms with low coupling constants. This data was further used to confirm the structure of the ligand and its NMR assignments.

2D NMR data from DEPT, HSQC and HMBC for **L1** was compiled and tabulated in Table 4.1 below.

Table 4.1: Summary of the 2D NMR data for **L1**

δ_C	DEPT	HSQC	HMBC
176.0	+ (CH)		
151.21	+ (CH)		
139.19	+ (CH)		
139.13	+ (CH)		
137.92	+ (CH)	8.2 *(s)*	
131.26	+ (CH)	7.15 *(d)*	8.2 *(s)*, 6.7 *(d)*
128.18	+ (CH)	7.2 *(t)*	
125.06	+ (CH)	7.0 *(t)*	7.65 *(t)*
124.56	+ (CH)		7.2 *(t)*
124.22	+ (CH)	7.65 *(m)*	7.2 *(t)*
124.07	+ (CH)		
23.37	-(CH$_2$)		1.15 *(t)*
15.22	+ (CH$_3$)	1.15 *(t)*	2.8 *(t)*

Homonuclear correlation spectroscopy (COSY) data for **L1** is as shown in figure 4.10. It shows protons that are coupled to each other.
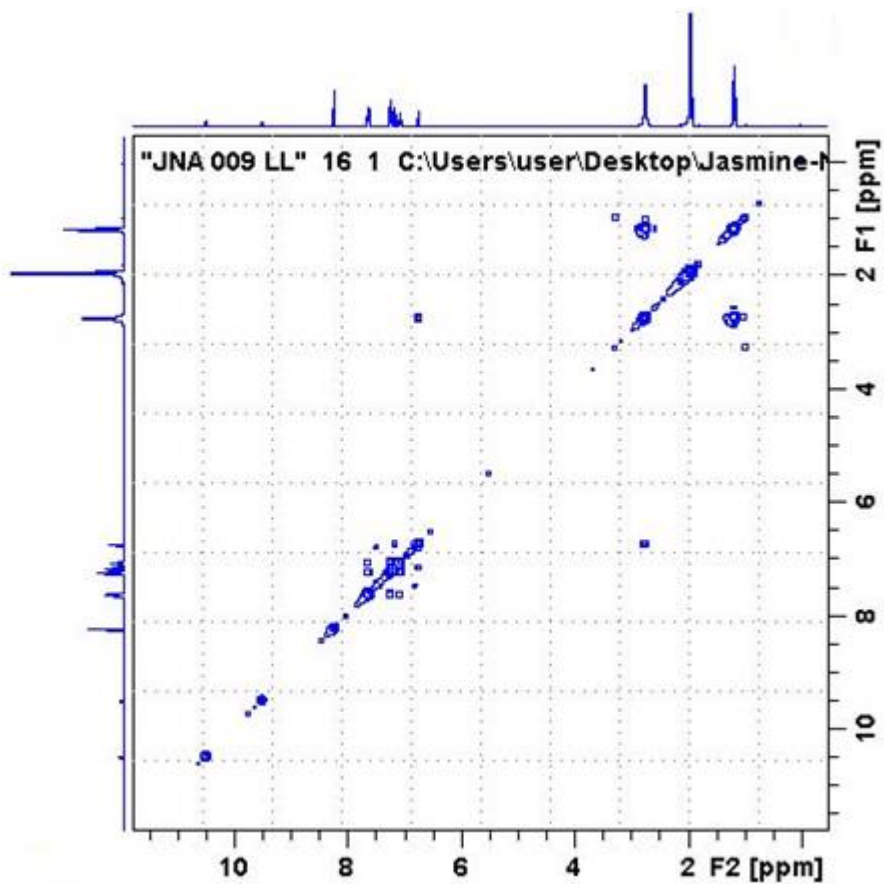
Figure 4.10: COSY peaks for **L1**

After considering all the data points, the following assignments were made, as shown in Table 4.2.

Table 4.2: Peak assignments made from the COSY spectrum

δH	COSY
10.50	
9.50	
8.23	
7.65	7.0, 7.2
7.20	7.65
7.15	
7.0	7.65
6.70	2.80
2.80	1.15
1.15	2.80

Upon considering data from both 1D and 2D NMR techniques, the ligand's structure was determined. **L1** structure with relevant assignments is as shown below.

L1

The experimental values of the elemental analysis of **L1** were; N, 21.51; C, 36.85; H, 3.91; S, 24.60 while the theoretical values were; N, 21.69; C, 37.0; H, 3.90; S, 24.82. The deviations in the experimental values were within the agreeable range of ±0.4% for N, C and H, and ±0.7% for S, confirming that the product of interest was synthesized and of expected purity.

After considering all the characterization techniques, the structure for **L1** was concluded to be as shown below

51

L1

4.2.2 Characterization and Structure of 2-((5-ethylthiophene-2-yl) methylene)-1-methylhydrazinecarbothiomide (L2)

L2 was a yellow solid with a melting point of 169°C. The yield was 89%. It dissolved in dichloromethane, dimethyl sulfoxide, acetone, acetonitrile, and dimethylformamide.

In the FTIR spectrum of **L2** (in the appendices), the aldehyde functional group previously observed at 1710.00 cm-^{1} was not present in the ligand's spectra. The appearance of an imine peak at 1622.08 cm-^{1} was synonymous with the formation of the thiosemicarbazone ligand. The peak observed at 1055.65 cm-^{1} was assigned to the C=S functional group. There was also a peak at 3285.95 cm-^{1} that was assigned to NH functional group. These observations confirmed that the product of interest had been formed. These results agree with previously published studies by Nyawade *et al.* (2020).

The UV – Vis spectrum of **L2** (in the appendices) displayed a $\pi \rightarrow \pi$ * transition at 341. 73 nm and $\eta \rightarrow \pi$ * transition at 247.20 nm. This corresponds to previous research on thiosemicarbazone ligands Motswainyana *et al.* (2013). The $\pi \rightarrow \pi$* transition is synonymous with molecules with pi bonds or those with a nonbonding orbital. In this case, the shift can be attributed to the aromatic units in the structure. The $\eta \rightarrow \pi$* transition observed at lower energy usually has high energies and consequently shorter wavelengths. It can be attributed to the N-C-S chromophore (Ahmad *et al.,* 2020). These bands can be associated with electronic transitions corresponding to HOMO (Highest Occupied Molecular Orbital) found in the imine region and LUMO (Lowest Unoccupied Molecular Orbital) in the thione.

From the ^{1}H NMR spectrum of **L2** (in the appendices), the singlet at δ 8.37 ppm is responsible for the proton attached to C=N, and it confirms the completion of the reaction between the amine and the aldehyde. This is supported by literature Mbugua *et al.* (2020). The first peak observed at

δ 1.29 ppm is a triplet assigned to the methyl protons attached to the thiophene ring. They appear as one peak in the ratio of 1:2:1 because they are in the same chemical environment and are observed upfield because they are highly shielded and have low energy. The second peak is at δ 2.87 ppm, which is assigned to the methylene protons next to the methyl protons because it is a quartet in the ratio of 1:3:3:1. Although it is highly shielded, it is not as much as the methyl protons, so it is not observed very downfield compared to the methyl peak. The third peak at δ 3.37 ppm is assigned to the methyl protons attached to the hydrazine nitrogen. It appears as a singlet in the ratio of 1:2:1 because the protons are coupling with each other. While it is highly shielded, it cannot be expected to appear as upfield as the other methyl peak because of its chemical environment. The fourth peak at δ 6.85 ppm is assigned to one of the aromatic protons on the thiophene ring. The peak is a doublet of a triplet because it is coupling with the other proton on the aromatic ring and the neighboring methylene proton peak. The fifth peak at δ 7.00 ppm was assigned to the amine protons because it is a singlet, as these protons don't have any neighbors they can couple with. The sixth peak at δ 7.30 ppm is assigned to the other aromatic proton on the thiophene ring.

Data from the ^{13}C NMR spectrum of **L2** (in the appendices) helps to confirm the assignments made from the ^{1}H NMR spectra. The first peak at δ 15.22 ppm is observed upfield and is assigned to the carbon atom with the methyl protons attached to the thiophene ring. This is because the carbon atom is in a highly shielded chemical environment and thus has lower energy. The second peak observed at δ 17.98 ppm is assigned to the carbon atom attached to the thiophene ring, which has methylene protons. This is because it is highly shielded. The third peak at δ 23.33 ppm is assigned to the carbon atom attached to the hydrazine nitrogen with methyl protons, making it highly shielded and thus appeared relatively upfield. The imine carbon is responsible for the peak observed at δ 124.46 ppm. The aromatic carbon atoms on the thiophene ring are assigned to the peaks at δ 130.00 ppm and δ 136.06 ppm. This data is confirmed by 2D NMR spectra; distortionless enhancement by polarization transfer, heteronuclear single quantum correlation, heteronuclear multiple bond correlation, and correlation spectroscopy. This peak is a doublet of a doublet because it couples only with the other aromatic proton.

The experimental values of the elemental analysis of **L2** were; N, 18.50; C, 47.33; H, 5.73; S, 28.31 while the theoretical values were; N, 18.48; C, 47.55; H, 5.76; S, 28.20. The deviations in the experimental values were within the agreeable range of $\pm 0.4\%$ for N, C and H, and $\pm 0.7\%$ for S, confirming that the product of interest was synthesized and of expected purity.

4.1.2.1 X-ray Diffraction Studies

L2 crystals for XRD analysis were grown by slow diffusion of *n*-hexane into DCM, which yielded needle-shaped yellow crystals. The crystallography data was obtained from Bruker SMART CCD APEXII and temperature was maintained at 100 K.

Table 4.3: Crystal data and refinement

Empirical formula	$C_9H_{13}N_3S_2$
Formula weight	227.35 g/mol
Temperature	100K
Wavelength	1.54056
Crystal system	Monoclinic
Space group	P 21/c

The XRD structure is shown below in figure 4.11.
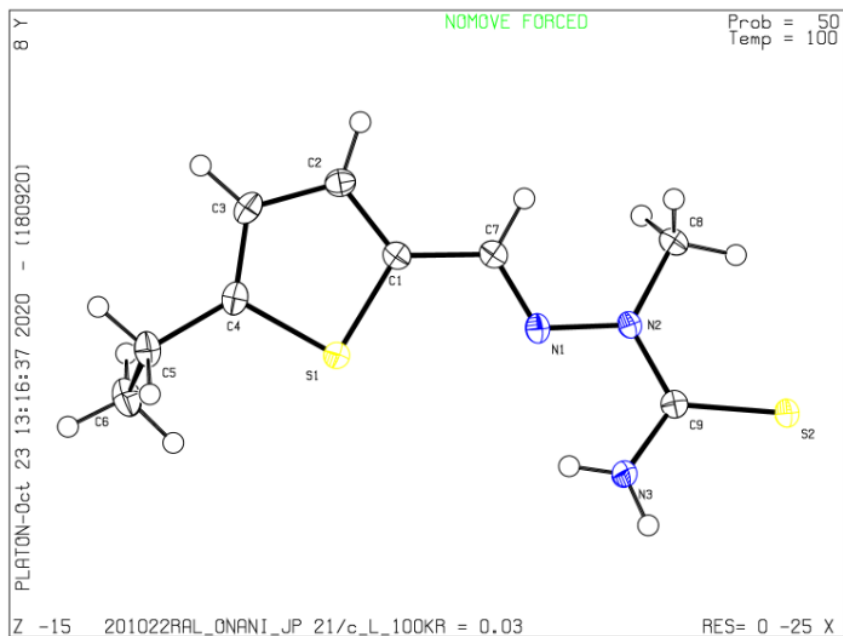
Figure 4.11: XRD structure for **L2**

L2 forms a monoclinic P21/c space system with 4-unit molecules packed into the crystal unit. It has three planes of symmetry. Figure 4.12 below illustrates the packing of the crystals.
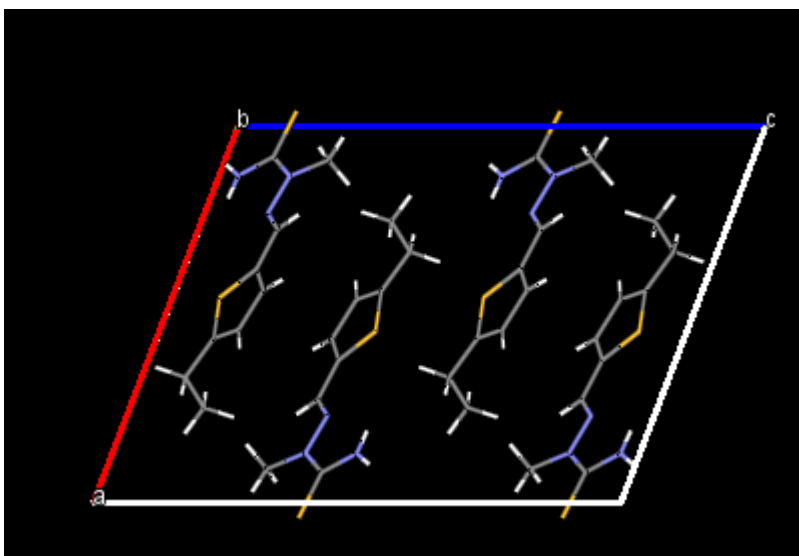
Figure 2.12: Crystal packing

Upon considering all the characterization techniques discussed above, the structure of **L2** was confirmed.
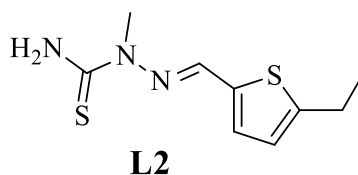

L2

4.2.3 Characterization and Structure of *N,N*–dimethyl–2-((4-nitrophene-2-yl)methylene)hydrazinecarbothiomide (L3)

L3 was an orange solid with a melting point of 183^OC – 184^OC. The yield was 99%. It dissolved in dimethyl sulfoxide, acetone and dimethylformamide.

In the FTIR spectrum of **L3** (in the appendices), the aldehyde functional group that had been previously observed at 1685.11 cm^{-1} was absent in the Fourier Transform Infrared Spectrum of the ligand. An imine peak was observed at 1551.01 cm^{-1}, a C=S peak at 1062.32 cm^{-1} and an NH peak at 3294.14 cm^{-1}. These observations confirmed that the product of interest had been formed. These results agree with previously published studies by Nyawade *et al.* (2020) and Mbugua *et al.* (2020).

The UV – Vis spectrum of **L3** (in the appendices) displayed a $\pi \rightarrow \pi$ * transition at 421.33 nm and $\eta \rightarrow \pi$ * transition at 276.00 nm. This corresponds to previous research on thiosemicarbazone ligands (Motswainyana *et al.,* 2013). The $\pi \rightarrow \pi^*$ transition is synonymous with molecules with pi bonds or those with a nonbonding orbital. In this case, the shift can be attributed to the aromatic units in the structure. The $\eta \rightarrow \pi^*$ transition observed at lower energy usually has high energies and consequently shorter wavelengths. It can be attributed to the N-C-S chromophore (Khanmohammoladi *et al.,* 2009). These bands can be associated with electronic transitions corresponding to HOMO (Highest Occupied Molecular Orbital) found in the imine region and LUMO (Lowest Unoccupied Molecular Orbital) in the thione.

In the ^{1}H NMR spectrum of **L3** (in the appendices), the imine proton peak is observed at δ 8.30 ppm, which confirms that the compound of interest has been formed and that the reaction

between the amine and the aldehyde is complete. This agrees with previous research, where the imine proton peak was observed within the same range (Mbugua *et al.,* 2020). The spectrum was elucidated further to confirm the structure of the compound. The first peak was observed at δ 3.57 ppm, and it was a quartet. This peak was assigned to the two sets of methyl protons attached to the aliphatic nitrogen atom. This is because all the protons are in the same chemical environment and thus share the same chemical shift. The observed quartet is attributed to the fact that the proton coupled with each other. The second peak is assigned to one aromatic proton and is observed at δ 7.38 ppm, which is also a doublet because it couples with the other aromatic proton. The third peak is observed at δ 7.99 ppm, which is assigned to the other aromatic proton on the thiophene ring; the one closer to the nitro group because it is likely to be more deshielded by the electrons from the nitro group, and thus vibrate at higher energy than the other proton. The peak is a doublet because it is coupling with the other aromatic proton. The peak that is furthest downfield at δ 11.29 ppm is assigned to the proton on the hydrazine nitrogen because it is the most deshielded of all the proton peaks, and is a singlet.

Data from the ^{13}C NMR spectrum of **L3** (in the appendices) helps to confirm the proton assignments. The first peak is observed at δ 29.53 ppm and is assigned to the two carbon atoms bearing the methyl protons. Because they are highly shielded, they appear upfield, and they are within the same chemical environment, which is why they share a chemical shift. The second peak at δ 129.60 ppm is assigned to the amine carbon. The third and fourth peaks at δ 135.38 ppm and 139.29 ppm are assigned to the carbon atoms on the thiophene ring bearing the aromatic protons. The fifth peak at δ 147.11 ppm is assigned to the quaternary carbon atom next to the imine carbon. The sixth peak at δ 205.08 ppm is assigned to the quaternary carbon attached to the nitro group, as it is very dishielded because of the high electron density of the nitro group, which is why it appears furthest downfield. This data is confirmed by 2D NMR spectra; distortionless enhancement by polarization transfer, heteronuclear single quantum correlation, heteronuclear multiple bond correlation, and correlation spectroscopy.

The experimental values of the elemental analysis of **L3** were; N, 14.45; C, 58.32; H, 5.24; S, 20.00 while the theoretical values were; N, 14.52; C, 58.10; H, 5.22; S, 22.16. The deviations in

the experimental values were within the agreeable range of ±0.4% for N, C and H, and ±0.7% for S, confirming that the product of interest was synthesized and of expected purity.

The characterization techniques discussed above confirmed the structure of **L3**

L3
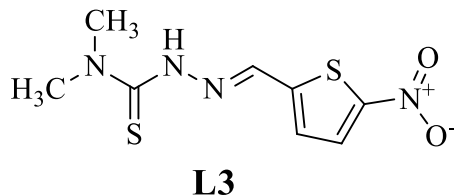
4.2.4 Characterization and Structure of L4

L4 was a yellow solid with a melting point of $229^{O}C - 230^{O}C$. The yield was 95%. It dissolved in dimethyl sulfoxide, acetone and dimethylformamide.

The Fourier Transform Infrared Spectrum of **L4** (in the appendices) confirmed the completion of the ligand formation reaction by exhibiting the disappearance of the aldehyde functional group 1701.03 cm^{-1} and the appearance of the imine peak 1577.98 cm^{-1}. The appearance of the C=S at 1003.68 cm^{-1} and NH at 3425.30 cm^{-1} confirmed that the product of interest had been formed. These results conform with previously published studies by Mbugua *et al.* (2020).

The UV – Vis spectrum of **L4** (in the appendices) displayed a $\pi \rightarrow \pi^*$ transition at 380.53 nm and $\eta \rightarrow \pi^*$ transition at 262.92 nm. This corresponds to previous research on thiosemicarbazone ligands (Motswainyana *et al.,* 2013). The $\pi \rightarrow \pi^*$ transition is synonymous with molecules with pi bonds or those with a nonbonding orbital. In this case, the shift can be attributed to the aromatic units in the structure. The $\eta \rightarrow \pi^*$ transition, observed at lower energy, usually has high energies and consequently shorter wavelengths. It can be attributed to the N-C-S chromophore (Ahmad *et al.,* 2020). These bands can be associated with electronic transitions corresponding to HOMO (Highest Occupied Molecular Orbital) found in the imine region and LUMO (Lowest Unoccupied Molecular Orbital) in the thione.

From the ^{1}H NMR spectrum of **L4** (in the appendices), the imine proton peak is observed at δ 8.00 ppm, which confirms the completion of the Schiff base condensation reaction between the

amine and the aldehyde. This data is supported by previous research Motswainyana *et al.* (2013). The other peaks were elucidated to determine the structure. The first peak was observed at δ 3.29 ppm, and it was assigned to the methyl protons because they are very shielded and thus appear the furthest upfield. It is also a singlet with a splitting ratio of 1:2:1, indicating that the peak is responsible for three protons that are in a chemically equivalent environment. The amine protons are observed at δ 7.42 ppm, and they appear as a singlet because they are also in a similar chemical environment. The aromatic protons on the thiophene ring attached to the imine are doublets and assigned to δ 7.15 ppm and δ 7.30 ppm. The aromatic proton peaks on the other thiophene ring are assigned δ 6.98 ppm, δ 7.24 ppm and δ 7.36 ppm, and they are all doublets of doublets because they couple with each other.

The ^{13}C NMR spectrum for **L4** (in the appendices) was used to confirm the chemical shift assignments and the ligand's structure. The first observed peak at δ 29.90 ppm is attributed to the carbon atoms attached to the methyl protons because the carbon atom is highly shielded and thus appears the furthest upfield. The imine carbon appears at δ 125.77 ppm. The carbon atoms on the thiophene ring close to the imine carbon are assigned δ 128.30 ppm, δ 131.48 ppm and δ 135.43 ppm. The quaternary carbon atoms are assigned δ 205.35 ppm since they are both in the same chemical environment. The carbon atoms on the second thiophene ring are assigned δ 124.15, 124.85 ppm and δ 125.77 ppm. This data is confirmed by 2D NMR spectra; distortionless enhancement by polarization transfer, heteronuclear single quantum correlation, heteronuclear multiple bond correlation, and correlation spectroscopy.

The experimental values of the elemental analysis of **L4** were; N,14.53; C,46.75; H,3.94; S,34.30 while the theoretical values were; N, 14.93; C, 46.95; H, 3.94; S, 34.18. The deviations in the experimental values were within the agreeable range of ±0.4% for N, C and H, and ±0.7% for S, confirming that the product of interest was synthesized and of expected purity.

After putting into account the characterization techniques discussed above, the **L4** structure was determined.

L4
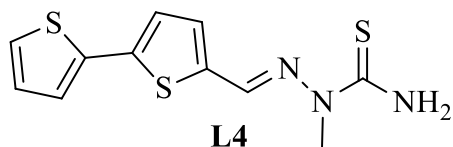
4.2.5 Summary of the Ligands

All the ligands were brightly-colored solid products with sharp melting points. The yields were between 89% and 99%. The Fourier transform infrared spectrum confirmed the completion of the ligand formation reaction by exhibiting the disappearance of the aldehyde functional group, which is usually observed between 1710 cm-^{1} and 1685 cm-^{1}, and the appearance of the imine peak between 1551 cm-^{1} and 1622 cm-^{1}. The ligands displayed strong imine stretching bands on FTIR spectra, ranging from 1551.21cm^{-1} and 1622.08 cm^{-1}. They also displayed thioamide stretching frequencies between 1003.68cm^{-1} and 1071.38cm^{-1}. These results are supported by Motswainyana *et al.*(2013) that had the bands within the same range. The $\pi \rightarrow \pi^*$ transition is synonymous with molecules with pi bonds or those with a nonbonding orbital. In this case, the shift can be attributed to the aromatic units in the structure. The $\eta \rightarrow \pi^*$ transition observed at lower energies usually has high energies and consequently shorter wavelengths. It can be attributed to the N-C-S chromophore (Ahmad *et al.*, 2020). The general trend of ^{1}H NMR for the ligands was that the imine proton was observed between 8.0 ppm and 8.43 ppm. On the other hand, the hydrazine protons were observed between 10.50 ppm and 11.29 ppm, while the hydrazine methyl proton peaks were observed between 3.29 ppm and 3.37 ppm. The TSC ligands exhibited two intra-ligand bands attributed to the n-π^* transitions and the π-π^* transitions. The π-π^*transitions are observed in systems with pi bonds or atoms with non-bonding electrons, which was the case for the TSC ligands. The π-π^* shifts ranged between 341 nm and 421 nm. The second transition observed in the TSC ligands was n-π^*, ranging between 246 nm and 276 nm. These results correspond to previous research on thiosemicarbazone ligands (Kayed *et al.*, 2013). The experimental results of the elemental analysis of the ligands agree with the theoretical data with deviations of ±0.4% for N, C and H, and ±0.7% for S, confirming that the product of interest was synthesized and of expected purity (Mbugua *et al.*, 2020).

4.3 Characterization of Complexes

All synthesized complexes, **C1** to **C4**, followed a similar synthesis method, where the respective ligand and K_2PtCl_4 were reacted in a molar ratio of 1:1. They were characterized using FTIR, ^{1}H NMR, UV-Vis, and elemental analysis.

4.3.1 Characterization and Structure of 2-((5-ethylthiophen-2-yl)methylene-*N*-phenylhydrazinecarbothiomide platinum(II) chloride (C1)

C1 was an orange solid with a melting point of 182^OC. The yield was 84%. It dissolved in dimethyl sulfoxide, acetone and dimethylformamide.

The FTIR spectroscopic data for **C1** is as shown in Figure 4.13.
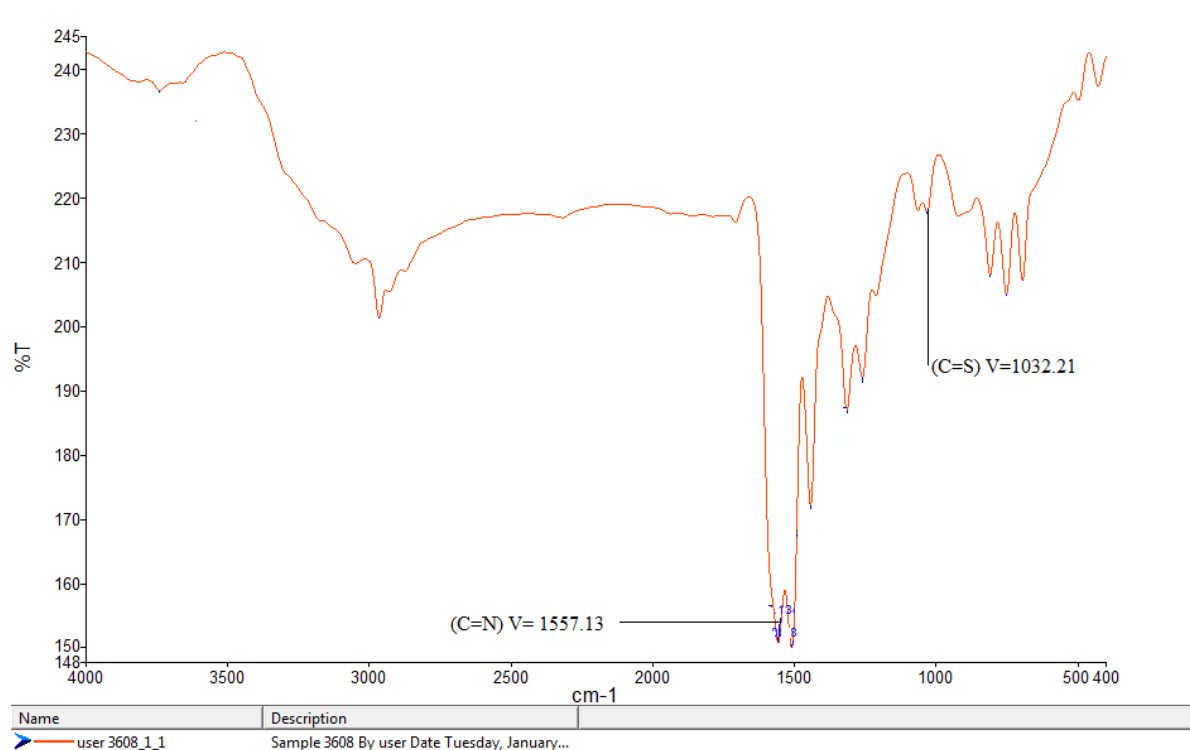
Figure 4.13: FTIR peaks for **C1**

The spectrum provides essential information on the atoms involved in coordinating the ligand to the central metal atom. From previous studies, the coordination was expected to involve the hydrazine nitrogen and sulphur. The C=S functional group was observed at 1032.21 cm^{-1}, while that of the ligand had been observed at 1071.38 cm^{-1}. The C=N functional group was observed at 1557.13 cm^{-1}, while that of the ligand had been observed at 1593.37 cm^{-1}. The observations

61

agree with previous publications (Mbugua *et al.,* 2020). The shift of the thioamide vibration to lower frequencies clearly indicates that the metal's coordination to the ligand was via the imine nitrogen and the sulphur atom. This is because the chelation of the ligand to the metal center reduces the electron density on the pi bonds, which in turn decreases the pi-character and thus weakens the bond. The ν (NH) was not observed in **C1**, which shows that complexation happened by proton loss.

UV – Vis spectroscopy data for **C1** is as shown in Figure 4.14.
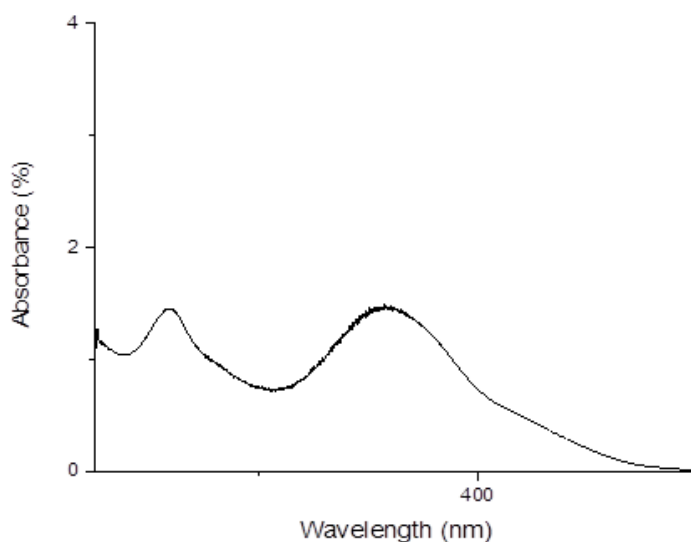
Figure 4.14: UV-Vis peaks for **C1**

It displayed a $\pi \rightarrow \pi$ * transition at 357.20 nm, which can be assigned to the MLCT (Metal to Ligand Charge Transfer) from the metal's d orbitals to the anti-bonding orbitals of the ligand. Similar results were reported by (Njogu *et al.,* 2019). The $\eta \rightarrow \pi$ * transition at 256.93 nm. This agrees with previous research on thiosemicarbazone complexes (Abu-Surraha *et al.,* 2010). The absorption bands were below 600 nm, suggesting large crystal field splitting concurrent with square-planar geometry.

The ¹H NMR spectrum of **C1** is as shown in Figure 4.15.
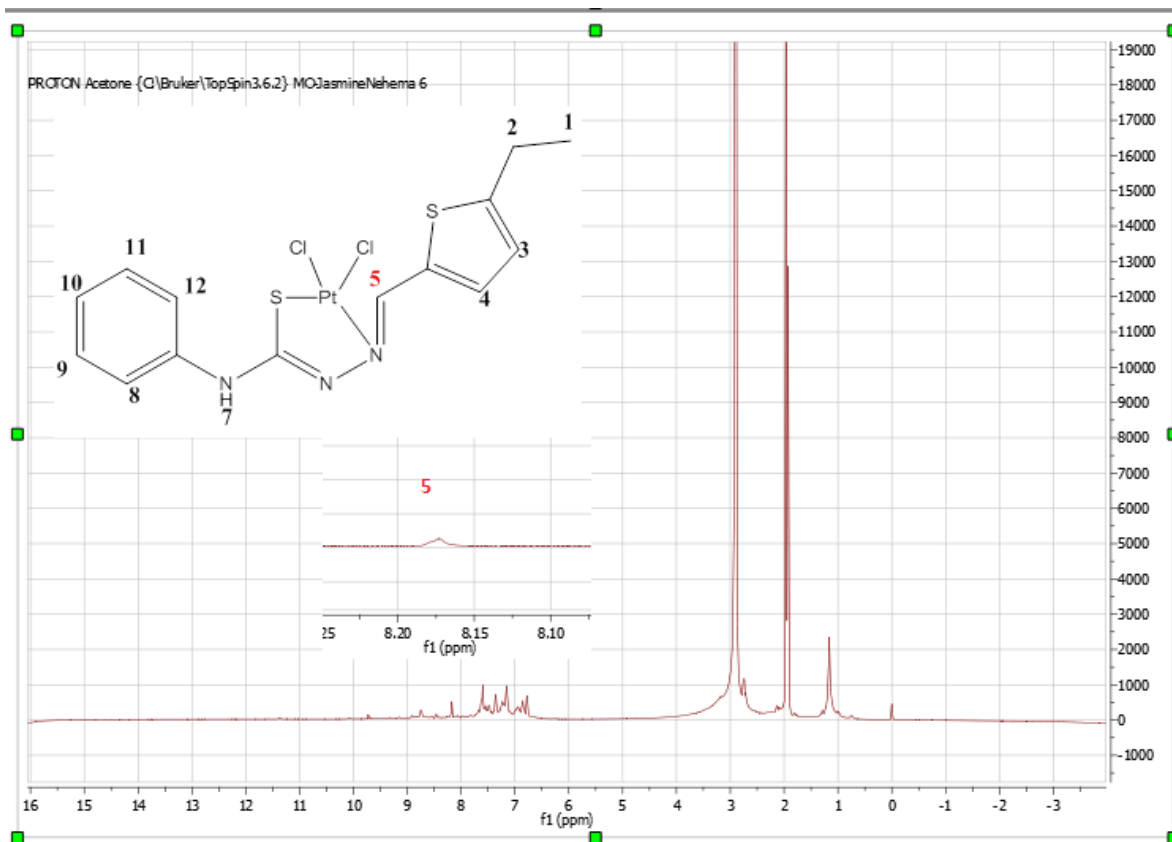
**Figure 4.15**: ^{1}H NMR peaks for **C1**

The peaks were obtained and compared to those of the ligands. The amine proton peak observed at 10.5 ppm in the ligand is not present in the complex spectrum, which indicates that complexation happened by proton loss. Furthermore, the imine proton peak is observed at 8.15 ppm, which is more upfield than the observed 8.2 ppm for the ligand. This confirms coordination via the thioamide sulphur and the imine nitrogen. This data agrees with previous research by Mbugua *et al.* (2020), who reported peaks within the same range.

The experimental values of the elemental analysis of **C1** were; N, 10.62; C, 18.20; H, 2.10; S, 12.12 while the theoretical values were; N, 10.67; C, 18.29; H, 2.11; S, 12.21. The deviations in the experimental values were within the agreeable range of ±0.4% for N, C and H, and ±0.7% for S, confirming that the product of interest was synthesized and of expected purity.

After considering the results from all the characterization techniques explained above, the structure of **C1** was determined.

C1
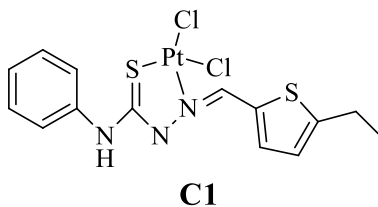
4.3.2 Characterization and Structure of 2-((5-ethylthiophene-2-yl) methylene)-1-methylhydrazine carbothiomide platinum(II) chloride (C2)

C2 was a yellow solid with a melting point of 180^OC. The yield was 88%. It dissolved in dimethyl sulfoxide, acetone and dimethylformamide.

The FTIR spectrum for **C2** (in the appendices) gives essential information on the atoms involved in binding to the central metal atom. From previous research, the reaction was expected to involve the hydrazine nitrogen and sulphur atom. The C=S functional group was observed at 1003.20 cm^{-1}, while that of the ligand had been observed at 1055.65 cm^{-1}. The C=N functional group was observed at 1581.12 cm^{-1}, while that of the ligand had been observed at 1622.08 cm^{-1}. The data agrees with previous publications (Serda *et al.,* 2014). The shift of the imine and the thioamide vibrations to lower frequencies indicates that the metal's coordination to the ligand was via the imine nitrogen and the sulphur atom. When the ligand binds with the metal center, it reduces the electron density on the pi bonds, thus reducing the pi-character and weakening the bond.

The UV – Vis spectrum of **C2** (in the appendices) displayed a $\pi \rightarrow \pi$ * transition at 345.73 nm attributed to MLCT (Metal to Ligand Charge Transfer) from the metal's d orbitals to the anti-bonding orbitals of the ligand. This corresponds to previous research on thiosemicarbazone complexes (Abu-Surraha *et al.,* 2010). The absorption bands were below 600 nm, suggesting large crystal field splitting synonymous with square-planar geometry. The n-π* transition is not observed, which indicates the possibility of a range below 200 nm, which could not be captured.

This mode of complexation can be confirmed by the ^{1}H NMR data (in the appendices), where the imine proton was observed at δ 8.37 ppm, as opposed to δ 8.43 ppm in the ligand, which agrees with previous research by Kayed *et.al.* (2016), who found peaks in the same range. This is proof that complexation involved imine nitrogen. However, unlike in the case of **C1** and **C3**, there was no proton loss in this compound. This could be because the methyl protons attached to the hydrazine nitrogen are harder to lose.

The experimental values of the elemental analysis of **C2** were; N, 8.48; C, 21.80; H, 2.63; S,12.89 while the theoretical values were; N, 8.52; C, 21.91; H, 2.66; S, 13.00. The deviations in the experimental values were within the agreeable range of ±0.4% for N, C and H, and ±0.7% for S, confirming that the product of interest was synthesized and of expected purity.

After considering all the data from the characterization techniques explained above, the structure of **C2** was determined.

C2
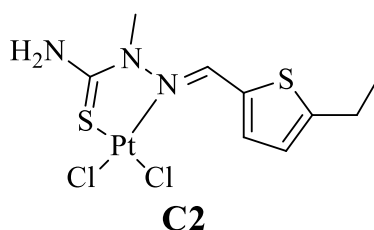
4.3.3 Characterization and Structure of *N,N*–dimethyl–2-((4-nitrophene-2-yl)methylene)hydrazinecarbothiomide platinum(II) chloride (C3)

C3 was a brown solid with a melting point of 192°C. The yield was 84%. It dissolved in dimethyl sulfoxide, acetone and dimethylformamide.

The FTIR spectroscopic data of **C3** (in the appendices) gives insight into the atoms involved in the coordination reaction. Previous studies suggest that hydrazine nitrogen and sulphur are fundamental donor atoms for thiosemicarbazones. The C=N was observed at 1524.32 cm^{-1}, while that of the ligand had been observed at 1551.21 cm^{-1}. The C=S was observed at 1059.83 cm^{-1}, while that of the ligand had been observed at 1062.32 cm^{-1}. This data agrees with the previous publication by Motswainyana *et al.* (2012), who reported shifts in the same region. The shift of

the imine and the thioamide vibrations to lower frequencies is a clear indication that the coordination of the metal to the ligand was via the imine nitrogen and the sulphur atom.

The UV – Vis spectrum of **C3** (in the appendices) displayed a $\pi \rightarrow \pi$ * transition at 355.86 nm because of the MLCT (Metal to Ligand Charge Transfer) from the metal's d orbitals to the anti-bonding orbitals of the ligand. The $\eta \rightarrow \pi$ * transition at 250.00 nm. This agrees with previous research on thiosemicarbazone complexes (Abu-Surraha *et al.,* 2010) found similar transitions in the synthesized complexes. The absorption bands were below 600 nm, suggesting large crystal field splitting concurrent with square-planar geometry.

From the ^{1}H NMR spectrum of **C3** (in the appendices), the imine proton is observed at δ 8.36 ppm, compared to the ligand, where it was observed at δ 8.30 ppm. The proton on the hydrazine nitrogen disappears. This confirms that the hydrazine nitrogen and the amine had been involved in the coordination to the metal center, and there was proton loss. These results agree with previous research by Kayed *et al.* (2016), who also found the coordination of some of the ligands synthesized to have involved the hydrazine nitrogen and the amine. Other notable changes on the ^{1}H NMR were: the methyl protons shifted from δ 3.57 ppm to δ 3.19 ppm, the aromatic protons on the thiophene ring shifted from δ 7.99 ppm and δ 7.38 ppm to δ 8.07 ppm and δ 7.83 ppm respectively.

The experimental values of the elemental analysis of **C3** were; N, 7.50; C, 30.10; H, 2.70; S, 11.40 while the theoretical values were; N, 7.57; C, 30.27; H, 2.72; S, 11.55. The deviations in the experimental values were within the agreeable range of ±0.4% for N, C and H, and ±0.7% for S, confirming that the product of interest was synthesized and of expected purity.

After considering all the characterization techniques used above, the structure of **C3** was determined.

C3
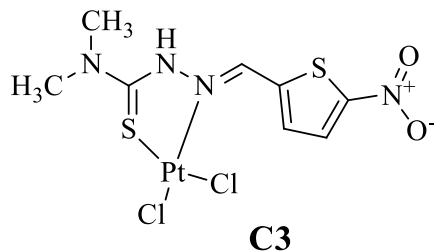
4.3.4 Characterization and Structure of 2-([2,2'-bithiophen]-5-ylmethylene-1-methylhydrazine carbothiomide platinum(II) (C4)

C3 was a yellow solid with a melting point of 242°C. The yield was 77%. It dissolved in dimethyl sulfoxide, acetone and dimethylformamide.

From the FTIR spectrum of **C4** (in the appendices), there is a minimal decrease in the IR frequencies, which can be attributed to its unique dimer coordination, which would result in a slight increase in the electron density on the pi-bonds and thus not much change in frequency is observed.

The UV – VIS spectrum of **C4** (in the appendices) displayed a $\pi \rightarrow \pi$ * transition at 384.00 nm, which may be attributed to the MLCT (Metal to Ligand Charge Transfer) from the metal's d orbitals to the anti-bonding orbitals of the ligand. This agrees with previous research on thiosemicarbazone complexes (Mbugua *et al.,* 2020). The absorption bands were below 600 nm, suggesting large crystal field splitting synonymous with square-planar geometry. The n-π* transition is not observed, suggesting a lower range below 200 nm that could not be observed.

Data from the ^{1}H NMR spectrum of **C4** (in the appendices) confirms that the imine proton formed the coordination compound because the shift increased from δ 8.00 ppm in the ligand to δ 8.44 ppm in the complex. Such shifts have been reported in (Serda *et al.,* 2014). The increase could be because this complex is bidentate, so there was increased electron density around the imine bond, and hence the proton peak was observed further downfield. No proton was lost in this complex, which could be because of the methyl protons on the hydrazine nitrogen, which are harder to lose than if it had been one proton. There were also slight changes across the entire structure, probably because of the chelate nature of the complex. However, all the proton peaks

maintained their multiplicity. The methyl protons were observed at δ 3.76 ppm. The amine protons were observed at δ 8.11 ppm. The aromatic protons on the thiophene ring attached to the imine shifted to δ 7.33 ppm and δ 7.47 ppm. The aromatic protons on the other thiophene ring shifted to δ 7.13 ppm, δ 7.41 ppm, and δ 7.56 ppm.

The experimental values of the elemental analysis of **C4** were; N, 11.00; C, 34.71; H, 2.92; S, 25.47 while the theoretical values were; N, 11.09; C, 34.86; H, 2.93; S, 25.38. The deviations in the experimental values were within the agreeable range of ±0.4% for N, C and H, and ±0.7% for S, confirming that the product of interest was synthesized and of expected purity.

The structure of **C4** was determined upon considering all of the characterization techniques explained above.

C4
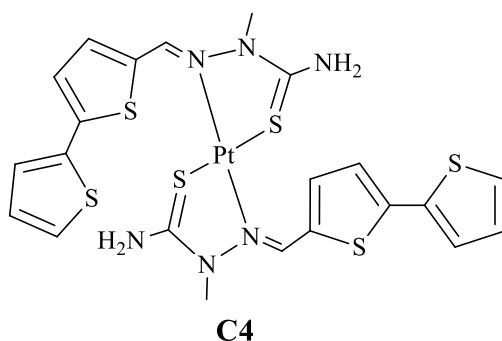
4.3.5 Summary of the Complexes

All the complexes were brightly-colored solid products with sharp melting points. The yields were between 77% and 88%. The FTIR spectroscopic data for the thioamide and imine vibrations provide crucial information regarding the coordination mode of the thiosemicarbazone ligands. There was a notable shift of the thioamide and imine functional groups vibrations to lower frequencies, which is a clear indication that coordination of the metal to the ligand was via the imine nitrogen and the sulphur atom. This is because the chelation of the ligand to the metal center reduces the electron density on the pi bonds, which in turn decreases the pi-character and thus weakens the bond. In this study, the amine frequencies ranged between 1524.32 cm^{-1} and 1709 cm^{-1}. This range is generally lower than that for the free ligands. All UV-Vis absorption bands were below 600 nm. The general trend observed for TSC complexes was that π-π* transition was observed at lower ranges. This can be attributed to the coordination of nitrogen

atoms to the metal center, which confirms its involvement in coordination. The n-π^* transition for **C2** and **C4** is not observed, thus suggesting a lower range (below 200) that could not be captured. Results from UV-Vis indicates that the complexes were square planar because no electronic transitions were observed at longer wavelengths, which is synonymous with large crystal-field splitting because of the large energy gap between the HOMO and the LUMO d-orbitals, which agrees with research by Mbugua *et al.* (2020), and Njogu *et al.* (2019) who had similar observations. The general trend observed for the NMR data of the complexes is the absence of the proton on the nitrogen atom of the NH-H group signal that was present in the spectra of the free ligands. This suggests that the coordination to the central metal atom occurred in the thione neutral form. The experimental results of the elemental analysis of the complexes agree with the theoretical calculations with deviations of ±0.4% for N, C and H, and ±0.7% for S (Mbugua *et al.,* 2020). This confirms the suggested structure and the coordination mode of the complexes. The data also confirms that the synthesized compounds were pure.

4.4 Anticancer Studies

The cytotoxicity of the TSC ligands and their respective complexes were screened against four human cell lines. Three of them (HELA, HT-29 and Caco-2) were cancerous, while the KMST-6 was a non-cancerous skin cell line. The cells were cultured before being treated with different concentrations of the ligands and complexes. Their responses to the treatments were assessed using an MTT assay. There were also notable morphological changes to the cells with regards to their sizes and shapes.

4.4.1 Cytotoxicity Assays

The cytotoxicity of the complexes was found to be better than their corresponding free ligands for **L1**, **L2** and **L4**. **L3** was an outlier, as it was lethal to HeLa (IC_{50} = 0.107 µg/mL), Caco-2 (IC_{50} = 3.412 µg/mL), and HT-29 (IC_{50} = 0.6886 µg/mL) cell lines at lower concentrations than *Cis*platin. However, it was also lethal to the non-cancerous cell line, KMST (IC_{50} = 2.1 µg/mL), meaning it has poor selectivity. Since **L3** has broad spectrum, targeted drug delivery can be considered when administering the compound. **C1** was toxic to HeLa (IC_{50} = 45.38 µg/mL) and Caco-2 (IC_{50} = 45.42 µg/mL), and had a minimal effect on the KMST-6 (IC_{50} = 78.99 µg/mL) cells. **C2** was better than *Cis*platin for HT-29 (IC_{50} = 31.63 µg/mL) and Caco-2 (IC_{50} = 41.82

μg/mL) cell lines and was minimally harmful to the non-cancerous KMST-6 (IC_{50} = 98.32 μg/mL) cells. **C3** was highly lethal on HeLa cells (IC_{50} = 0.0001973 μg/mL) and did not affect the non-cancerous KMST-6 cells at all, showing high selectivity. However, **C3** was not toxic on Caco-2 and HT-29 cell lines. **C4** did not affect the non-cancerous cell line, but it was not as good as **C2** and **C3** on the cancerous cell lines. It had (IC_{50} = 95.27 μg/mL) HeLa and (IC_{50} = 0.62.33 μg/mL) Caco-2. The excellent selectivity in the complexes can be attributed to the N and S donor ligands used. Other platinum-based drug molecules like *cis*platin have been found to have high resistance and low selectivity because of their affinity for bioligands with Sulphur donors like peptides, proteins and amino acids (Motswainyana *et al.,* 2013). In the case of *cis*platin, platinum is activated by binding to water molecules when it is introduced into a biological system. However, sometimes it coordinates with Sulphur-containing bioligands, such as cysteine, glutathione, methionine, and metallothionein (Qi *et al.,* 2019). When this happens, the platinum-based drug is unable to function as it should. Since some cancer cells contain high levels of these bioligands, they are likely to disturb the functioning of the medications before reaching the targeted DNA. This observation is believed to lead to the resistance of many of the current metal-based anti-tumour drugs. That is why this study emphasizes complexes with N and S donor ligands like the thiosemicarbazone complexes. The IC_{50} (μg/mL) values for ligands and complexes are as shown in Table 4.4. The results were compared to *cis*platin as indicated in the last row.

Table 4.4: IC_{50} (μg/mL) values for ligands and complexes

COMPOUND	HeLa	Caco-2	HT-29	KMST-6
L1	>100	>100	>100	>100
L2	>100	>100	>100	>100
L3	0.107	3.412	0.6886	2.1
L4	>100	>100	>100	>100
C1	45.38	45.42	39.77	78.99
C2	57.53	41.82	31.63	98.32
C3	0.0001973	>100	>100	>100
C4	95.27	62.33	>100	>100
*Cis*platin	0.1099	48.83	35.5	100

70

4.4.2 Cell Viability Graphs

As shown in Figures 17, 18, and 19, different compounds showed varying effects on the cell lines, and some of them were better than *cis*platin in terms of cell viability. Compounds that were lethal to cancerous cell lines (HeLa, Caco-2 and HT-29) have good potential for anti-cancer agents. However, those that were lethal to KMST-6, a non-cancerous cell line lack selectivity.
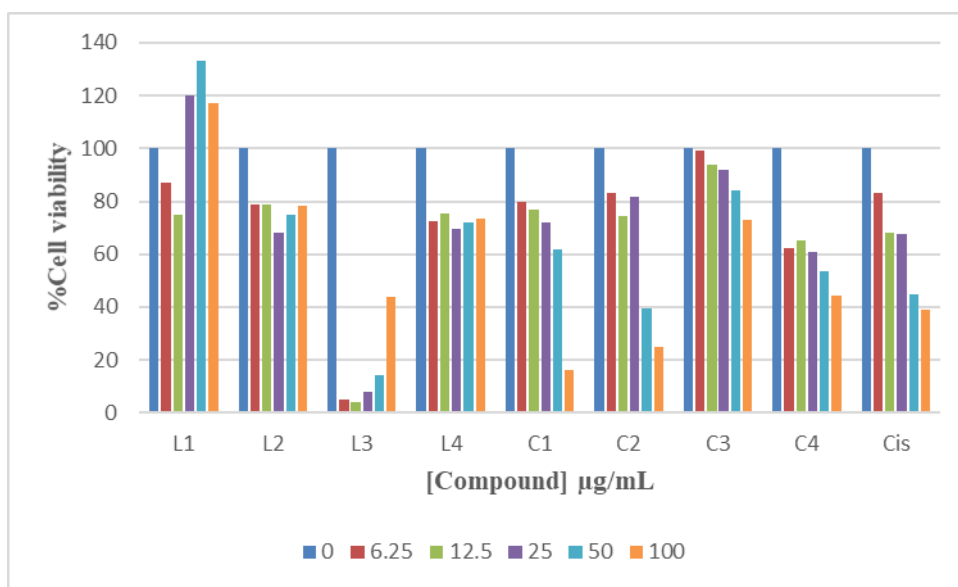
Figure 4.16 represents the HeLa viability graph of the compounds at 6.25, 12.5, 25, 50 and 100 µg/mL. **L3** was toxic at 6.25, 12.5, 25, and 50 µg/mL. Its toxicity at 6.25, 12.5, and 25 µg/mL was constant. However, it was not toxic at 100 µg/mL. **C1** was toxic at 50 and 100 µg/mL, but the highest toxicity was experienced at 100 µg/mL. **C3** was toxic at all the concentrations; (6.25, 12.5, 25, 50 and 100 µg/mL). It exhibited the highest toxicity at 25, 50 and 100 µg/mL, and the toxicity remained constant at the three concentrations. **C2** and **C4** was toxic at the highest concentration of 100 µg/mL. **L1, L2,** and **L4** were not toxic, even at the highest concentration tested (100 µg/mL).
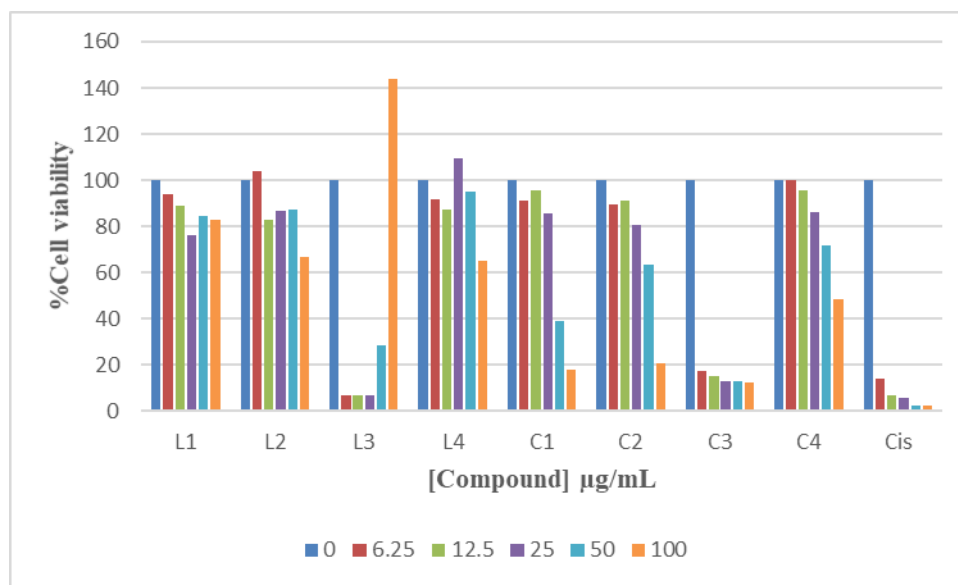
Figure 4.16: HeLa viability graph

Figure 4.17 represents the Caco-2 viability graph of the compounds at 6.25, 12.5, 25, 50 and 100 µg/mL. **L3** was toxic at all the concentrations and was most toxic at 12.5 µg/mL. **C1**, **C2** and **C4**

were toxic at 100 µg/mL. **L1, L2, L4**, and **C3** were not toxic, even at the highest concentration tested (100 µg/mL).

Figure 4.17: Caco-2 viability graph

Figure 4.18 represents the KMST-6 viability graph of the different compounds at 6.25, 12.5, 25, 50 and 100 µg/mL. **L3** was toxic at all concentrations tested. **C1** and **C2** were toxic at 100 µg/mL. **L1, L2, L4**, **C3** and **C4** were not toxic at the highest concentration tested (100 µg/mL).
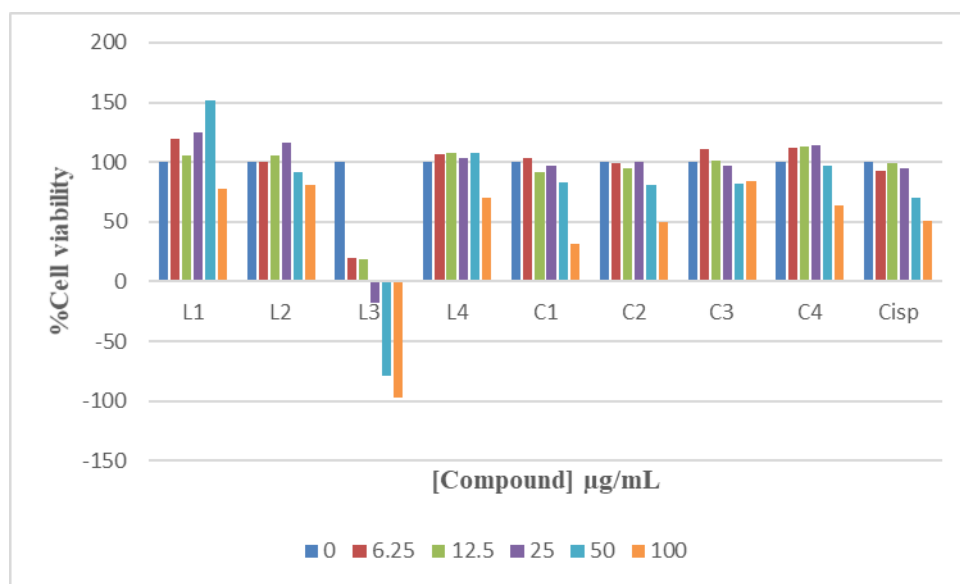
Figure 4.18: KMST-6 viability graph

4.4.3 Morphological Changes Observed in the Cells

As observed in Figure 20, bioassay tests on the HeLa cell line showed apparent morphological changes in the cells by **C1** and **C2**.

Untreated cells

C2

C1

Cisplatin

Figure 3: Illustration of observed morphological changes

The morphological changes include cell shrinking, membrane blebbing, formation of apoptotic bodies, and cell detachment. The effects were compared to *cis*platin, and they showed some similarities. The changes indicate that the cells were affected by the compounds. Comparable results were observed in other cell lines and by different complexes. These results conform with what (Qi *et al.,* 2018). The tests were done in a 24-hour period with μg/mL concentration of the compounds.

CHAPTER 5
CONCLUSION AND RECOMMENDATIONS

5.1 Conclusion

Four thiosemicarbazone ligands were successfully synthesized and characterized usingFTIR, UV-Vis, ^{1}H NMR, ^{13}C NMR, elemental analysis and XRD for the available crystals. FTIR was used to confirm the successful synthesis of the ligands, and the structure was elucidated from both 1D and 2D NMR techniques. Data from UV-Vis confirmed that the compounds were aromatic and had atoms with non-bonding orbitals because they showed two intra-ligand bands, which are attributed to the n-π* transitions and the **π-π*** transitions. XRD data confirmed the structure **L2** forms a monoclinic P21/c space system with 4-unit molecules packed into the crystal unit and has three planes of symmetry. Elemental analysis of the ligands confirmed their purity, as the experimental values had minor deviations from the theoretical values.

Four platinum(II) thiosemicarbazone complexes were successfully synthesized from the respective thiosemicarbazone ligands and characterized using FTIR, ^{1}H NMR and elemental analysis. FTIR and ^{1}H NMR data were used to confirm the coordination mode of the complexes, and it suggests that the ligands coordinated in the thione form. The ligands also coordinated to the platinum metal atom in a bidentate manner via the sulphur and nitrogen atoms, and **L4** was a chelate. **L1** coordinated to the metal center by proton loss. UV-Vis data proves that the complexes are square planar. Elemental analysis was used to confirm the purity of the complexes as the experimental values had minor deviations from the theoretical values.

Anti-cancer analysis on the four ligands and complexes for HELA, Caco-2, HT-29 and KMST-6 human cell lines were completed successfully, and *Cis*platin was made. Some morphological changes were observed, including cell shrinking, membrane blebbing, formation of apoptotic bodies, and cell detachment. Unlike the other ligands that had less activity than their complexes, **L3** was an outlier, as it was lethal to Caco-2, HT-29 and HeLa cell lines at low concentrations than *Cis*platin. **C1** was a good choice for Caco-2 and HT-29 and had a minimal effect on the KMST-6 cells. **C2** was better than *Cis*platin for HT-29 and Caco-2 cell lines and was minimally harmful to the non-cancerous KMST-6 cells. **C3** was highly lethal on HeLa cells and did not

76

affect the non-cancerous KMST-6 cells at all. Although **C4** did not affect the non-cancerous cell lines, it didn't have as many positive effects as **C2** and **C3** on the cancerous cell lines.

Generally, most complexes had better anti-cancer activity than the free ligands, suggesting that complexation improved the biological activity of the compounds. **C1**, **C2** and **C3** had better activity than *cis*platin on some cell lines, showing that bulkier ligands could indeed have better activity than their lighter counterparts. This means that the bulky ligands protect the metal center to prevent unnecessary ligand exchange reactions and give better selectivity. However, **C4**, which as a dimer, had lower activity than **C2** and **C3**, meaning that very bulky ligands might have reduced biological activity to some extent.

5.2 Recommendations

1. Since this work focused on using platinum metal centers, it is essential to carry out further research to understand the effect of other metal centers on cytotoxicity. Ruthenium would be a good candidate for further investigation since it is relatively inert, a member of the platinum group and some studies show that ruthenium complexes have good biological properties.

2. *In vivo* studies on (**C2)** and (**C3)** could be undertaken to determine their effectiveness in treating colorectal cancer because of their positive effects on Caco-2 and HT-29.

3. It is essential to conduct *in vivo* tests on (**C3)** to further survey its effectiveness on cervical cancer, owing to its positive *in vitro* results on HeLa cell line.

4. Further biological tests such as DNA binding studies should be conducted on the viable complexes (**C1**, **C2** and **C3**), and viable ligand (**L3**) to determine their mechanism of action. This will help to determine the usefulness of these compounds as anti-cancer therapies.

5. The compounds ought to be tested against more cell lines to explore their application to other cancer types. From previous studies, they are likely to have good activity against breast cancer, uterine cancer, liver cancer, kidney cancer, bone marrow cancer, and spleen cancer cell lines.

6. Thiosemicarbazone ligands and complexes have been used in other studies as anti-infective, psychotropic, anti-HIV agents. Therefore, these compounds need to be examined for other biological uses because they may have great potential.

REFERENCES

Abu-Surraha, A. S., Safieha, K. A., Ahmadb, I. M., Abdallac, M. Y., Ayouba, M. T., Qarousha, A. K., (2010). New palladium(II) complexes bearing pyrazole-based Schiff base ligands:Synthesis, characterization and cytotoxicity. *European Journal of Medicinal Chemistry, 45*, 471-475.

Ahmad, N., Anouar, E. H., Tajuddin, a. M., Ramasamy, K., Yamin, B. M., & Bahron, H. (2020). Synthesis, characterization, quantum chemical calculations and anticancer activity of a schiff base NNOO chelate ligand and Pd (II) complex. *PloS one*, 15(4), e0231147

Ahrens, Sebastian, Strassner, & Thomas. (2006). Detour-free synthesis of platinum-bis-NHC chloride complexes, their structure and catalytic activity in the CH activation of methane. *Inorganica Chimica, 389*(15), 4789–4796.

Archna, S. Pathania, P.A. Chawla, (2020). Thiophene-based derivatives as anticancer agents: An overview on decade's work, *Bioorganic Chemistry,* 1, 104026

Archibald, S., & Smith, R. (2013). Protein-Binding Metal Complexes: Noncovalent and Coordinative Interactions. In S. Archibald, & R. Smith, *Comprehensive Inorganic Chemistry II (Second Edition)* 3 (1). 661-682).

Bouchal P, Jarkovsky J, Hrazdilova K, Dvorakova M, Struharova I, Hernychova L, Damborsky J, Sova P & Vojtesek B (2011). The new platinum-based anticancer agent LA-12 induces retinal binding protein 4 in vivo. *Proteome Science,* 9 ,1–9.

Chaturvedi, A.; Herbst, L.; Pusch, S.; Klett, L.; Goparaju, R.; Stichel, D.; Kaulfuss, S.; Panknin, O.; Zimmermann, K.; Toschi, L. (2017). Pan-Mutant-IDH1 Inhibitor BAY1436032 is Highly Effective Against Human IDH1Mutant Acute Myeloid Leukemia In Vivo. *Leukemia*, 1 (31), 2020−2028

Corint, D., Coletti, C., Re, N., Piccirillo, S., Giampà, M., Crestoni, M. E., (2017). Hydrolysis of *cis*- and *trans*platin: structure and reactivity of the aqua complexes in a solvent-free environment. *Royal Society of Chemistry, 7*, 15877-15884

Dasari S & Tchounwou PB (2014). *Cis*platin in cancer therapy: molecular mechanisms of action. *European Journal of Pharmacology* 740 364–378

De Oliveira, J. F., da Silva, A. L., Vendramini-Costa, D. B., da Cruz Amorim, C. A., Campos, J. F., Ribeiro, A. G., … Alves de Lima, M. do C. (2015). Synthesis of thiophene-

thiosemicarbazone derivatives and evaluation of their in vitro and in vivo antitumor activities. *European Journal of Medicinal Chemistry*, 104, 148–156

Ellena J, Gozzo C, Cominetti MR, (2015). Chiral platinum(II) complexes featuring phosphine and chloroquine ligands as cytotoxic and monofunctional DNA-binding agents. *Inorg Chem*. 54(24):11709–11720.

El-Saied, F., El-Aarag, B., Salem, T., Said, G., Khalifa, S., & El-Seedi, H. R. (2019). Synthesis, Characterization, and In Vivo Anti-Cancer Activity of New Metal Complexes Derived from Isatin-N(4)antipyrinethiosemicarbazone Ligand Against Ehrlich Ascites Carcinoma Cells. *Molecules (Basel, Switzerland),* 24(18), 3313-3315.

Graham, J., Muhsin, M. & Kirkpatrick, P. (2004). Oxaliplatin. *Nat Rev Drug Discov,* 3 (1), 11–12

Goldie, J.H. (2001). Drug Resistance in Cancer: A Perspective. *Cancer Metastasis* Rev 20, 63–68

Gunnar, F., Nordberg, Bruce, A. F., & Monica, N. (2014). *Handbook on the Toxicology of Metals* (Vol. 1). Academic Press, 224-500

Johnstone TC, Park GY & Lippard SJ (2014). Understanding and improving platinum anticancer drugs – phenanthriplatin., *Anticancer Research,* 34, 471–476

Jurca, T., Eleonora, M., Vicaş, L., Mureşan, M., & Fritea, L., (2017). Metal Complexes of Pharmaceutical Substances, Spectroscopic Analyses - Developments and Applications, , *IntechOpen*, Retrieved from: https://www.intechopen.com/books/spectroscopic-analyses-developments-and-applications/metal-complexes-of-pharmaceutical-substances on 9th July 2021. DOI: 10.5772/65390

Kayed A. Abu-Safieh, Adnan S. Abu-Surrah, Hani D. Tabba, Huda A. AlMasri, Randa M. Bawadi, Fadila M. Boudjelal, Lubna H. Tahtamouni, (2016). Novel Palladium(II) and Platinum(II) Complexes with a Fluoropiperazinyl Based Ligand Exhibiting High Cytotoxicity and Anticancer Activity In Vitro, *Journal of Chemistry*, vol. 2016, Article ID 7508724, 1-7.

Kellinger MW, Park GY, Chong J, Lippard SJ & Wang D. (2013) Effect of a monofunctional phenanthriplatin-DNA dduct on RNA polymerase II transcription fidelity and translesion synthesis. *Journal of the American Chemical Society,* 135, 13054–13061

Kettle, S. (1996). *Physical Inorganic Chemistry: A Coordination Chemistry Approach.* Springer, 95-120

Khanmohammadi, H., Salehifaed, M., & Abnosi, M (2009). Synthesis, characterization, biological and thermal studies of Cu (II) complexes of Salen and tetrahedrosalen ligands. Journal of the Iranian Chemical Society, 6(2), 300-309

Kozubík A, Horváth V, Švihálková-Šindlerová L, Soucek K, Hofmanová J, Sova P, Kroutil A, Žák F, Mistr A & Turánek J (2005). High effectiveness of platinum (IV) complex with adamantylamine in overcoming resistance to *cis*platin and suppressing proliferation of ovarian cancer cells in vitro. *Biochemical Pharmacology,* 69, 373–383.

Kumble, D., Geetha, P. M., & Asha, P. F. (2017). Application of Metal Complexes Of Schiff Bases As An Antimicrobial Drug: A Review Of Recent Works. *Internation Journal of Current Pharmaceutical research, 9*(3), 27-30.

Lee, J. (2009). *Concise inorganic chemistry* (Vol. 6). Blackwell Science Ltd, 500-720.

Lévi, F., Metzger, G., Massari, C. (2012). Oxaliplatin. *Clin Pharmacokinet,* 38 (1), 1–21

Liu K-J, Guan Z-Z, Liang Y, Yang X-Q, Peng J, Huang H, Qing-Xiang S, Meng-Zhao W, Zhu Y-Z & Wu C-P. (2014). A double-blind, randomized phase II study of dicycloplatin plus placlitaxel versus carboplatin plus paclitaxel as first-line therapy for patients with advanced non-small-cell lung cancer. *Archives of Medical Science,* 10 (1). 717–724

Marko´, I, E, S. Ste´rin, O. Buisine, G. Mignani, P. Branlard,B. Tinant and J.-P. (2002) *Declerq, Science*, 298 (1), 204

Mbugua, S. N., Njenga, L. W., Odhiambo, R. A., Wandiga, S. O., Meyer, M., Sibuyi, N., Onani, M. O. (2020). Synthesis, Characterization, and DNA-Binding Kinetics of New Pd(II) and Pt(II) Thiosemicarbazone Complexes: Spectral, Structural, and Anticancer Evaluation. *Journal of Chemistry*, 2020 (1), 1–17.

Mbugua, S. N., Sibuyi, N. R. S., Njenga, L. W., Odhiambo, R. A., Wandiga, S. O., Meyer, M., Onani, M. O. (2020). New Palladium(II) and Platinum(II) Complexes Based on Pyrrole Schiff Bases: Synthesis, Characterization, X-ray Structure, and Anticancer Activity. ACS Omega, 5 (25), 14942-14954.

Motswainyana, W. M., Onani, M. O., & Madiehe, A. M. (2012). Bis(ferrocenylimine)palladium(II) and platinum(II) complexes: Synthesis, molecular structures and evaluation as antitumor agents. *Polyhedron, 41*(1), 44-51.

Motswainyana, W., Onani, M. O., Madiehe, A. M., Morounke, S., Jeroen, J., & Lucvan, M. (2013). Imino-quinolyl palladium(II) and platinum(II) complexes: Synthesis, characterization, molecular structures and cytotoxic effect. *Inorganica Chimica Acta, 400*, 197-202.

Nabil, Y., Ahmed, M., El-Seidya, M., Schiavonib, B., Castanob, F., & Ragainib, E. ((2012). Thiosemicarbazone copper complexes as competent catalysts for olefin cyclopropanations. *Journal of Organometallic Chemistry, 714*(1), 94-103.

Ndagi, U, Mhlongo, N, Soliman, M, (2017). Metal complexes in cancer therapy – an update. *Drug Design, Development and Therapy*. 11(1), 599–616

Netalkar, P. P., Netalkar, S. P., & Revankar, V. K. (2015). Transition metal complexes of thiosemicarbazone: Synthesis, structures and invitro antimicrobial studies. *Polyhedron, 100*(1), 215-222.

Niioka T, Uno T, Yasui-Furukori N, (2007). Pharmacokinetics of low-dose nedaplatin and validation of AUC prediction in patients with non-small-cell lung carcinoma. *Cancer Chemother Pharmacol*. 59(5):575–580

Njogu, R., Fodran, P., Tian, Y., Njenga, L., Kariuki, D., & Amir, Y.,(2019). Electronically Divergent Triscyclometalated Iridium(III) 2-(1-naphthyl)pyridine Complexes and Their Application in Three-Component Methoxytrifluoromethylation of Styrene. *Synlett, 30*, A-G.

Nyawade, E. A., Sibuyi, N. R. S., Meyer, M., Lalancette, R., & Onani, M. O. (2020). Synthesis, characterization and anticancer activity of new 2-acetyl-5-methyl thiophene and cinnamaldehyde thiosemicarbazones and their palladium (II) Complexes. Inorganica Chimica Acta, 2021 (1), 120036.

Odhiambo, R. A., Aluoch, A. O., Njenga, L. W., Kagwanja, S. M., Wandiga, S. O., & Wendt, O. F. (2018). Synthesis, characterisation and ion-binding properties of oxathiacrown ethers appended to $[Ru(bpy)_2]^{2+}$. Selectivity towards Hg^{2+}, Cd^{2+} and Pb^{2+}. *Royal Society of Chemistry (RSC) Adv 8*(7), 3663-3672.

Pan, S. Y., Litscher, G., Gao, S. H., Zhou, S. F., Yu, Z. L., Chen, H. Q., Zhang, S. F., Tang, M. K., Sun, J. N., & Ko, K. M. (2014). Historical perspective of traditional indigenous medical practices: the current renaissance and conservation of herbal resources. Evidence-based complementary and alternative medicine : *eCAM*, 525340.

Parkin DM, Youlden DR, Chitsike I, Chokunonga E, Couitchéré L, Gnahatin F, Nambooze S, Wabinga H, Aitken JF. (2021). Stage at diagnosis and survival by stage for the leading childhood cancers in three populations of sub-Saharan Africa. *Int J Cancer.* 148(11):2685-2691.

Prajapati, N. P., & Patel, H. D. (2019). Novel thiosemicarbazone derivatives and their synthesis. *Synthetic Comunications, 49*(21), 2767-2804.

Pitt, J. M.; Vetizou, M.; Daillere, R.; Roberti, M. P.; Yamazaki, T.; Routy, B.; Lepage, P.; Boneca, I. G.; Chamaillard, M.; Kroemer, G., (2016). Resistance Mechanisms to Immune Checkpoint Blockade in Cancer: Tumor-Intrinsic and -Extrinsic Factors. *Immunity,* 1 (44), 1255−1269

Richard A. Ward, Stephen Fawell, Nicolas Floc'h, Vikki Flemington, Darren McKerrecher, and Paul D. Smith. (2021). *Chemical Reviews*, 121 (6), 3297-3351

Saad, H.A., Youssef M.M., Mosselhi M.A., Microwave assisted synthesis of some new fused 1, 2, 4-triazines bearing thiophene moieties with expected pharmacological activity, *Molecules.* 16 (2011) 4937-4957

Sava G & Dyson PJ (2006) Metal-based antitumour drugs in the post genomic era. *Dalton Transactions* 16 1929–1933

Serda, M., Kalinowski, D. S., Rasko, N., Potůčková, E., Mrozek-Wilczkiewicz, A., Robert, M., (2014). Exploring the Anti-Cancer Activity of Novel Thiosemicarbazones Generated through the Combination of Retro-Fragments: Dissection of Critical Structure-Activity Relationships. *Plos One.* 9(10), e110291

Sidney, Fran*cis*, Alan, & Kettle. (1969). *Coordination compounds.* Nelson, 94-118.

Shah, R., & Verma, P. K. (2018). Therapeutic importance of synthetic thiophene. *Chemistry Central journal*, 12(1), 137s

Shimada, M., Itamochi, H., & Kigawa, J. (2013). Nedaplatin: a *cis*platin derivative in cancer chemotherapy. *Cancer management and research*, 5, 67–76.

Subasi, E., Atalay, E. B., Erdogan, D., Betül, S., Pakyapan, B., & Kayali, H. A. (2019). Synthesis and characterization of thiosemicarbazonefunctionalized organoruthenium (II)-arene complexes:. *Materials Science & Engineering* 106-108.

Sung, H, Ferlay, J, Siegel, R, Laversanne, M, Soerjomataram, I, Jemal, A, Bray, F, (2021). Global cancer statistics 2020: GLOBOCAN estimates of incidence and mortality

worldwide for 36 cancers in 185 countries. *CA: A cancer journal for clinicians.* https://doi.org/10.3322/caac.21660. Retrieved from https://acsjournals.onlinelibrary.wiley.com/doi/10.3322/caac.21660. On 11th April 2021.

Qi, L., Luo, Q., Zhang, Y., Jia, F., Zhao, Y., & Wang, F. (2019). Advances in toxicological research of the anticancer drug *cis*platin. *Chemical research in toxicology.* 32 (8), 1469-1486

Velazquezd, H. D. and Verpoort, F. (2012). N-heterocyclic carbene transition metal complexes for catalysis in aqueous media. *Chemical Society Reviews.* 41(21), 7032

Wei , L., Easmon , J., Nagi, R., Muegge , B., Meyer, L., & Lewis, J. (2006). 64Cu-azabicyclo[3.2.2]nonane thiosemicarbazone complexes: radiopharmaceuticals for PET of topoisomerase II expression in tumors. *Pubmed, 47*(12), 2034-2041.

Wexselblatt E & Gibson D (2012) What do we know about the reduction of Pt (IV) pro-drugs? *Journal of Inorganic Biochemistry,* 117 220–229

WHO. (2019). Global Cancer Burden in 2018. Retrieved from https://www.who.int/cancer/PRGlobocanFinal.pdf. on 9th July 2020

Xuan, W., Haiyun, Z., & Xiaozhuo, C. (2019). Drug resistance and combating drug resistance in cancer. *Cancer Drug Resist, 2*, 141-160

Yu JJ, Yang X, Song Q, Mueller MD & Remick SC (2014) Dicycloplatin, a novel platinum analog in chemotherapy: synthesis of chinese preclinical and clincal profile and emerging mechanistic studies. *Anticancer Research*, 34 (1). 455–464

Zalba S & Garrido MJ (2013) Liposomes, a promising strategy for clinical application of platinum derivatives. *Expert Opinion on Drug Delivery* 10(1). 829–844

Zhang, Y., Chen, X., Gueydan, C., & Han, J. (2018). Plasma membrane changes during programmed cell deaths. Cell research, 28(1), 9-12

Zhao, M., Cui, Y., Zhao, L., Zhu, T., Lee, R. J., Liao, W., Sun, F., Li, Y., & Teng, L. (2019). Thiophene Derivatives as New Anticancer Agents and Their Therapeutic Delivery Using Folate Receptor-Targeting Nanocarriers. *ACS omega*, 4(5), 8874–8880

Appendix (I) – FTIR Spectra
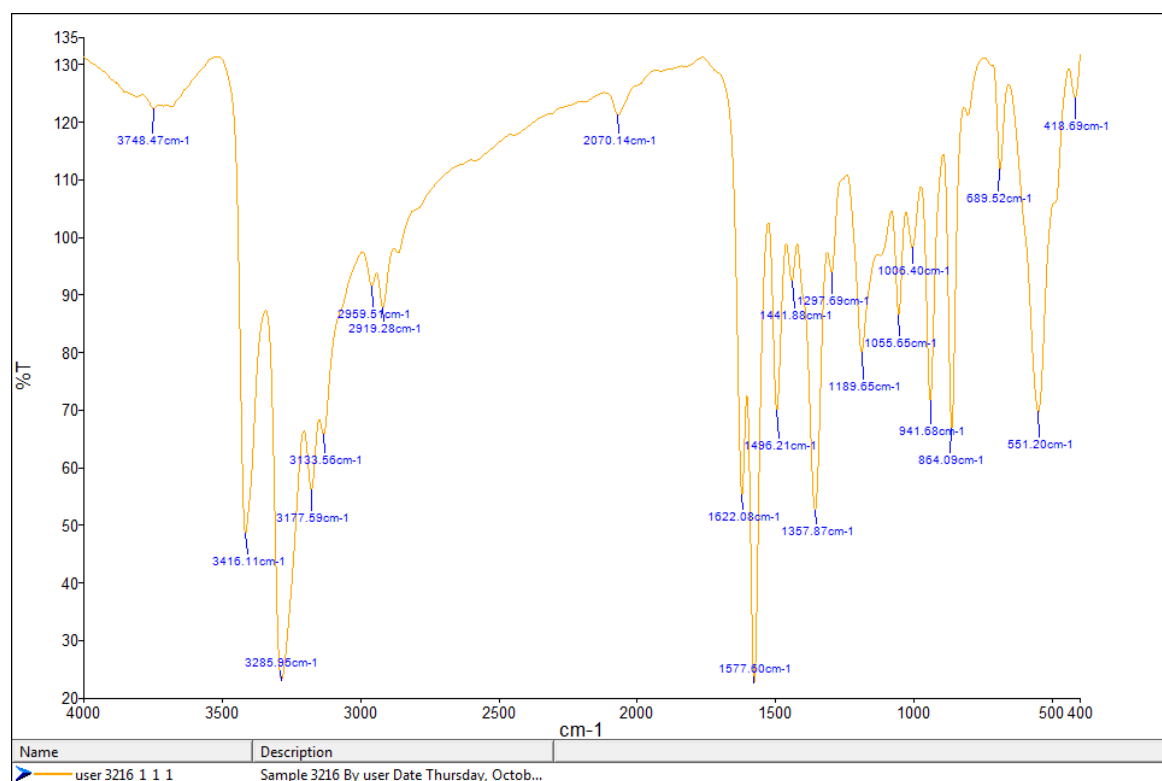
a – **FTIR spectra for L2**
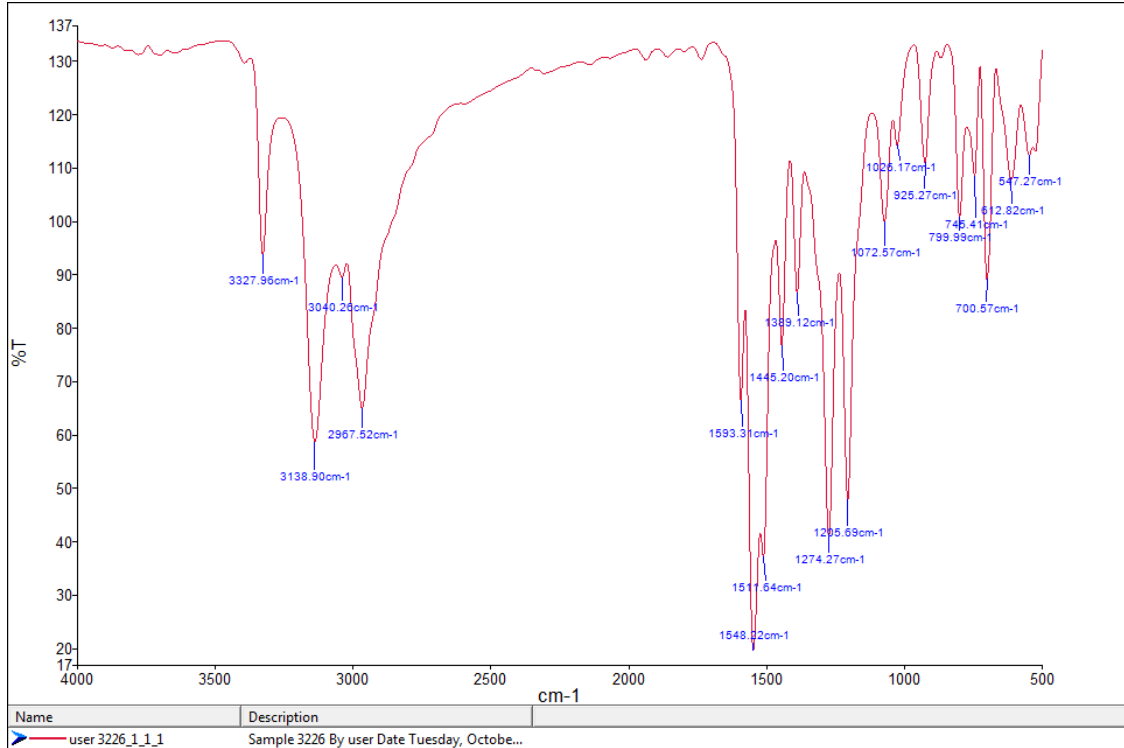
b - **FTIR spectra for L3**
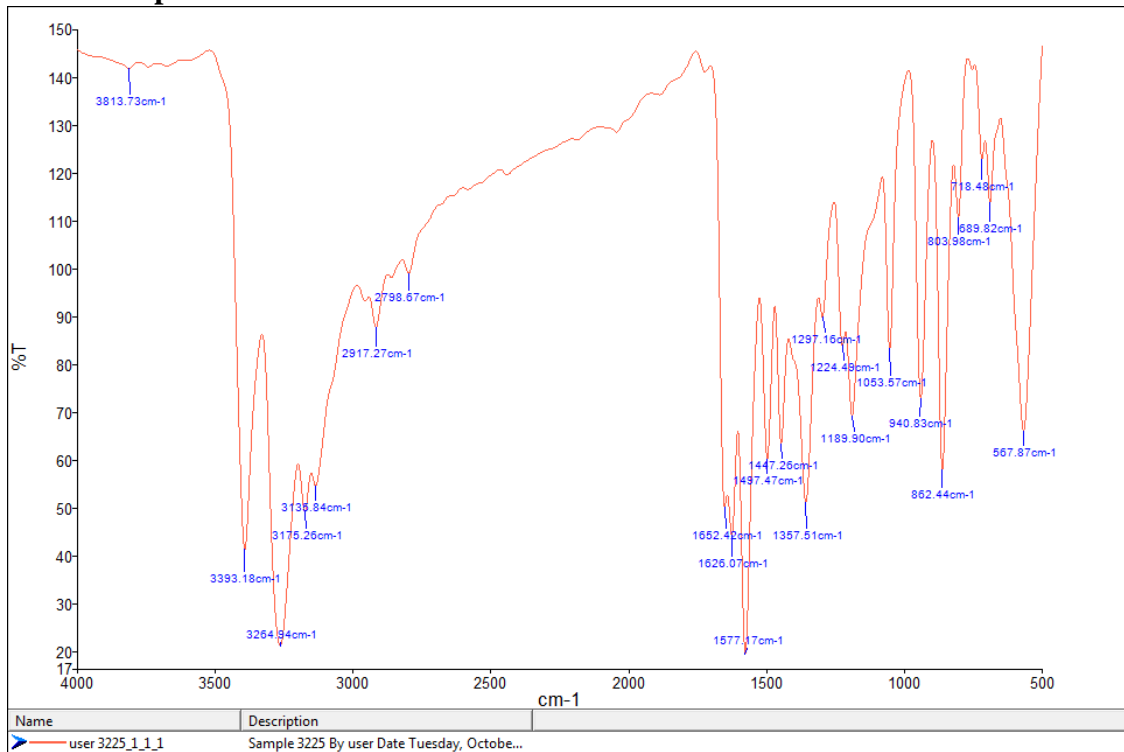
c - **FTIR spectra for L4**
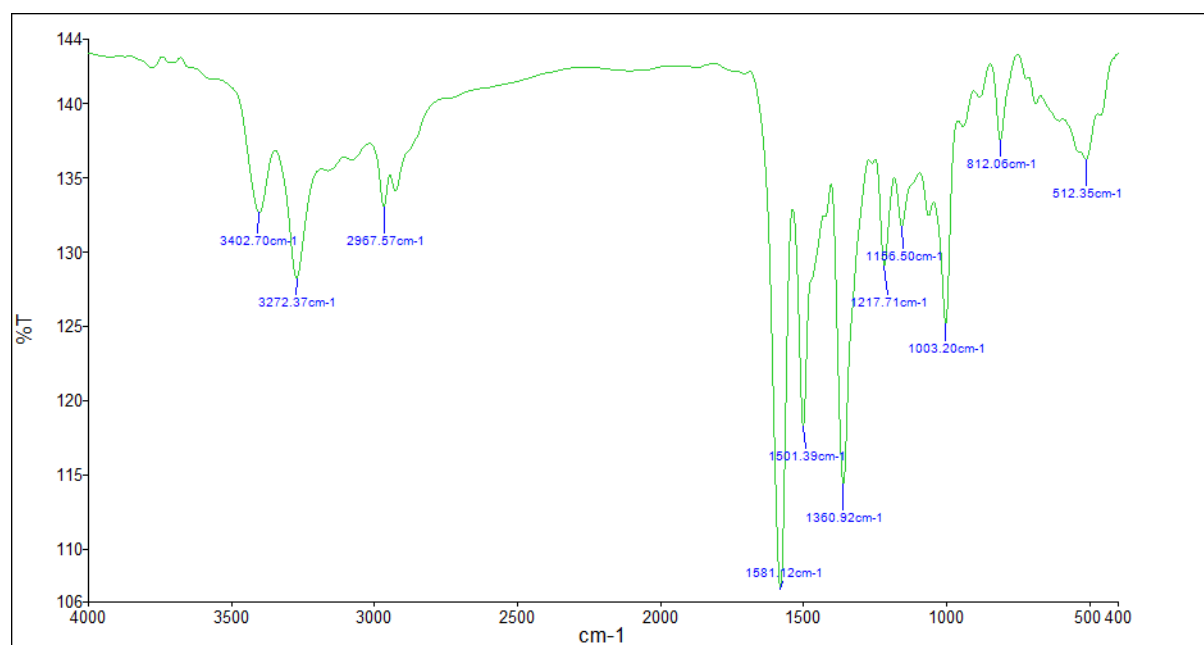
d - **FTIR spectra for C2**
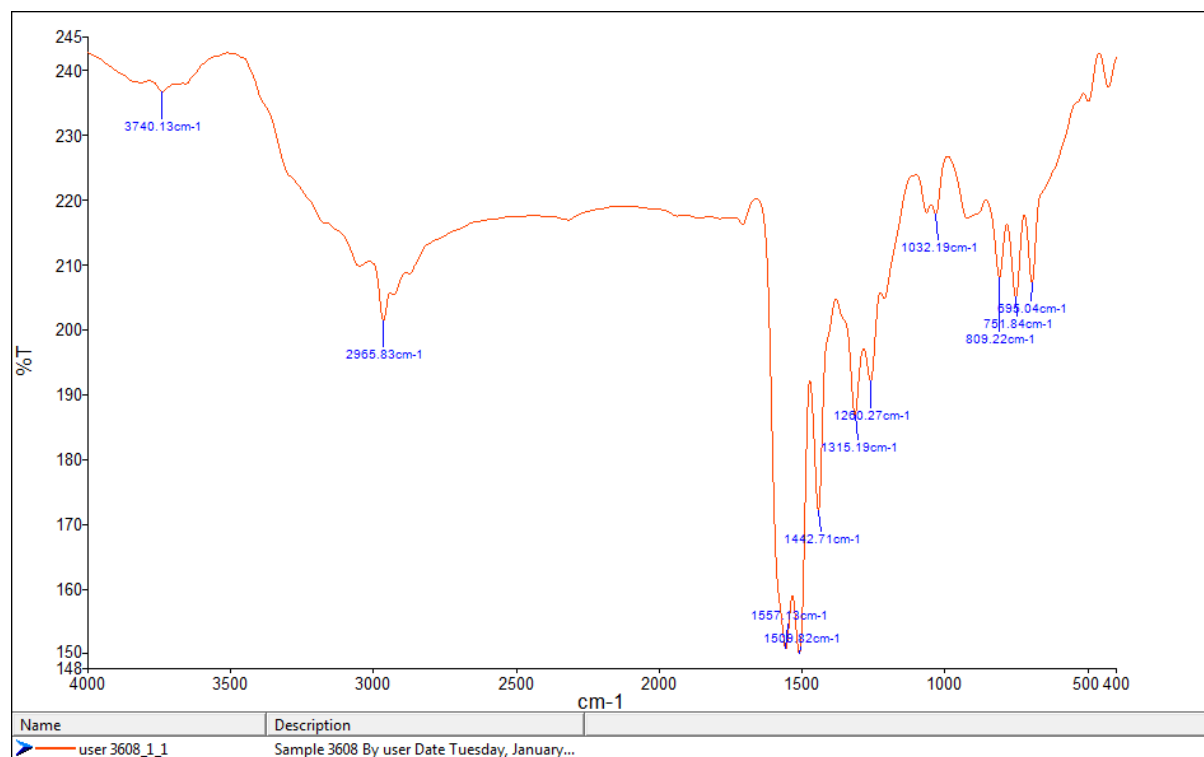
e - **FTIR spectra for C3**
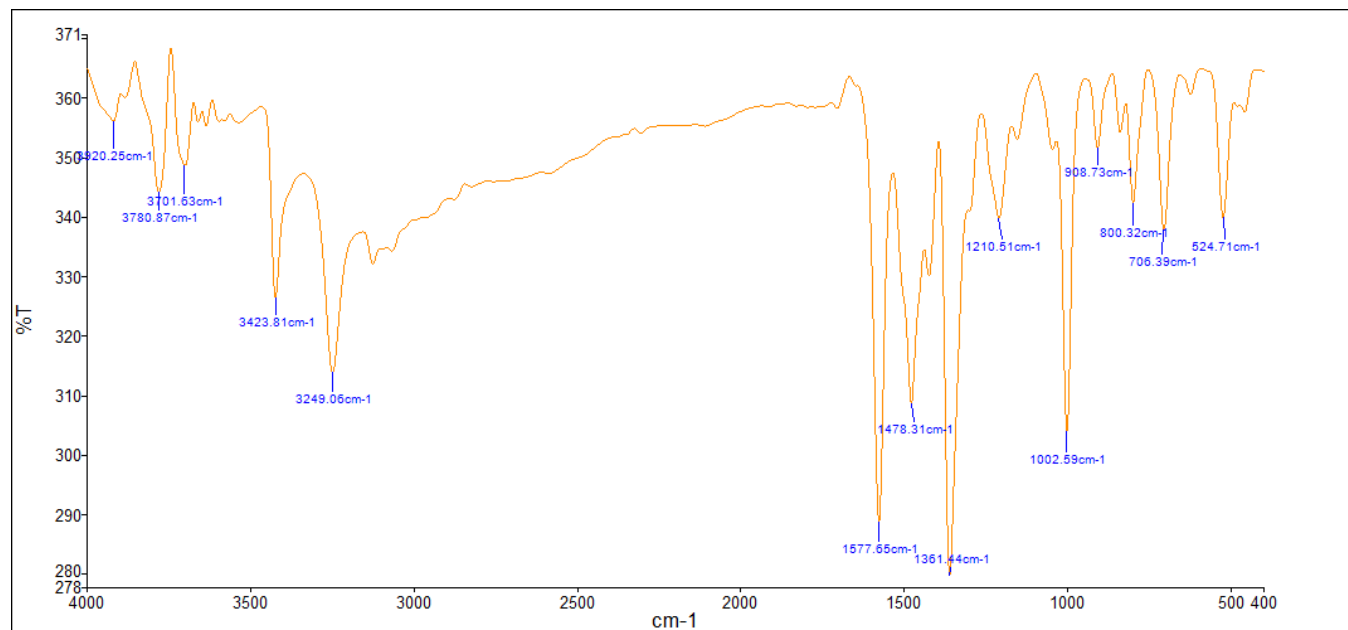
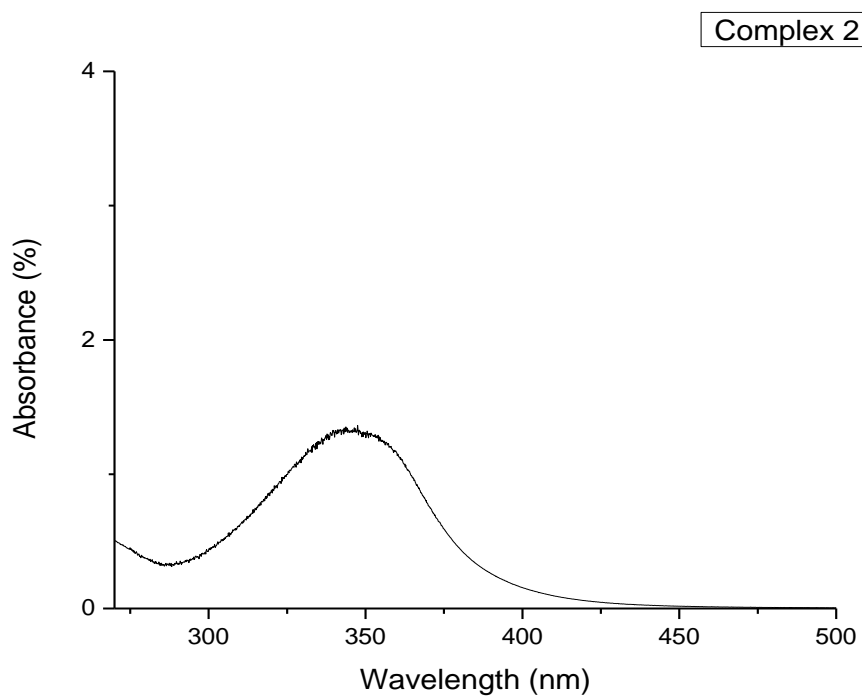**f - FTIR spectra for C4**

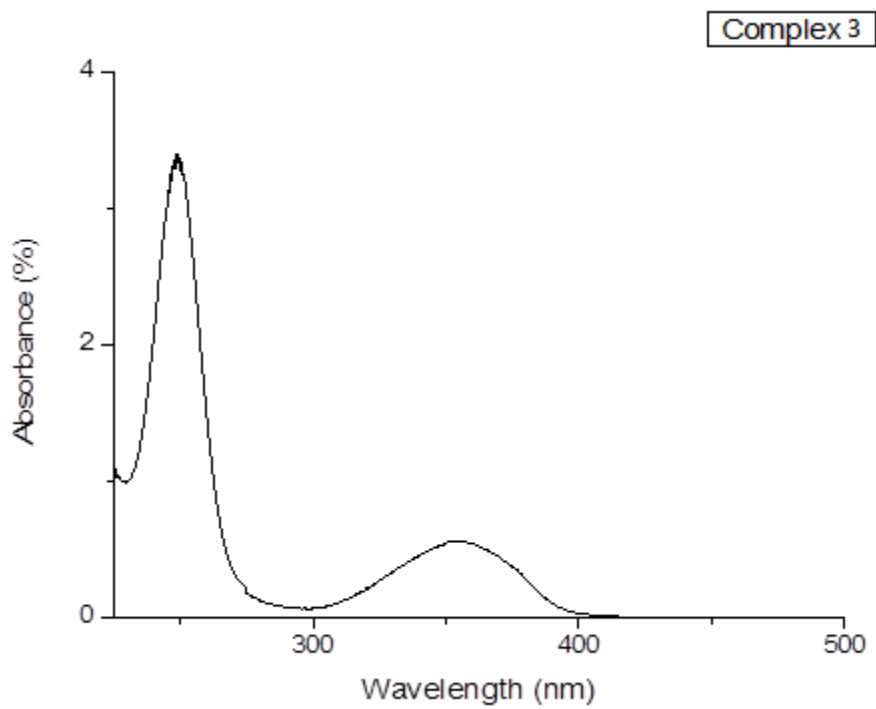## Appendix (II) - UV-Vis Spectra
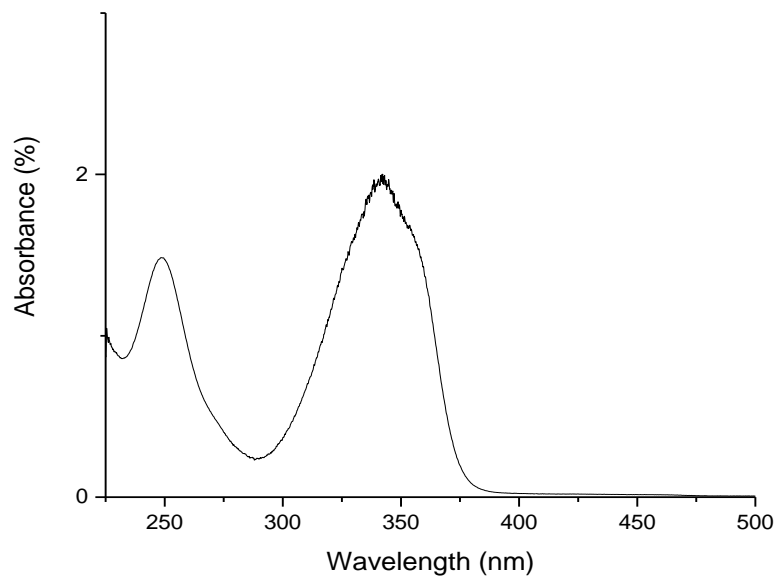
a - UV-Vis spectra for L2
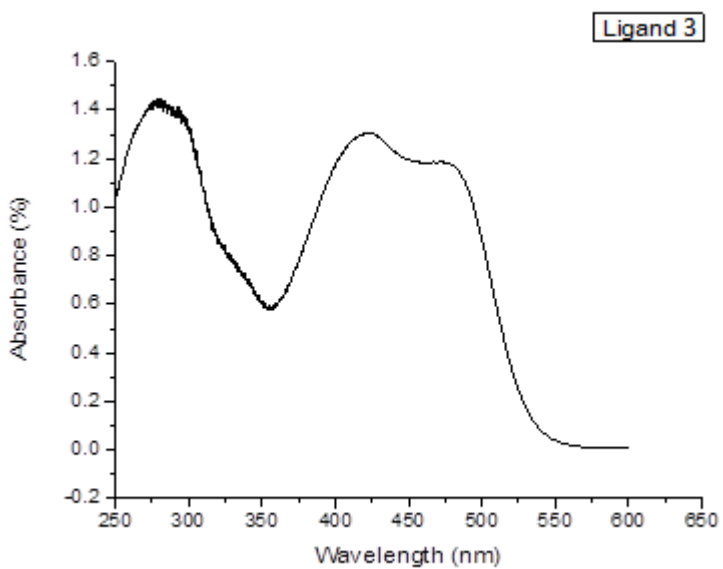
b - UV-Vis spectra for L3
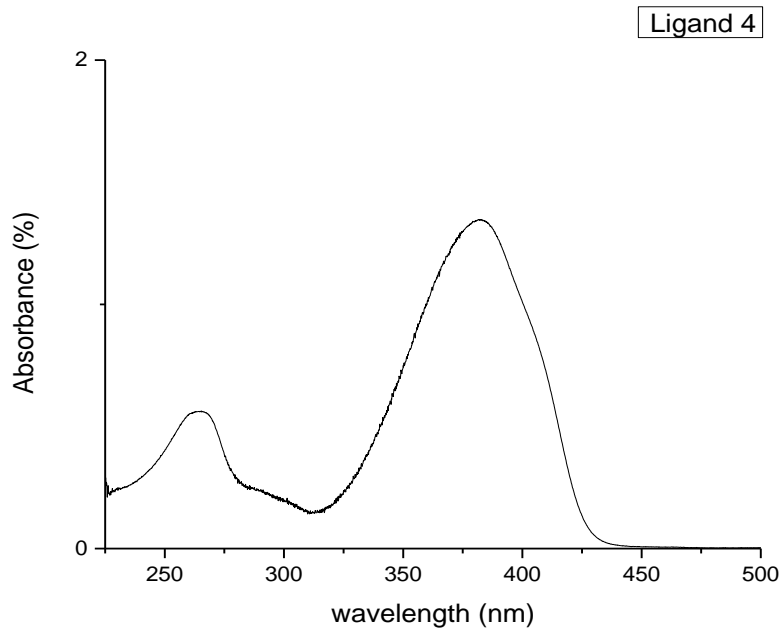
c- UV-Vis spectra for L3
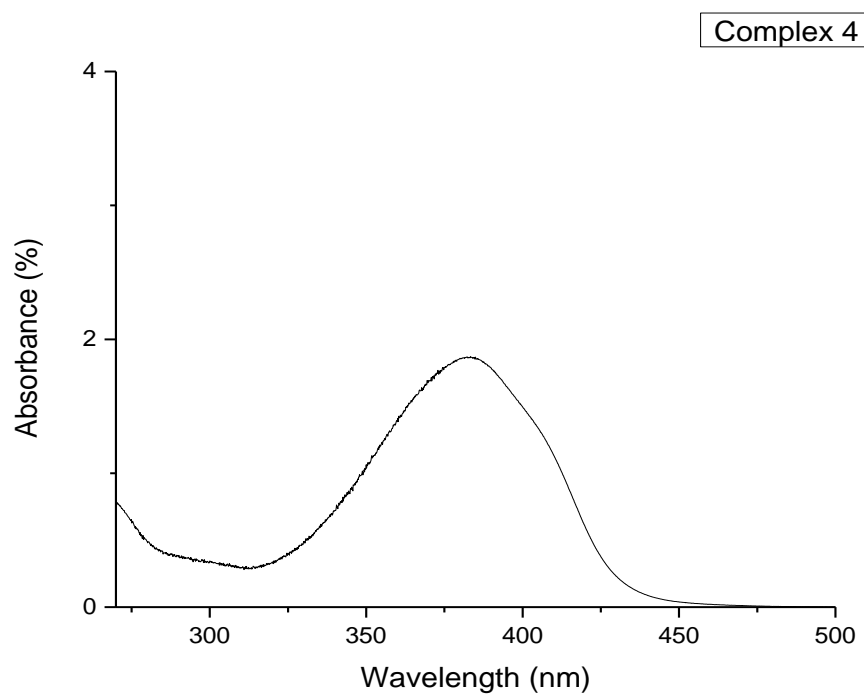
d - UV-Vis spectra for C2

e - UV-Vis spectra for C3
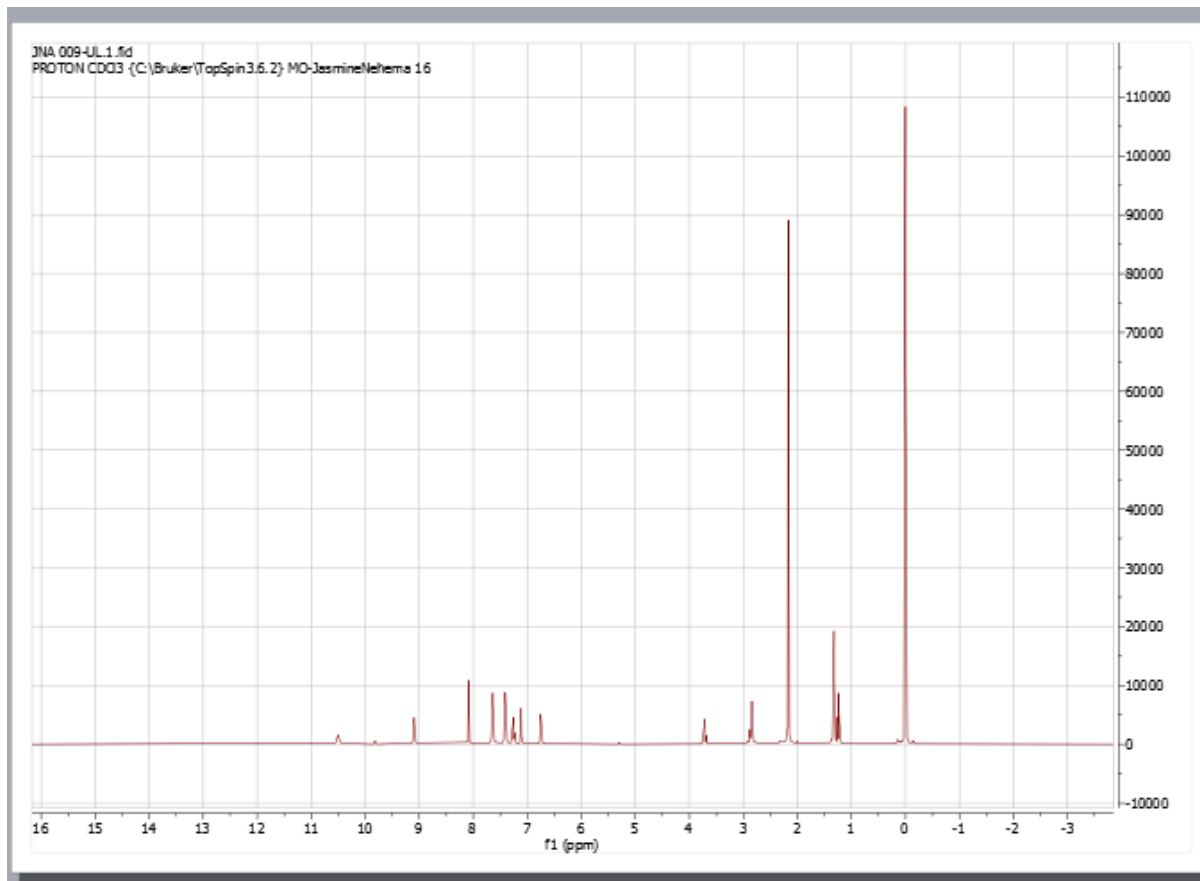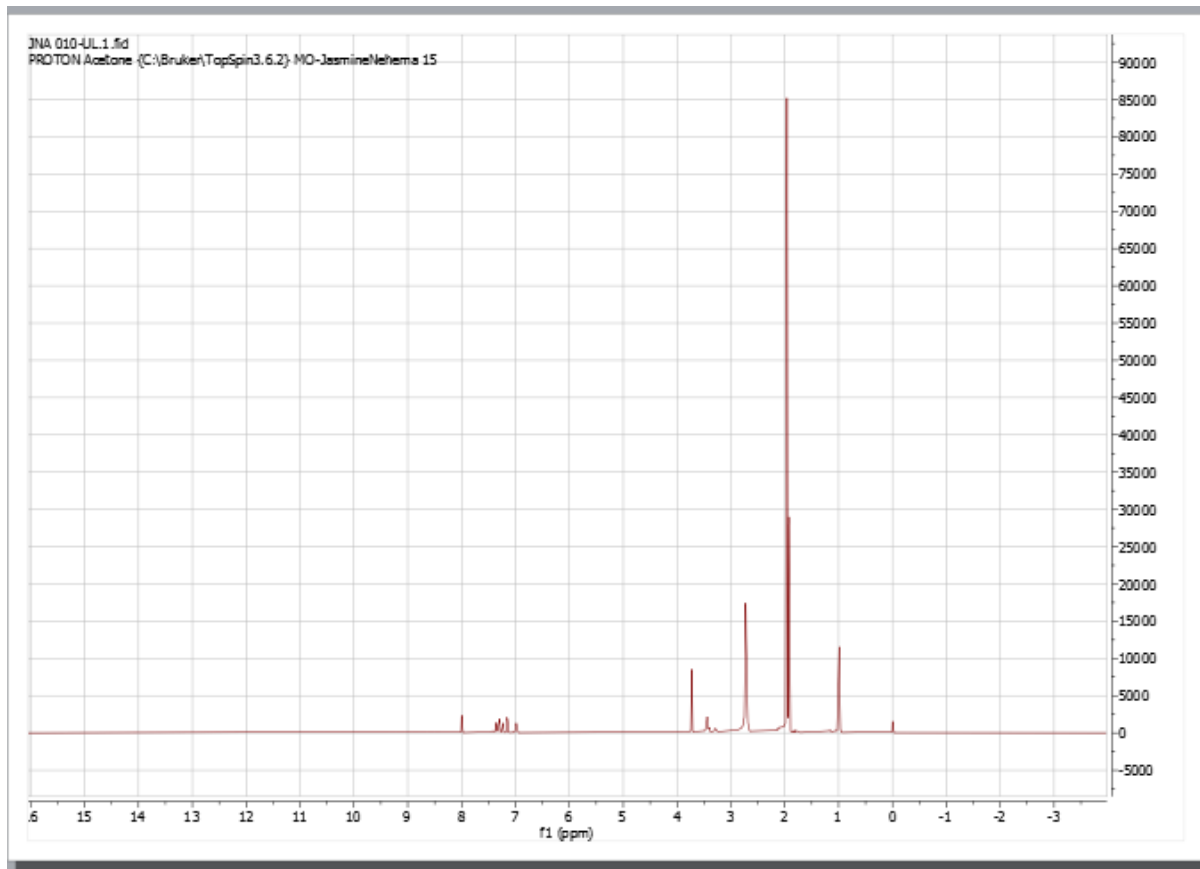
f - UV-Vis spectra for C4

Appendix (III) – ^{1}H NMR Spectra

JNA 008-UL.1.fid
PROTON Acetone {C:\Bruker\TopSpin3.6.2} MO-JasmineNehema 17
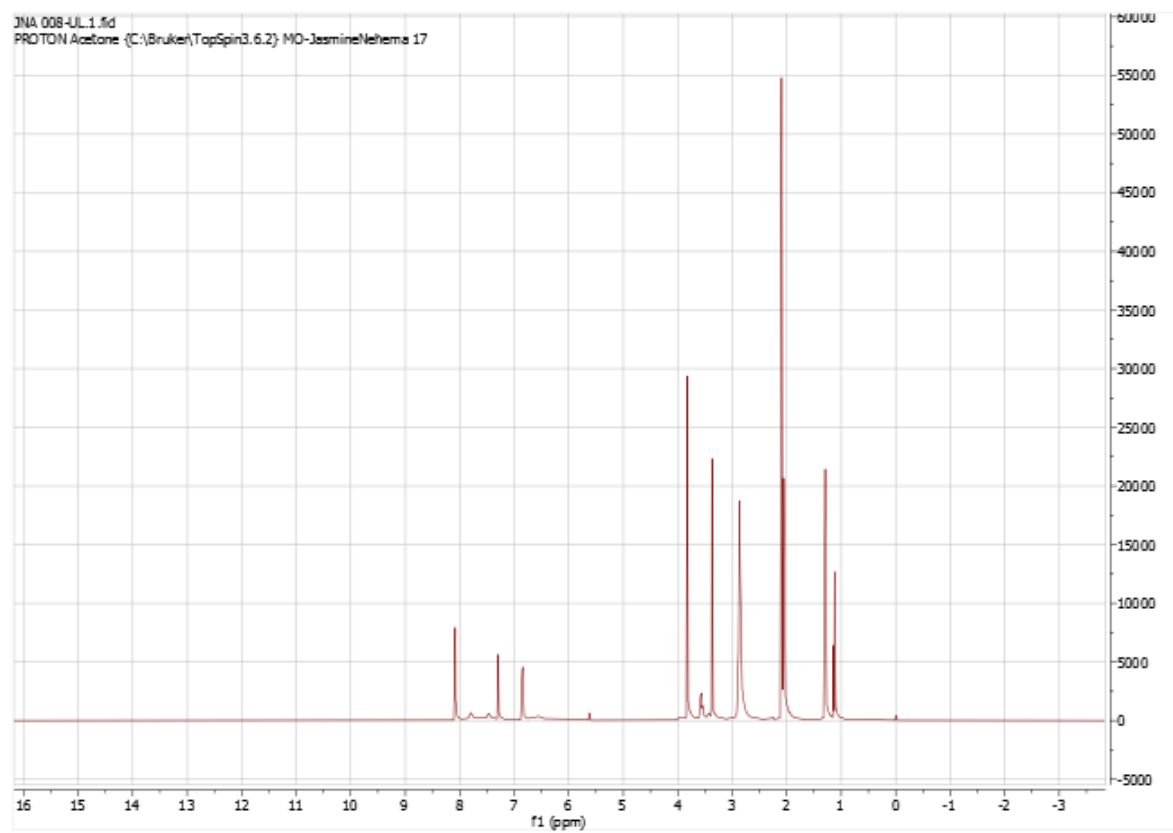
a - ^{1}H NMR Spectra for L2

b - ¹H NMR Spectra for L3

c - ¹H NMR Spectra for L4

d - **¹H NMR Spectra for C2**

PROTON DMSO{C:\Bruker\TopSpin3.6.2} MO-JasmineNehema 22
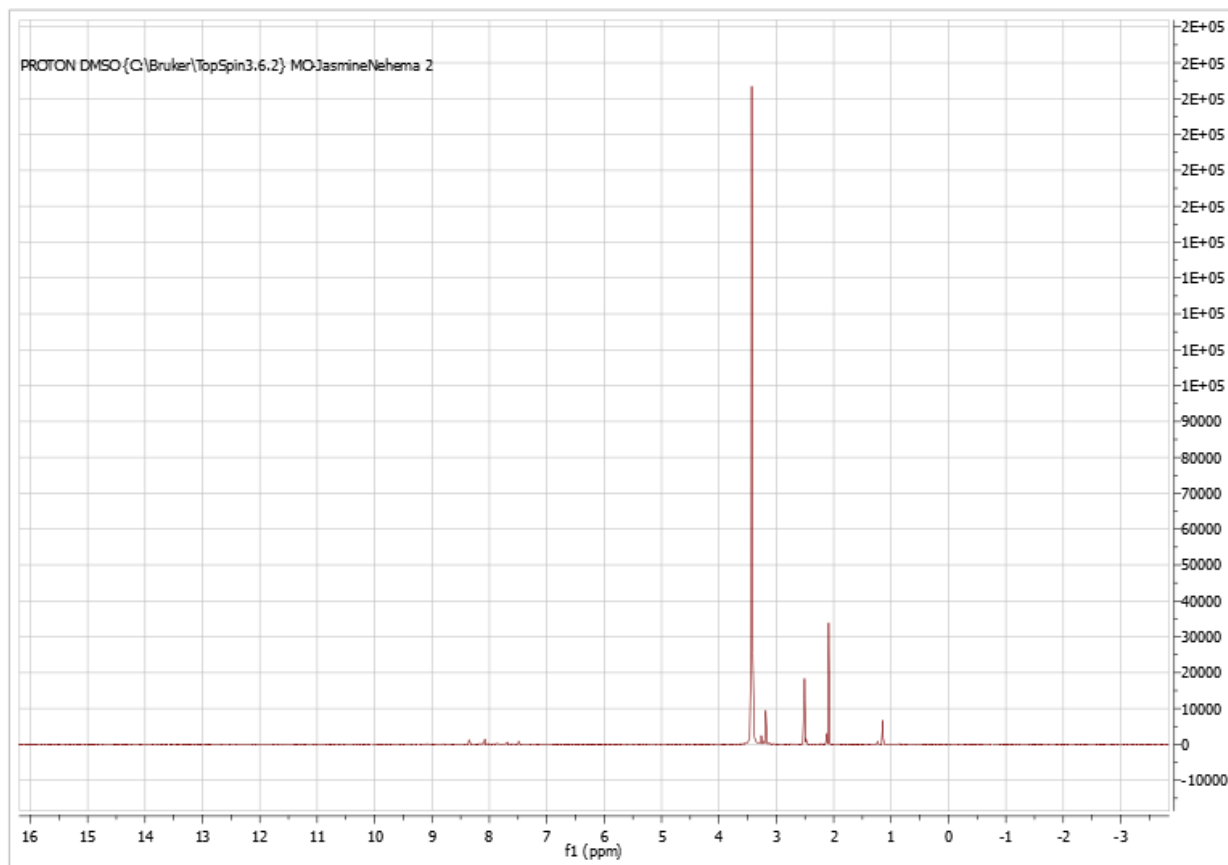
e - ¹H NMR Spectra for C3
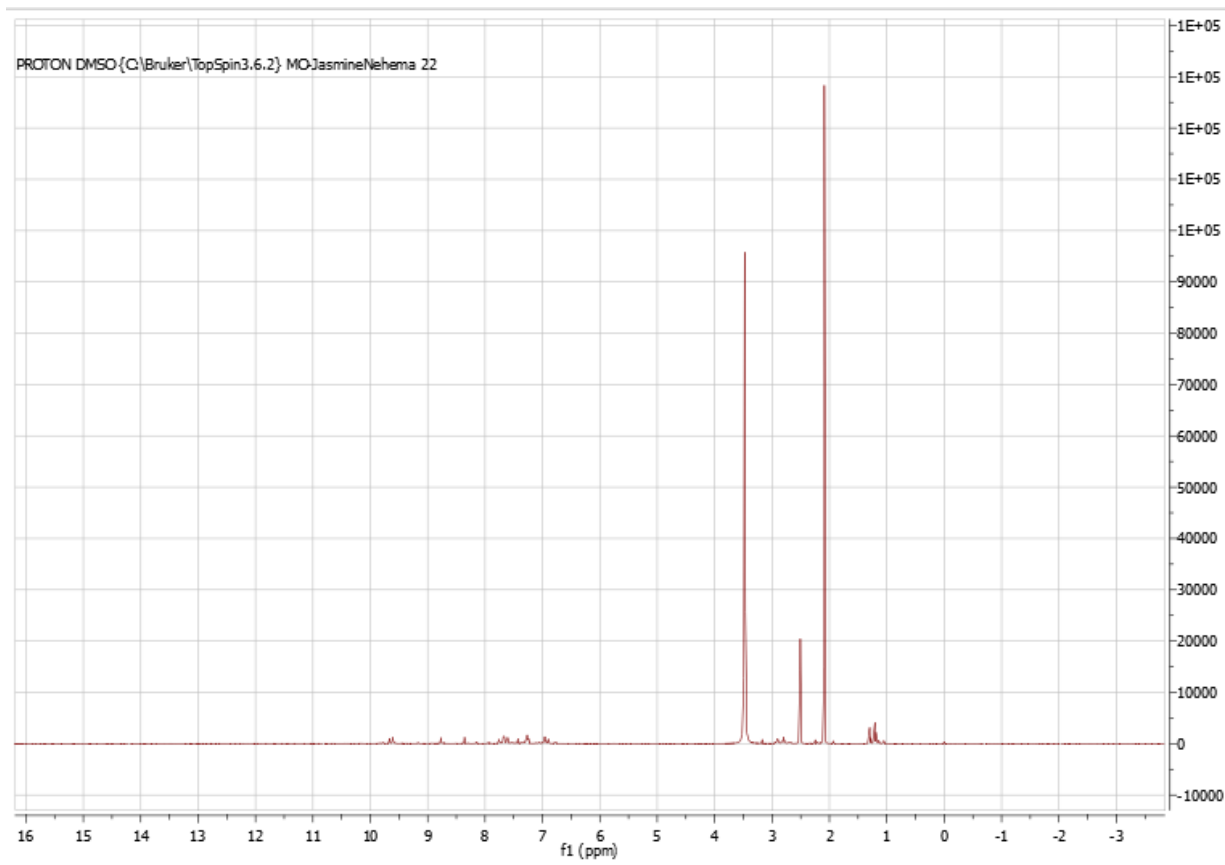
PROTON DMSO {C:\Bruker\TopSpin3.6.2} MO-JasmineNehema 3
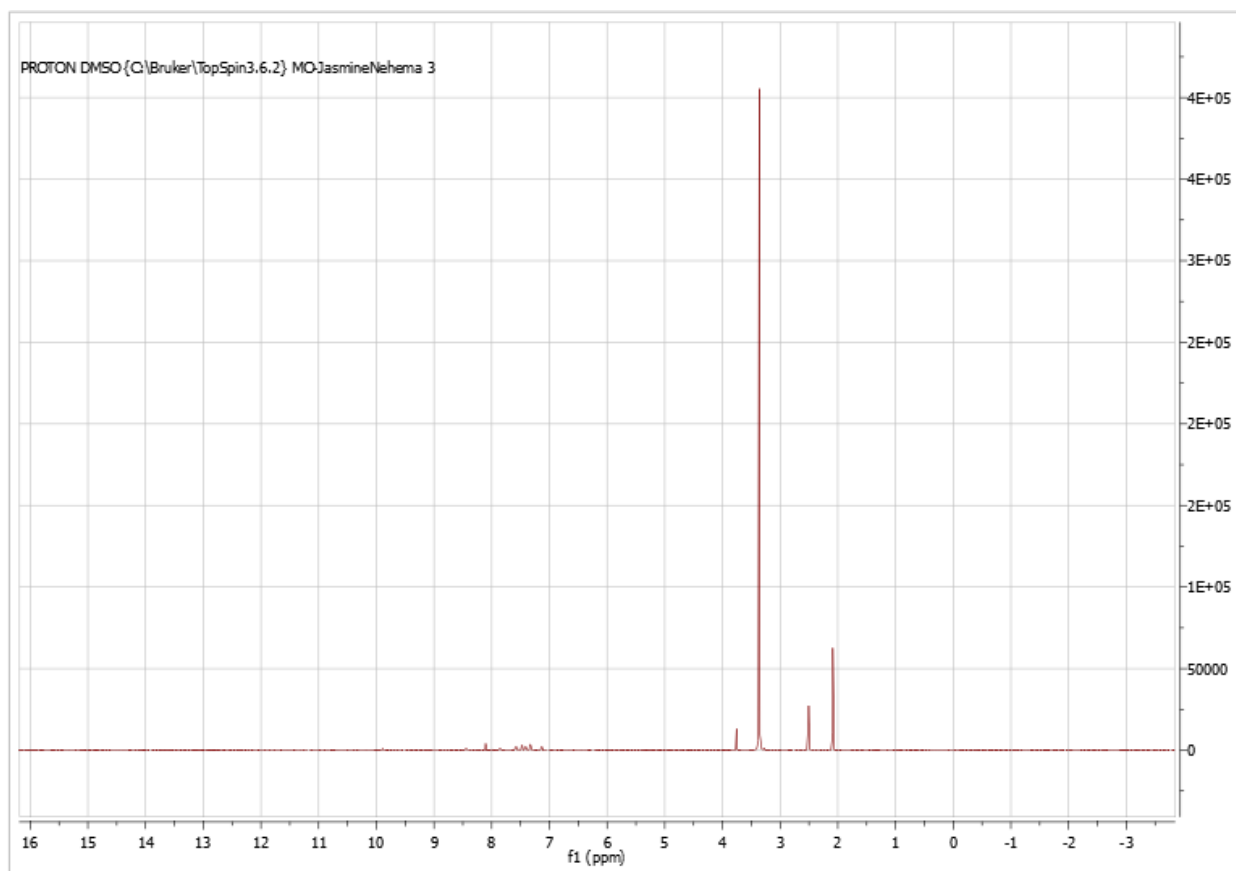
f - ¹H NMR Spectra for C4

Appendix (IV) - ^{13}C NMR Spectra

JNA 008-UL.2.fid
C13CPD Acetone {C:\Bruker\TopSpin3.6.2} MO-JasmineNehema 17
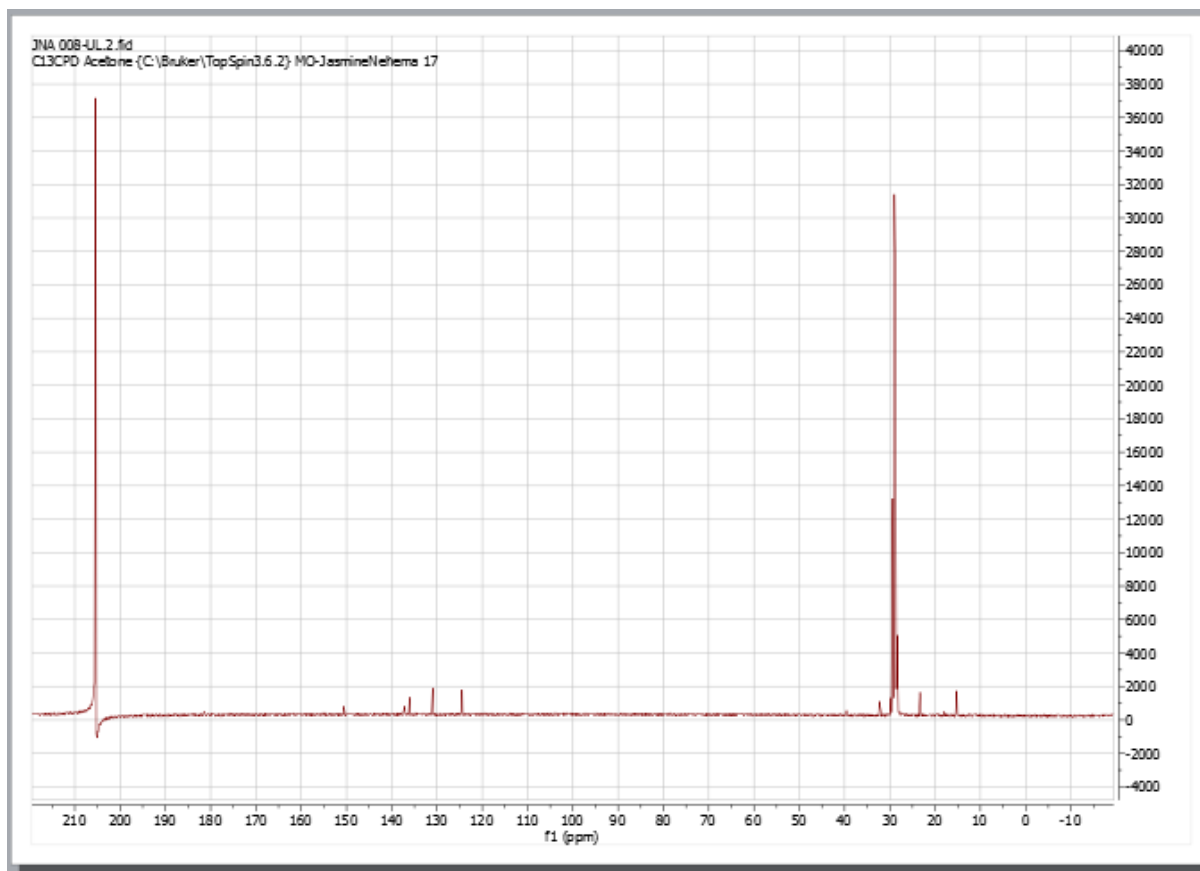
a - ^{13}C NMR Spectra for L2
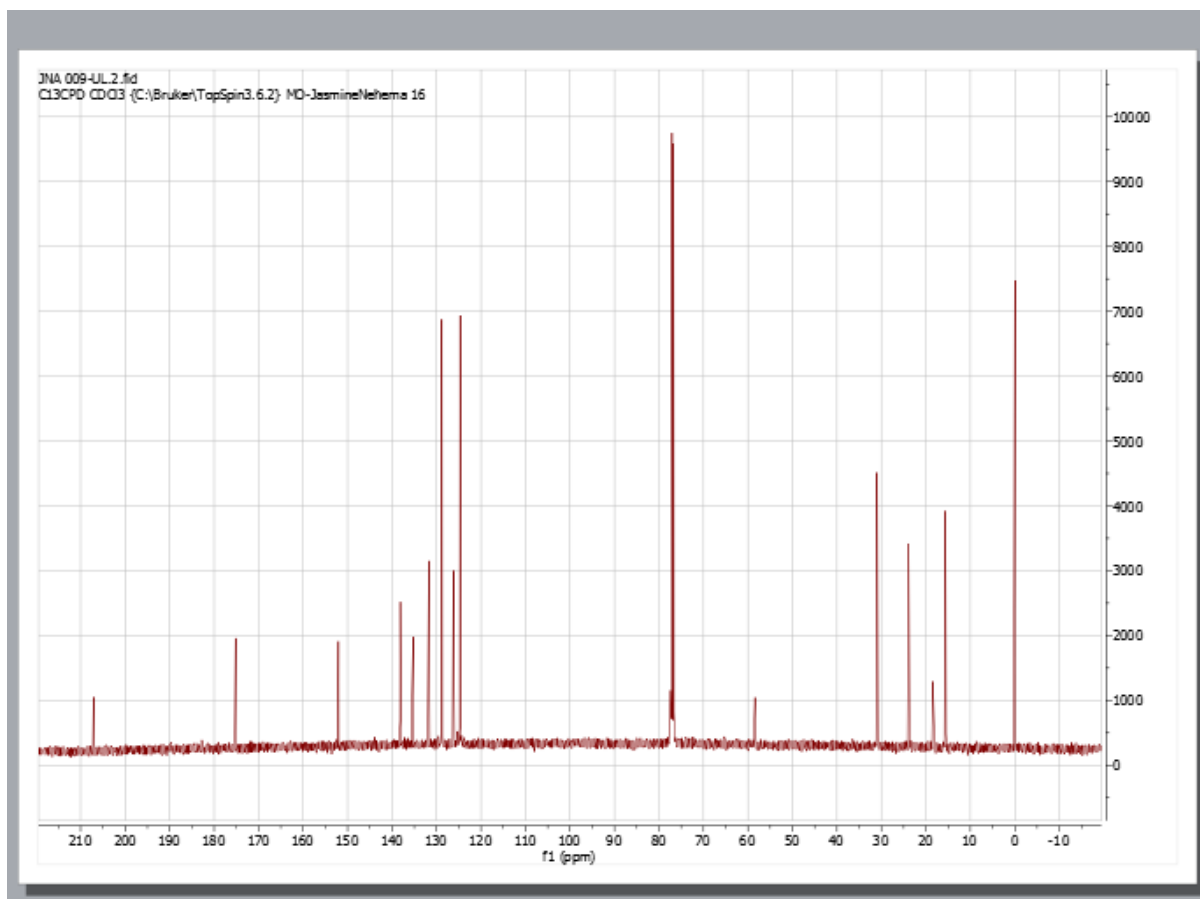
b - ^{13}C NMR Spectra for L3
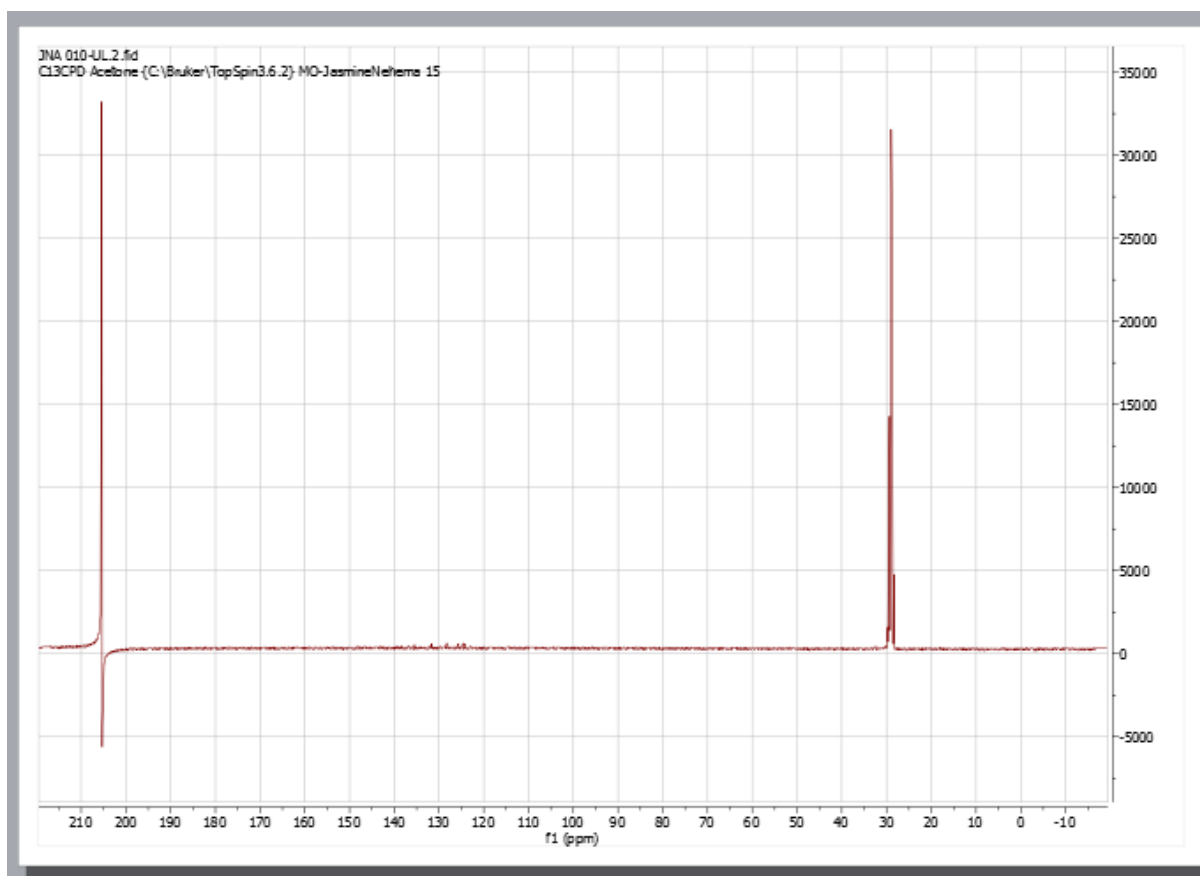
c - ^{13}C NMR Spectra for L4

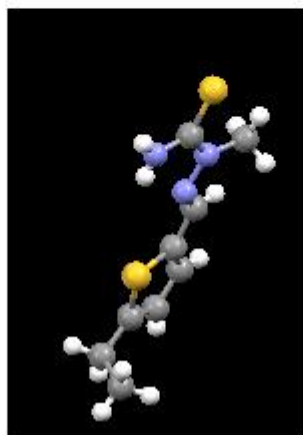**Appendix (V) - XRD data for L2**
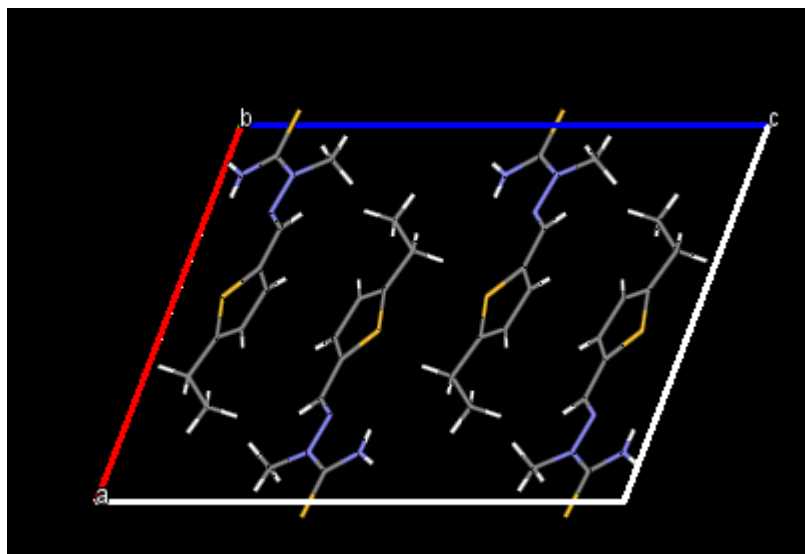
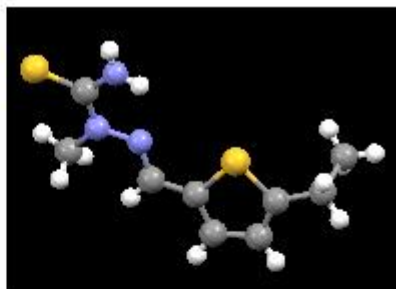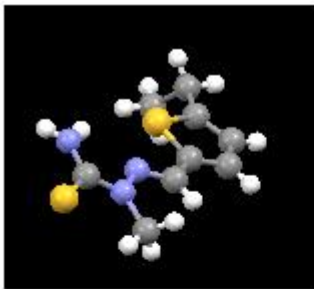**1 - Crystal packing of the ligand**
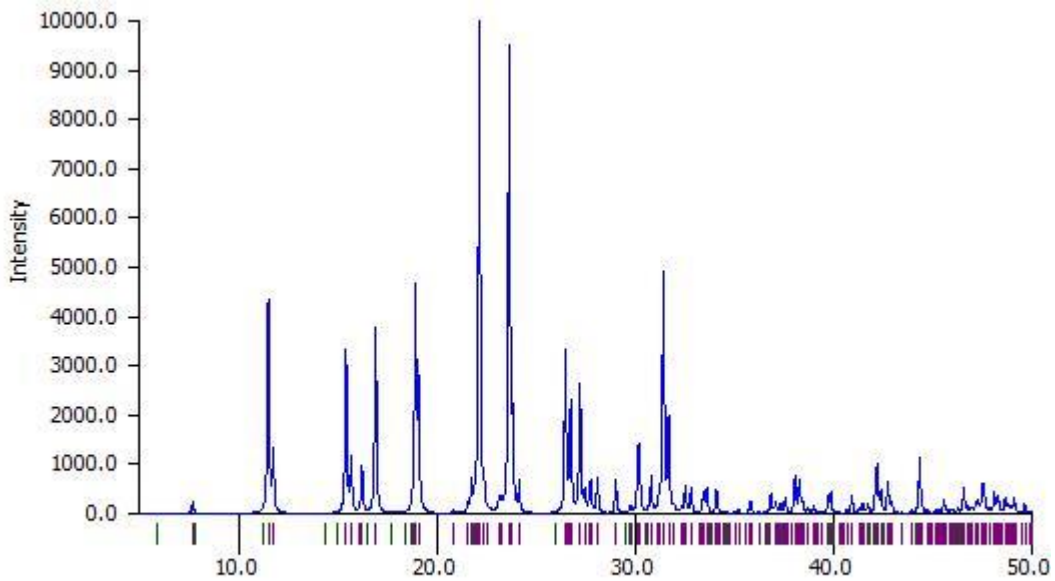
Wavelength: 1.54056   2 theta   14.989, 10407   h, k, l = 0, 1, 0

2 - Powder data

3 **- Lines of symmetry**